SOCIETY OF PETROLEUM ENGINEERS JOURNAL

VOLUME 1, NO 1, MARCH, 1961

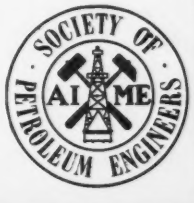

New Versatility in Polarographic Analysis

WIDE-RANGE FISHER ELECDROPODE®

- Manual or automatic operation
- Measures concentrations of 0.01 to 0.00001 equivalents per liter
- Increased potential range (−3 to +2 volts)
- Line-operated, without tubes or batteries
- Separate polarographic cell permits thermostating
- Accessory for amperometric titrations

Oil chemists will find the all-new Model 65 Elecdropode highly useful for determining metals in lubricating oils, greases and gasolines . . . for halogenated hydrocarbons . . . mercaptans . . . and many other positive and negative ions. Modern electronic design has increased the usefulness of the Elecdropode. Its extended potential range makes possible the accurate qualitative and quantitative analysis of a greater variety of inorganic, organic and biological materials.

Use of a Model 66 Recorder makes determinations fully automatic and doubles the 400-to-1 sensitivity range. The Amperometric Titrimeter® accessory carries the range down to 10^{-6} or lower.

The stable power supply requires no vacuum tubes or batteries, except a mercury reference cell. The Elecdropode runs directly on any 115-volt, 50- or 60-cycle a-c line.

For free Bulletin FS-278, please write your nearest Fisher branch or Fisher Scientific Company, 150 Fisher Building, Pittsburgh 19, Pa. F-134

FISHER SCIENTIFIC

World's Largest Manufacturer-Distributor of Laboratory Appliances & Reagent Chemicals

Boston • Chicago • Ft. Worth • Houston • New York • Odessa • Philadelphia • Pittsburgh • St. Louis • Washington • Montreal • Toronto

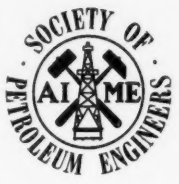

SOCIETY OF PETROLEUM ENGINEERS JOURNAL

JOE B. ALFORD
Executive Publisher

R. WILLIAM TAYLOR
Editor

DAVID L. RILEY
Assistant Editor

ANN GIBSON
Assistant Editor

CAROLYN BLACK
Editorial Assistant

MAURICE D. BRATT
Advertising Manager

VOLUME 1 • NUMBER 1 • MARCH, 1961

SOCIETY OF PETROLEUM ENGINEERS JOURNAL is published quarterly by the Society of Petroleum Engineers of AIME at 6300 North Central Expressway, Dallas 6, Tex. Subscription $15 per year for non-SPE members in United States and North, South and Central America; $5 to public libraries. The Society of Petroleum Engineers is not responsible for any statement made or opinion expressed in its publications. **Registered cable address, AIME. Printed in U.S.A. Application for second class mail privileges is pending at Dallas, Tex.**

Editorial

With this first issue of the *Society of Petroleum Engineers Journal,* the SPE reaches another milestone in its history of disseminating technical information to engineers of the petroleum industry. Publishing of this new journal represents another step taken by SPE and AIME over the years to constantly improve our publications program.

The first AIME *Transactions* volume was published in 1873, but publication of periodicals in addition to the bound volume did not start until 1905 with a journal called *The Bulletin.* First appearing on a bi-monthly basis, *The Bulletin* became a monthly publication in 1909.

In 1919 *Mining and Metallurgy* replaced *The Bulletin* and was published through 1948, serving all members of AIME. It contained no Technical Papers, but included many technical articles. During the earlier days of its publication, the Technical Papers were issued as separates which members requested by mail. Then in 1934, the first of the four *Technologies* was originated to complement *Mining and Metallurgy* and to handle Technical Papers dealing with specific fields of technology.

Metals Technology was issued first in 1934, *Mining Technology* in 1937, *Petroleum Technology* in 1938 and *Coal Technology* in 1946. They were published irregularly as bi-monthlies or quarterlies. Then in 1949 publication of *Journal of Petroleum Technology* in Dallas was started and, simultaneously, *Journal of Metals* and *Mining Engineering* were founded in New York.

In 1958 the increasing flow of technical material again caused expansion of the publications programs. The Society of Petroleum Engineers began to publish some papers as separates, with summaries, appearing in *Journal of Petroleum Technology* and the complete text in the annual *Transactions* volume. At the same time, The Metallurgical Society of AIME separated metals *Transactions* papers from *Journal of Metals,* placing them in a bi-monthly *Transactions of the Metallurgical Society.* Prior to that time, since 1953, *Journal of Metals* had issued three to five supplements per year carrying additional *Transactions* papers.

The Society of Mining Engineers decided in 1960 to begin the practice of publishing most of their *Transactions* material in the annual volume only. Now, in 1961, the Society of Petroleum Engineers begins publication of *Society of Petroleum Engineers Journal.*

Looking back over the years in this manner, it is interesting to see how the three societies of AIME have developed their publications programs similarly, even though they have approached the problem independently, particularly in recent years.

The primary purpose of a professional society is to provide a forum for technical information which will aid its members in better fulfilling their jobs. So it is with the Society of Petroleum Engineers as we inaugurate this new publication with great hopes and expectations for its future. Its success, however, depends not upon the ability of the Society to publish the material, but upon the efforts of individual members in supplying outstanding Technical Papers for presentation here. This is your publication; your contributions will be the foundation for its growth and service to the profession.

R. WILLIAM TAYLOR
Editor

Experiments on Mixing During Miscible Displacement in Porous Media

WILLIAM E. BRIGHAM
JUNIOR MEMBER AIME
PHILIP W. REED
JOHN N. DEW
MEMBERS AIME

CONTINENTAL OIL CO.
PONCA CITY, OKLA.

ABSTRACT

The paper describes experiments on miscible displacement in various porous media and the results of these experiments. Both glass bead packs and natural cores were used. Bead diameters varied from 0.044 to 0.47 mm, and pack lengths varied from 83 to 678 cm. Natural cores used were Berea and Torpedo sandstone.

By taking samples as small as 0.5 cc and using refractive index for analysis, the data on breakthrough curves could be plotted to within ± 0.5 per cent. To plot the data correctly on error function paper, a parameter $(V_P - V)/\sqrt{V}$ *was used which allowed for the predicted growth of the front as it moved past the observer.*

The change in the amount of mixing (length of mixed zone) was studied by varying velocity, length of travel, bead size, viscosity ratio and pack diameter. When the displaced material was less viscous than the displacing material (favorable viscosity ratio), these changes were adequately predicted by theory. When natural cores were used, rather than glass beads, the amount of mixing was greatly increased – also qualitatively predicted by theory.

In experiments with favorable viscosity ratios in which the ratio was varied from 0.175 to 0.998, it was found that the rate of mixing was changed by a factor of 5.7. Thus, the rate of mixing is strongly affected by viscosity ratio, even when the theoretical error function relationship for mixing is valid.

Experiments using fluids with viscosity ratios near 1.0 showed that the instability effects of even a slightly unfavorable viscosity ratio (1.002) caused disproportionately more elongated breakthrough curves than found with a favorable viscosity ratio (.998). When the viscosity ratio was as high as 5.71 these instability effects were much more pronounced, as evidenced by the shape of the breakthrough curve. The displacements at viscosity ratios above 1.0 no longer followed the theoretical error function curve.

It was found that at reservoir rates in natural reservoir materials the rate of mixing (as measured by the dispersion coefficient K) was considerably higher than in glass bead packs. The higher mixing rate is caused by the inhomogeneity of reservoir rock as compared to glass beads. The amount of inhomogeneity is expressed in terms of a mixing coefficient α.

Data on length of mixed zone vs velocity showed that there exists a velocity at which the zone length is a minimum. At this velocity, diffusional mixing contributes only a small fraction of the total mixing.

INTRODUCTION

Data have been taken on the amount of mixing between two miscible fluids during the displacement of one fluid by another using various systems of porous media and various fluids. The porous media were packs of relatively uniform spherical glass beads (which form an ideal medium for flow studies) and consolidated sandstone cores. The effects of displacing rate, bead size, length of travel, diameter of bead pack and viscosity ratio were investigated.

EQUIPMENT AND EXPERIMENTAL PROCEDURE

The glass beads were packed in Lucite tubes which had an inside diameter of 3.19 cm and a wall thickness of 0.64 cm, except for those packs used to study diameter effects. Porous stainless steel discs were set in the ends of the tube to contain the beads. Minnesota Mining and Manufacturing Co. "Superbrite" beads were used. The consolidated cores were mounted in Lucite tubes, which had been heated to the softening point and bonded to the cores using external pressure. Data on the bead packs and cores are given in Table 1. The prefix numbers on the bead packs (107, 113 and 117) are the Minnesota Mining and Manufacturing code numbers for the particular bead size used.

Fluid movement at any desired rate was obtained by a Zenith gear-type pump driven through a variable

Original manuscript received in Society of Petroleum Engineers Office Nov. 30, 1959. Revised manuscript received Oct. 13, 1960. Paper presented at AIChE-SPE Joint Symposium, Dec. 6-9, 1959, in San Francisco.

speed transmission. The bead packs (or cores) were mounted vertically with the displacing oil injected at the bottom. Oils of matched density were used. Oil compositions are given in Table 1. The diffusion coefficient of these fluids was found experimentally to be 3.2×10^{-6} cm^2/sec. The proportion of each oil in the effluent was determined from refractive index (R.I.) measurements since one oil was mainly Soltrol (an isoparaffinic oil with a low R.I.) and the other was mainly commercial kerosene with a high R.I. For convenience in identification and visual observation of the fluid displacement, one of the pair of oils was dyed red with a dye which did not change the refractive index.

In preparation for a run, a pack was saturated with oil to be displaced. The oil-saturated pack was inverted, the header filled with displacing oil and the tubing carrying displacing oil was connected. The pack was re-inverted so that the inlet was at the bottom, the outlet header was emptied and the run started immediately. In this way, an exact material balance could be made on the effluent. The effluent was caught in a graduate until the approximate arrival of the mixed zone. Incremental samples of suitable size were then taken as the effluent accumulated in the header. Samples were taken with a hypodermic syringe so that each sample emptied the header; thus, each sample was exactly representative of the oil passing the end of the pack during the small time interval of that sample. The refractive index was measured and the proportions of displacing and displaced oil determined from an experimental calibration curve. By taking samples as small as 0.50 cc, the data on breakthrough curves could be plotted within ±0.5 per cent.

EXPERIMENTAL RESULTS

EFFECT OF LENGTH OF TRAVEL

Taylor's[1] theory of displacement in capillary tubes, Scheidegger's[2] statistical theory of porous media, Keulemans'[3] "eddy diffusion" theory and Frankel's[4] "stagnant pockets" theory all predict that longitudinal dispersion will be governed by the following equation.

$$\frac{\partial C}{\partial t} = K \frac{\partial^2 C}{\partial x_1^2} \quad \ldots\ldots\ldots\ldots\ldots (1)$$

Eq. 1 is identical in form to the well known diffusion equation; however, the rate of dispersion or mixing of the flood front is governed by a dispersion coefficient (K) rather than the Fick diffusion coefficient (D), as in the diffusion equation. Also, since the flood front is moving through the porous medium, the space variable used is the distance from the midpoint of the flood front (x_1) rather than the distance from the inlet end of the porous medium (x). The variables x and x_1 are simply related as follows:

$$x_1 = x - ut = x - \frac{L}{T} t \quad \ldots\ldots\ldots\ldots (2)$$

The solution of Eq. 1 with appropriate boundary conditions is well known in the following form.

$$C = 1/2 \left[1 - \text{erf}\left(\frac{x_1}{2\sqrt{Kt}}\right)\right] \quad \ldots\ldots (3)$$

where

$$\text{erf}(\xi) = \frac{2}{\sqrt{\pi}} \int_o^{\xi} e^{-\xi^2} d\xi .$$

Eq. 3 defines the well known "S" shaped curve of the error function integral, and a plot of this equation is a straight line on arithmetic probability co-ordinate paper.

The argument of the error function in Eq. 3 ($x_1/2\sqrt{Kt}$) indicates that at a constant rate of flow and with a constant dispersion coefficient the spread of the mixed zone will be proportional to the square root of the distance traveled. It is of interest to determine the validity of this "square root law"; however, first it is necessary to change

[1]References given at end of paper.

TABLE 1 – POROUS MEDIA AND FLUIDS

Pack or Core No.	Length (cm)	Diameter (cm)	Pore Vol. (cc)	Porosity (per cent)	Permeability (darcies)	Avg. Bead Dia. (mm)
117-1	83.2	3.19	221	33.2	0.65	.044
113-1	83.3	3.19	230	34.6	7.1	.100
107-1	83.5	3.19	215	32.2	115	.470
113-2	167.2	3.20	500	37.1	7	.100
113-3	83.4	14.00	4615	36.0	7	.120
113-4	83.5	1.30	47	37.0	7	.100
113-6	678	3.19	1946	35.8	7	.100
B-1	82.2	7.60	725	20.0	0.300	Berea Sandstone .042 (Calculated)
T-1	82.2	4.88	346	22.5	0.258	Torpedo Sandstone .036 (Calculated)

Oils for Favorable Viscosity Ratio Runs:

Displaced Oil – 89.4 vol. per cent Soltrol, 10.6 per cent Carbon Tetrachloride
Density 0.840 gm/cc, Viscosity 1.25 cp at 25°C.

Displacing Oil – 50 vol. per cent Mineral Oil, 50 vol. per cent Kerosene
Density 0.840 gm/cc, Viscosity 7.14 cp at 25°C.

Oils for Runs at Approximately Equal Viscosity Ratios:

Clear Oil – 94.9 vol. per cent Soltrol, 5.1 per cent Carbon Tetrachloride
Density 0.795 gm/cc, Viscosity 1.296 cp at 25°C.

Red Oil – 94.8 vol. per cent Kerosene, 5.2 per cent Heptane
Density 0.795 gm/cc, Viscosity 1.299 cp at 25°C.

the equation variables somewhat. Eq. 3 defines the concentration profile in the porous medium at a given time, while the experimental data give the concentration at a given point as the constantly growing mixed zone moves past the observer. The following substitutions can be made:

$$x_1 = L\left(\frac{V_p - V}{V_p}\right) \quad \ldots\ldots\ldots\ldots \quad (4)$$

$$t = T\left(\frac{V}{V_p}\right) \quad \text{or} \quad t = \frac{x}{u} \quad \ldots\ldots\ldots \quad (5)$$

Thus, the argument of the error function becomes,

$$\frac{x_1}{2\sqrt{Kt}} = \frac{L(V_p - V)}{2\sqrt{TKV_pV}} = \frac{L}{2\sqrt{KTV_p}}(U) \quad \ldots\ldots \quad (6)$$

where

$$U = \frac{V_p - V}{\sqrt{V}} \ .$$

The error function parameter U serves two purposes. First, it accounts for the predicted growth of the mixed zone as it passes an observer stationed at a fixed point. Second, with displacements varying only in length of travel, plots of U vs concentration should fall on the same line if the "square root law" holds.

As a test of the square root law, runs were made at approximately the same rate (5.2 to 6.3 $\times$ 10^{-3} cm/sec) at a viscosity ratio of 0.175. Three bead packs of 3.19-cm ID were used – Pack Nos. 113-1, 2 and 6. The lengths of these packs were 83.3, 167.2 and 678 cm, respectively. The results of these runs are plotted in Fig. 1. As can be seen, the data fall on a straight line in the concentration range of 5 to 80 per cent displacing fluid. This shows that the theoretical equation for the composition profile (the error function) is valid over most of the concentration range, although at high concentrations the profile is somewhat longer than predicted. Further, since all the data fall on the *same* straight line, the square root law is also valid.

It appears appropriate at this point to define the relationship between the error function parameter U and the rate of growth of the mixed zone which is

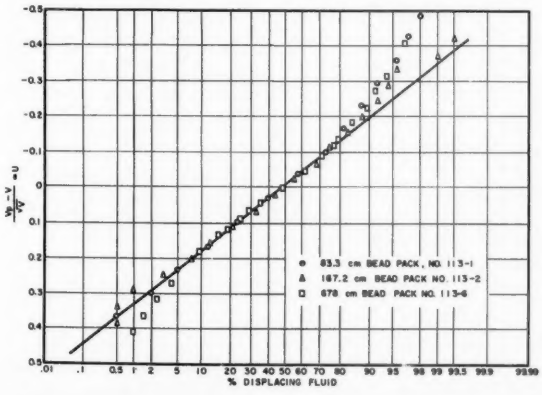

FIG. 1 – EFFECT OF LENGTH OF TRAVEL ON ERROR FUNCTION PLOT.

characterized by the dispersion coefficient K. Taylor[1] has shown that K can be related to the length of the transition zone between any two specified compositions. For instance, if x_{10} is defined as the distance to the point of 10 per cent displacing fluid and x_{90} is the distance to the point of 90 per cent displacing fluid, the length of transition zone so defined is $x_{90} - x_{10}$, and the dispersion coefficient is defined as follows.

$$K = \frac{1}{t}\left[\frac{x_{90} - x_{10}}{3.625}\right]^2 \quad \ldots\ldots\ldots\ldots \quad (7)$$

However, for our purposes it is necessary to relate the dispersion coefficient K to the error function parameter U. The following method is used. The best straight line is drawn through the data points. Values of U are read from this line at the 10 per cent (U_{10}) and 90 per cent (U_{90}) concentration values. The dispersion coefficient is then defined as follows.

$$K = \frac{1}{V_P T}\left[\frac{L\,(U_{90} - U_{10})}{3.625}\right]^2 \quad \ldots\ldots \quad (8)$$

Eq. 8 is identical to Eq. 7, as can be shown by substituting Eqs. 5 and 6 into Eq. 7. If a person prefers to use other concentration values, such as 20 and 80 per cent, the form of the equations would be the same as Eqs. 7 and 8, but a different constant would be necessary (e.g., 2.380 for 20 and 80 per cent concentrations). These constants can be obtained from any standard table of error integrals.

EFFECT OF VISCOSITY RATIO

Data were run in the 113-1 bead pack at viscosity ratios of 0.175, 0.998, 1.002 and 5.71 at a constant velocity ($\cong$ 6.0 $\times$ 10^{-3} cm/sec). The effluent composition curves are shown in Figs. 2 and 2A. In Fig. 2 only the 5.71 and 0.998 viscosity ratio data are shown due to crowding of the other curves near 1.0 pore volume injected. In Fig. 2A the central portion of the effluent composition plot of Fig. 2 has been greatly expanded, and the data at 0.175 and 1.002 viscosity ratios have also been included. Of course, on this expanded plot only a small portion of the 5.71 viscosity ratio curve can be seen.

Fig. 2 best shows the marked difference when the viscosity ratio of 0.998 (a favorable viscosity ratio) is compared to a ratio of 5.71 (an unfavorable viscosity ratio). The favorable ratio curve is the typical "S" shaped curve of the error function, as defined by Eq. 3. The unfavorable viscosity curve is greatly extended, no longer follows the theoretical "S" shaped curve and exhibits a number of bumps and irregularities in composition. The irregularities are caused when "fingers" of displacing fluid run ahead of the bulk of the flood front. These fingers could be easily observed since the displacing fluid was dyed red; also, they have been reported visually by Blackwell, *et al.*[5]

In Fig. 3, the data of Fig. 2A have been plotted

on probability co-ordinates. The most noticeable phenomenon is that increasing the viscosity ratio also increases the value of $U_{90} - U_{10}$ and, thus, increases K and the rate of dispersion. For instance, compare the data at viscosity ratios of 0.175 and 0.998. Both of these are favorable ratios and both follow the theoretical error function of Eq. 3. But, it is evident that the change in viscosity ratio caused an increase in mixing rate (shown through $U_{90} - U_{10}$). This phenomenon has not been adequately studied to date, so no generalization can be made about the effect of viscosity ratio on mixing rate. But this points out the need to view with care data from different authors who may be using different viscosity ratios.

Another important effect of viscosity ratio is found by comparing the 0.998 data with the 1.002 data. The instability effects of only a slightly unfavorable viscosity ratio (1.002) cause a disproportionately large change in the effluent concentration curve. Also, along with a greater amount of mixing, the unfavorable viscosity ratio data no longer plot a straight line on the probability co-ordinates of Fig. 3. The 5.71 viscosity ratio data are not plotted on Fig. 3, but these data exhibit even more curvature. So Eq. 3 cannot be considered valid for displacements at a viscosity ratio greater than unity.

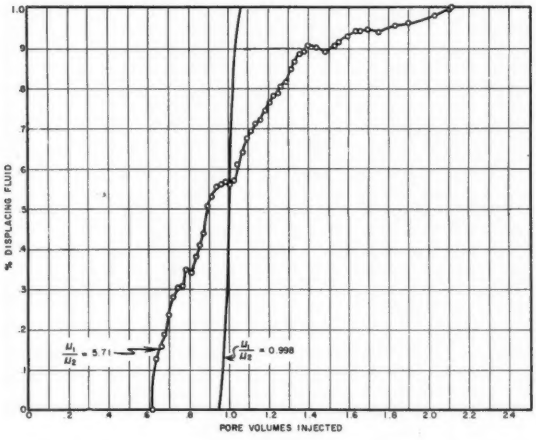

FIG. 2 – EFFECT OF VISCOSITY RATIO ON EFFLUENT CONCENTRATION CURVE, BEAD PACK NO. 113-1.

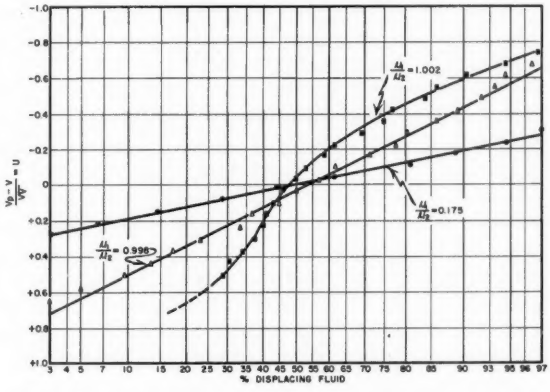

FIG. 3 – EFFECT OF VISCOSITY RATIO ON ERROR FUNCTION PLOT, BEAD PACK NO. 113-1.

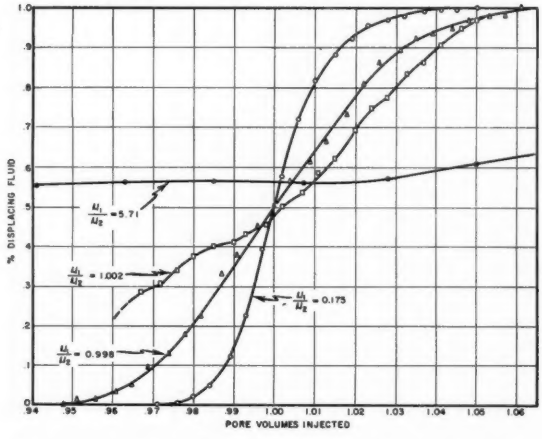

FIG. 2A – EFFECT OF VISCOSITY RATIO ON EFFLUENT CONCENTRATION CURVE, BEAD PACK NO. 113-1.

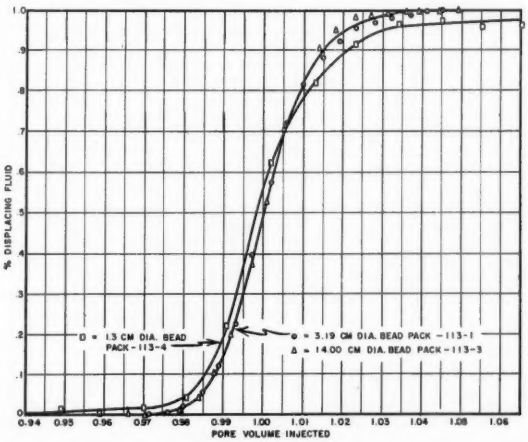

FIG. 4 – EFFECT OF BEAD PACK DIAMETER ON EFFLUENT COMPOSITION CURVE.

EFFECT OF PACK DIAMETER

Displacements were run in 14.00-cm (113-3), 3.19-cm (113-1) and 1.30-cm (113-4) packs to determine the effect of over-all pack diameter. The beads used in all three packs were 0.100-mm average diameter, and the viscosity ratio used was 0.175. As can be seen in Fig. 4, the 3.19 and 14.00-cm packs show almost identical breakthrough curves; but, the 1.30-cm pack definitely exhibits more dispersion. There are two possible reasons for the greater mixing found in the small-diameter pack. One reason can be deduced from the nature of the mixing theories in porous media.[2, 3, 4] All these theories assume a cross section large enough that boundary or wall effects are negligible, and it is likely that this assumption is not valid in the 1.30-cm pack. Another reason for greater dispersion may

be the difficulty in achieving uniform packing in a small tubing; but, whatever the reason, the data of Fig. 4 emphasize the need for viewing with caution any data acquired from small-diameter packs (less than approximately 3-cm diameter).

EFFECT OF FLOW VELOCITY

Keulemans[3] has suggested that one source of dispersion at higher flow rates is due to the separation and rejoining of channels of flow in the porous medium and has termed this "eddy diffusion". If one considers a particular porous medium, the amount of dispersion introduced with each centimeter of distance traveled is the same, regardless of the velocity of flow through that medium. The dispersion is entirely due to the amount of separation and rejoining that is inherent in the medium itself. However, the dispersion coefficient (K) is a measure of the *rate* of dispersion, not the amount, and thus would be proportional to velocity. Also, when considering two similar porous media differing only in size of flow channels and particles, the amount of dispersion is directly proportional to particle size. So, for Keulemans' "eddy diffusion",

$$E = \lambda\, u\bar{r} \quad \ldots\ldots\ldots\ldots\ldots\ldots \quad (9)$$

where λ is a term which expresses the amount of irregularity of packing and, thus, the amount of eddy diffusion characteristic of the particular porous medium. It is often desirable to express variables in dimensionless form, and Eq. 9 suggests the following form.

$$\frac{K}{D} \sim \frac{\bar{r}u}{D} \quad \ldots\ldots\ldots\ldots\ldots\ldots \quad (10)$$

Taylor's capillary tube theory and Frankel's "stagnant pockets" theory both reduce to the following proportionality,

$$K \sim \frac{(\bar{r}u)^2}{D} \quad \ldots\ldots\ldots\ldots\ldots\ldots \quad (11)$$

which, again in dimensionless form, becomes

$$\frac{K}{D} \sim \left(\frac{\bar{r}u}{D}\right)^2 \quad \ldots\ldots\ldots\ldots\ldots\ldots \quad (12)$$

By referring to Expressions 10 and 12, it would appear reasonable to plot $\bar{r}u/D$ vs K/D, both for the purpose of correlation of data and to test the validity of these theories. Accordingly, a plot of all the data has been made in Fig. 5 using K/D and $\bar{r}u/D$ as co-ordinates, as done by Blackwell, *et al.*[5] A log-log co-ordinate system is preferable here because of the wide range of variables covered and because $\bar{r}u/D$ is expressed as a power function in the above proportionalities.

EFFECT OF FLOW VELOCITY – LOW FLOW RATES

To understand the amount of mixing which occurs at low velocity, one should consider the limiting case where velocity is zero. At non-flow conditions, the only case of mixing should be ordinary molecular (Fick) diffusion, and the dispersion coefficient K will be constant. In Fig. 5, the data on 0.100-mm beads approaches this condition at a value of $\bar{r}u/D$ of about 0.2. Thus, at low rates the equation for the dispersion coefficient in glass bead packs becomes

$$\frac{K}{D} = 0.7 \quad \ldots\ldots\ldots\ldots\ldots\ldots \quad (13)$$

Blackwell, *et al*[5] and Carman[6] have also found this relationship at low flow rates for spherical glass bead packs. The number 0.7 should not be considered a universal constant, for diffusion in a porous medium is directly analogous to the electrical resistivity of the medium. Thus, K/D is related to the formation factor F and porosity ϕ, and a more exact equation at low rates is

$$\frac{K}{D} = \frac{1}{F\phi} \quad \ldots\ldots\ldots\ldots\ldots\ldots \quad (14)$$

The term $1/F\phi$ will commonly vary between 0.15 and 0.7, depending on the lithology of the porous medium.[7]

EFFECT OF FLOW VELOCITY – HIGH FLOW RATES

At high flow rates, as stated, Keulemans' theory predicts that the term K/D is proportional to $\bar{r}u/D$ to the first power. The other theories predict a second power dependence. The data of Fig. 5 show that none of these theories is exact but, rather, that the result lies somewhere between them. The exponent was found experimentally to be 1.24, 1.20 and 1.19 in the 0.470-mm beads, 0.100-mm beads and the Berea core, respectively. These data compare closely with the 1.17 power reported by Blackwell, *et al*,[5] and the 1.20 power shown by Aronofsky and Heller[8] on data reported by von Rosenburg.[9]

From these data it appears that, for glass bead packs and fairly homogeneous sandstone, a reasonable value to use for the exponent is 1.20. Thus, we get the empirical equation

$$\frac{K}{D} = a\left(\frac{\bar{r}u}{D}\right)^{1.20} \quad \ldots\ldots\ldots\ldots\ldots\ldots \quad (15)$$

The exponent (1.20) may not be a constant, valid for all porous media, since it has only been tested for bead packs and sandstone. It lies between the 1.00 and 2.00 limits of the mixing theories, so it

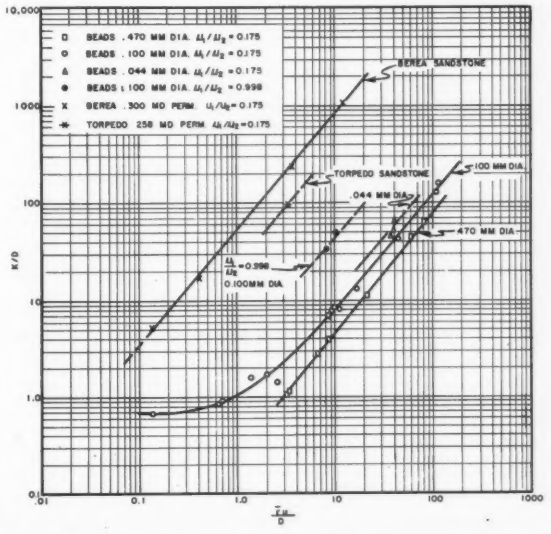

FIG. 5 – EFFECT OF RATE AND TYPE OF POROUS MEDIUM ON DISPERSION RATE.

appears that both eddy diffusion of Keulemans' model and statistical dispersion of either the Scheidegger or Frankel type play a part in determining the rate of mixing. Also, since the result is close to the first power, eddy diffusion must be the dominant factor in these media.

Eq. 14 for low rates can be combined with Eq. 15 for high rates to give a single equation expressing the dispersion coefficient as a function of velocity and lithology. Thus, we get

$$\frac{K}{D} = \frac{1}{F\phi} + a\left(\frac{\bar{r}u}{D}\right)^{1.20} \quad \ldots\ldots\ldots\ldots (16)$$

It will be noted that no attempt has been made to give an exact numerical value for the mixing coefficient (a) in these equations. The reason is that a is not a constant, as implied in other work[5] but, rather, varies widely depending on the geometry of the porous medium and the viscosity ratio of the flowing fluids. A further discussion on the effect of porous medium type on a is found in the next section, and a comparison of a values has been made in Table 2. The authors feel that, with more experimental evidence, the mixing coefficient (a) could be used with success to characterize porous media, for a is a measure of the inhomogeneity of a medium in a dynamic situation, while the present pore size distribution techniques are based on non-flow measurements.

Upon studying Eq. 16, one observes an interesting relationship between the dispersion coefficient K and the molecular diffusion coefficient D. At high flow rates with all other variables held constant, K is inversely proportional to $D^{0.2}$; this means that, if the fluids had a larger diffusion coefficient, the amount of mixing would be slightly less. No attempt has been made to study this possibility here, but the data of Handy[10] at least qualitatively substantiate that mixing rate is decreased somewhat when using a fluid with a greater diffusion coefficient.

EFFECT OF POROUS-MEDIUM TYPE

Keulemans' eddy diffusion term includes the coefficient λ which expressed the inhomogeneity of the flow channels. Let us assume we have two porous media which are geometrically similar with different particle sizes, such as two identically packed bead packs differing only in diameter of beads. These packs would have identical values for λ according to Keulemans' theory. Scheidegger's theory contains a dispersivity term a which from its definition would also be constant under the afore-mentioned conditions, and Frankel's stagnant pockets theory gives the same result. However, in practice, λ (and, thus, a and a) has experimentally been found to increase with finer particles. Klinkenberg and Sjenitzer[11] report values of λ increasing from one to eight as particle diameters drop from 1.0 to .05 mm. The data of Fig. 5 and Table 2 on 0.470, 0.100 and .044-mm beads also point out this trend, for the values of a increase as the bead diameters decrease.

TABLE 2 – EFFECT OF VISCOSITY RATIO AND POROUS MEDIUM ON a, FOR $K/D = a\,(\bar{r}u/D)^{1.20}$

Porous Medium	Viscosity Ratio	a
.044-mm Beads	.175	0.69
.100-mm Beads	.175	0.49
.100-mm Beads	.998	2.78
.470-mm Beads	.175	0.30
Torpedo Sandstone	.175	23.2
Berea Sandstone	.175	53

Why then is a not constant? Keulemans suggested that this increase with small particles is due partially to the difficulty in packing smaller particles uniformly and partially to the greater variation in particle size usually found with finer particles. That is, the larger a is caused by more inhomogeneity in the porous medium. The data reported here from glass bead packs corroborates this theory, for the small beads have a greater variation in particle size than the large beads.

Also, we can compare the values for a reported here to those cited by Blackwell[5] and Klinkenberg.[11] The a values found in this paper are considerably smaller than found by these two authors. Part of this difference is caused by viscosity ratio (explained earlier), but even the 0.998 viscosity ratio data give less mixing than reported by Blackwell and Klinkenberg. Again, this is caused by the narrow particle-size range of these beads – that is, by the more homogeneous porous media.

To plot the Berea and Torpedo sand data on Fig. 5 for comparison with the bead pack data, an assumption must be made on average particle radius to be used for these natural porous media. The following equations were used to calculate average pore radii and particle radii.

$$\bar{r}_p \cong \sqrt{\frac{8k\,\tau^2}{\phi}} \times 10^{-4} \quad \ldots\ldots\ldots\ldots (17)$$

$$\bar{r} \cong 3\bar{r}_p \quad \ldots\ldots\ldots\ldots\ldots\ldots (18)$$

where

$\tau \cong 2.0$

Using these equations, the average sand-grain radii calculated 2.0×10^{-3} cm for the Berea sandstone and 1.8×10^{-3} cm for the Torpedo sandstone. These average grain radii are, of course, not exact, but they are close enough to show without doubt the tremendously increased importance of the a term (the inhomogeneities) in naturally occurring porous media when the data are compared in Fig. 5 to the homogeneous bead pack. Handy's[10] data obtained from a Boise consolidated sandstone show the same results. In Table 2, the a values for the bead pack data and the natural core data may be easily compared.

To more readily see the effect of inhomogeneities on rate of mixing at reservoir rates, let us consider a displacement at 3.0×10^{-4} cm/sec (0.85 ft/day). In the .100-mm glass bead pack, the dispersion rate was controlled almost entirely by molecular diffusion. But, in the Berea core used in this study, the dispersion rate was 9.2 times as great as in the glass bead pack because natural sandstone is more

heterogeneous. This result is reflected directly in the values for a found in Table 2.

EFFECT OF VELOCITY ON ZONE LENGTH

It is of considerable interest to know the effect of velocity on the length of the mixed zone. Consider Eqs. 7 and 16. We can substitute $\frac{LV}{uV_p}$ for t in Eq. 7, and then solve these equations simultaneously for $x_{90} - x_{10}$ as a function of velocity. The result is

$$\left(\frac{x_{90}-x_{10}}{3.625}\right)^2 = \frac{1}{F\phi}\frac{DLV}{uV_p} + a\left(\frac{\bar{r}u}{D}\right)^{1.20}\left(\frac{DLV}{uV_p}\right) \quad \ldots\ldots\ldots\ldots\ldots\ldots\ldots\ldots (19)$$

A glance at Eq. 19 will show that there exists a velocity at which the mixed zone length is a minimum. Eq. 19 can be differentiated with respect to velocity and set equal to zero to solve for this velocity.

$$u = \frac{D}{\bar{r}}\left(\frac{1}{.2aF\phi}\right)^{1/1.20} \quad \ldots\ldots\ldots\ldots (20)$$

Using the data for the 113-1 bead pack (0.70 for $1/F\phi$ and 0.49 for a), the velocity for minimum mixing is found from Eq. 20 to be 3.3×10^{-3} cm/sec. Fig. 6 shows the data on velocity and zone length for this pack along with the calculated minimum.

Another method of fixing this "minimum" velocity is to draw a 45° line on Fig. 5 tangent to the curve. The point of tangency corresponds to the minimum point. By this procedure it is apparent that this velocity will be lower as the porous medium becomes more heterogeneous. For instance, assuming $1/F\phi$ equals 0.50 for the Berea sandstone and a equals 53, the velocity for minimum mixing in Berea is calculated to be 1.2×10^{-4} cm/sec. Also, it can be seen from the K/D value that only about 20 per cent of the total dispersion coefficient is caused by diffusion at the "minimum mixing" velocity.

SUMMARY AND CONCLUSIONS

This investigation has found that the viscosity ratio during displacement greatly affects dispersion rate in the following ways.

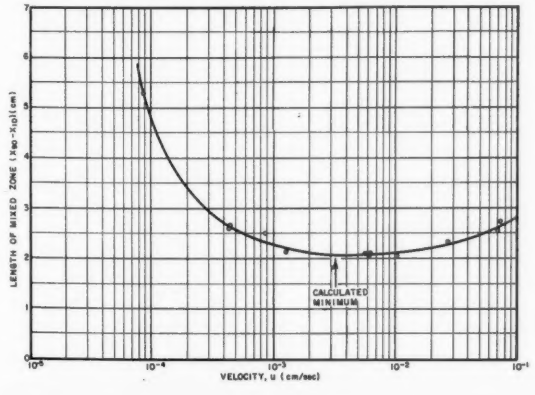

FIG. 6 – EFFECT OF VELOCITY ON ZONE LENGTH, BEAD PACK NO. 113-1, VISCOSITY RATIO 0.175.

1. When a favorable viscosity ratio was changed by a factor of 5.7 (0.175 to 0.998), the dispersion coefficient was also changed by a factor of 5.7. Although this seems to suggest a linear relationship, there are not enough data available to substantiate such a conclusion. This should be investigated further.

2. When changing only slightly from a favorable (0.998) to an unfavorable (1.002) viscosity ratio, the mixing rate was disproportionately increased and the predicted error function curve was no longer valid.

3. When the viscosity ratio was 5.71, the effluent concentration curve was greatly extended, and there was both visual and analytical evidence of distinct "fingers" of displacing fluid running ahead of the average displacement front.

4. At viscosity ratios above 1.0, the theoretical error function curve no longer was valid.

The following conclusions can be drawn for displacements at a favorable viscosity ratio (viscosity ratio $\leq$ 1.0).

1. The "square root law", which concludes that the amount of mixing is proportional to the square root of the distance traveled, is valid.

2. Diameter of the pack can be an important variable, and data from small-diameter packs should be treated with caution. Data obtained using .100-mm diameter beads were consistent for packs 3.2 cm in diameter and larger.

3. At very low rates of flow, the dispersion coefficient K is directly proportional to the Fick diffusion coefficient, as expected.

$$\frac{K}{D} = \frac{1}{F\phi} .$$

4. At high rates of flow, the dispersion coefficient is characterized by the following relation for sandstones and glass bead packs.

$$\frac{K}{D} = a\left(\frac{\bar{r}u}{D}\right)^{1.20} .$$

5. a in this equation is not a constant but, rather, is a function of the viscosity ratio of the flowing fluids and the inhomogeneity of the porous medium.

6. In natural sandstones at reservoir rates, the dispersion coefficient K is proportional to $(u)^{1.20}$, as in the above equation, and the rate of dispersion is considerably higher than found in glass bead packs.

7. The length of the mixed zone is a function of velocity. The zone length increases at very low flow rates and very high flow rates, and there exists a velocity at which the zone length is a minimum. At this velocity, diffusion contributes only a small fraction of the total dispersion coefficient.

NOMENCLATURE

C = concentration (cc/cc)
t = time (seconds)
x_1 = distance from midpoint of flood front (cm)
K = dispersion coefficient (cm^2/sec)

D = Fick diffusion coefficient (cm^2/sec)
x = distance from inlet end of porous medium (cm)
u = average pore velocity (cm/sec) $u = L/T$
L = length of porous medium (cm)
T = time required to inject or produce one pore volume of fluid (seconds)
V_p = pore volume of porous medium (cc)
V = volume of fluid recovered at time of sample (cc)
U = error function parameter $(V_p - V)/\sqrt{V}$
$\bar{r}$ = average radius of glass beads or sand grains (cm)
E = Keulemans' eddy diffusion coefficient (cm^2/sec)
λ = Keulemans' packing coefficient
F = formation resistivity factor
ϕ = fractional porosity
α = mixing coefficient
a = Scheidegger's dispersivity
$\bar{r}_p$ = average pore radius (cm)
k = permeability (darcies)
Viscosity Ratio = the ratio of the displaced phase viscosity to the displacing phase viscosity

ACKNOWLEDGMENTS

The authors wish to express their appreciation to the management of Continental Oil Co. for permission to publish this paper, to Byron Dyche and Wilbur Hullet for performing many of the experiments, and to Stanley Frankel for his helpful comments and suggestions.

REFERENCES

1. Taylor, G. I.: "Dispersion of Soluble Matter in Solvent Flowing Slowly Through a Tube", *Proc.*, Royal Society (1953) Vol. 219, 186.
2. Scheidegger, A. E.: "Statistical Hydrodynamics in Porous Media", *Jour. Appl. Phys.* (1954) Vol. 25, No. 8, 994.
3. Keulemans, A. I. M.: *Gas Chromatography*, Reinhold Press, N. Y. (1957).
4. Frankel, Stanley: "Mixing of Fluid Flowing in a Porous Medium", Conference on Theory of Fluid Flow in Porous Media, U. of Oklahoma (March 23-24, 1959).
5. Blackwell, R. J., Terry, W. M. and Rayne, J. R.: "Factors Influencing the Efficiency of Miscible Displacement", *Trans.*, AIME (1959) Vol. 216, 1.
6. Carman, P. C.: *Flow of Gases Through Porous Media*, Reinhold Press, N. Y. (1956).
7. Pirson, S. J.: *Oil Reservoir Engineering*, McGraw-Hill Book Co., Inc., N. Y. (1958).
8. Aronofsky, J. S. and Heller, J. P.: "Diffusion Model to Explain Mixing of Flowing Miscible Fluids in Porous Media", *Trans.*, AIME (1957) Vol. 210, 345.
9. von Rosenburg, D. U.: "Mechanics of Steady-State Single-Phase Fluid Displacement from Porous Media", *AIChE Jour.* (March, 1956) Vol. 2, No. 1, 55.
10. Handy, L. L.: "An Evaluation of Diffusion Effects in Miscible Displacement", *Trans.*, AIME (1959) Vol. 216, 61.
11. Klinkenberg, A. and Sjenitzer, F.: *Chem. Engrg. Science* (1956) Vol. 5, 528.

***

Stability Theory and Its Use to Optimize Solvent Recovery of Oil

RICHARD L. PERRINE
MEMBER AIME

U. OF CALIFORNIA AT LOS ANGELES
LOS ANGELES, CALIF.

ABSTRACT

This paper shows how stability theory can be used to optimize solvent recovery of oil. Application of the theory leads to definition of the limiting conditions required for stable displacement to occur. One of these conditions is that the size of a solvent "slug" must at least equal a prescribed minimum. The criteria to be satisfied are miscibility and stability. Stability implies that no viscous fingering will occur and that mixing will be caused only by a dispersion process. Miscibility implies that complete recovery will be obtained from the swept regions. Thus, for any specified set of reservoir conditions, an optimum use of solvent is defined.

INTRODUCTION

The early outlook for solvent flooding as a means to increase oil recovery was very favorable. Some laboratory results indicated that a "slug" containing perhaps 2 to 3 per cent of a hydrocarbon pore volume could be successful. However, other data suggested as much as 30 per cent would be required. The difference is of considerable economic importance. A theoretical explanation for these divergent results has been advanced by the author.[1,2] Stability theory defines conditions for two distinct flow regimes. In stable displacement, solvent and oil become mixed by a dispersion process, and the solvent requirement is small. On the other hand, unstable displacement can degenerate into viscous fingering. The practical result is a considerable increase in the extent of mixing and, thus, in the solvent required.

The present paper shows how to use stability theory to optimize solvent recovery of oil. Oil is usually considered to be displaced by a small amount, or a slug, of solvent. Gas in turn follows solvent. Any fingering will permit contact of nearly solvent-free gas and oil, leading to immiscibility and reduced recovery. Thus, our optimum is defined by two restrictions – stable flow and miscibility. Although an immiscible solvent process could prove more profitable than any miscible process, such processes lie outside the selected definition of an optimum. The usefulness of computations based on the present work will depend on the validity of the general theory. Because the important idealizations required tend to minimize the predicted solvent requirement, the results should state correctly the limiting conditions required. Therefore, theoretical calculations should have practical value.

This paper first reviews several principles that result from stability theory. The following section describes use of these ideas in relatively simple systems which symmetry makes appear one-dimensional. Of particular importance is the step-by-step design of a stable minimum-solvent slug. The use of stability theory in cases of multi-dimensional displacement is discussed and, finally, suggestions are given for simplified practical application of the theoretical results.

PRINCIPLES OF STABILITY THEORY

The use of perturbation methods to derive stability conditions has been shown by the author.[1] The discussion is presented in terms of the fractional concentration of solvent in the single hydrocarbon phase. Quite generally, any disturbance can be represented as a Fourier series, of which only the least stable term need be considered. Denoting this term at time $t = 0$ by c_n,

$$c_n = \tilde{c}_n \cos \alpha x L^{-1} \cos \beta y L^{-1} \cos n\pi z L^{-1} \quad \ldots\ldots (1)$$

The initial growth of this least stable term is calculated according to

$$\exp(-\gamma t) \quad \ldots\ldots (2)$$

where

$$\gamma = L^{-2}\left[\alpha^2 D_1 + (\beta^2 + n^2\pi^2) D_3\right] + u_0 \delta^{-2}\left[\alpha n\pi \frac{\partial \bar{c}}{\partial x} - (\alpha^2 + \beta^2)\frac{\partial \bar{c}}{\partial z}\right] g_3 + u_0 \delta^{-2}\left[\alpha n\pi \frac{\partial \bar{c}}{\partial z} - (\beta^2 + n^2\pi^2)\frac{\partial \bar{c}}{\partial x}\right] g_1 \quad \ldots\ldots (3)$$

Original manuscript received in Society of Petroleum Engineers office May 23, 1960. Revised manuscript received Oct. 27, 1960.

[1] References given at end of paper.

and the functions are defined by

$$g_1 = \frac{d \ln \mu}{dc} + \frac{k}{\bar{\mu}} \frac{d\rho}{dc} \frac{g \sin \theta}{\phi u_0}$$

$$g_3 = \frac{k}{\bar{\mu}} \frac{d\rho}{dc} \frac{g \cos \theta}{\phi u_0}$$

$$\delta^{-2} = (\alpha^2 + \beta^2 + n^2\pi^2)^{-1} \ldots\ldots\ldots (4)$$

The least stable term has the highest growth rate, yet stability requires that no growth occur. This means that the stability coefficient γ must be zero or positive, and Eq. 3 shows how this requirement restricts displacement conditions.

The derivation assumed flow in the x-direction within a reservoir of large x and y dimensions and limited thickness L in the z-direction. D_1 is the axial and D_3 the lateral dispersion coefficient.[3-5] The constant, stable volumetric flow rate per unit of cross-sectional area and per unit of porosity is u_0. Flow symmetry maintains solvent concentration $\bar{c}$ for stable flow independent of y. Viscosity $\bar{\mu}$ is for a fluid mixture of solvent concentration $\bar{c}$. From Eq. 1, α, β and n are Fourier expansion parameters depending on the initial disturbance. Other symbols are k for permeability, ϕ for porosity, ρ for density, g for the acceleration of gravity and θ for the dip angle of the formation. For downward tilt in the direction of flow, θ is negative.

Consider what happens as solvent moves through a reservoir displacing oil. Dispersion will cause mixing and a gradual transition from oil to solvent. Values of γ will vary within the solvent bank depending on the relative importance of gravity, viscosity and dispersion. So long as any part of the system is unstable, viscous fingers can grow to dominate flood behavior. The problem is to keep the most negative value of γ zero, forcing all others to be positive. No real system is simple. However, several useful generalizations can be derived and are presented in the following discussions.

THE PRINCIPLE OF GRAVITY STABILIZATION

The most important stabilizing mechanism is gravity segregation. The function g_1 in Eq. 4 is positive when gravity is dominant, but it becomes negative when gravity is subordinate to viscous forces. Thus, it measures the relative importance of gravity. This assumes "normal" solvent-oil density, viscosity and displacement conditions. Gravity stabilization can be achieved by controlling rate.

THE MINIMUM-SLUG-SIZE PRINCIPLE

The stability limit is marked by $\gamma = 0$. This same condition defines the minimum solvent slug for stable displacement. Take the simple example in which concentration is independent of z and make the assumption that α is negligible. Inserting these conditions together with $\gamma = 0$ and re-arranging terms in Eq. 3,

$$\frac{\partial \bar{c}^*}{\partial x} = \frac{(\beta^2 + n^2\pi^2)D_3}{u_0 L^2 g_1} \ldots\ldots\ldots (5)$$

The asterisk indicates a critical, or limiting, relationship. Stability results whenever either one of the following occurs.

1. g_1 is positive and (a) the concentration gradient has any negative value or (b) the concentration gradient has a positive value no larger than that indicated by Eq. 5.

2. g_1 is negative and (a) the concentration gradient has any positive value or (b) the concentration gradient has a negative value no larger in magnitude (no more negative) than indicated by Eq. 5.

While a solvent slug should be kept small, at high rates stability and an abrupt change from oil to solvent may be incompatible.[6] Maximum gradients for a given rate will depend on system properties.

SOURCES OF REQUIRED DATA

Most information required to apply Eqs. 3 through 5 is readily obtained. Although the dispersion coefficients D_1 and D_3 are new parameters, measurement techniques have been developed.[3,7-9] These coefficients characterize the mixing capability of a porous medium in much the same way that permeability denotes flow capacity. Because at very low rates the lateral dispersion process will reduce to molecular diffusion, these coefficients must be measured under appropriate experimental conditions.

The remaining new parameters arise from the Fourier series representation of possible disturbances in solvent concentration. They are denoted by the letters α, β and n. As shown by Eq. 1, these parameters reflect the scale, or "wave length", of disturbances propagated as a result of inhomogeneity in reservoir properties. The principal cause would be permeability inhomogeneity. Means for proper determination of α, β and n will require research into the variation characteristic of porous media. Such studies have yet to be made.

From theory,[1] however, together with even cursory observation of natural oil-reservoir rocks, we can draw several useful conclusions. The first is that very frequently α, and perhaps also β, can be neglected. The most important quantity is n. It must be an integer and must be greater than or equal to one. Thus, conservative practice would dictate the values $\alpha = 0$, $\beta = 0$ and $n = 1$ when estimates must be used.

Before assuming that this crude approach will always be necessary, consider possible sources of information. What we require is a measure of the greatest distance between successive extreme values of permeability characteristic of the formation. In the vertical direction, for example, suppose that permeability maxima occur (at most) each L' units apart. Then, it is reasonable to expect the fundamental component of a resulting disturbance to be periodic with the approximate interval L'. That is, we expect that it will contain as its long wave-length Fourier component of appreciable amplitude a term with $n \approx 2L/L'$. One source of such characteristic maxima might be well logs that have been properly interpreted. Certainly this should be true for n because it is characteristic of vertical variation. It is fortunate that precise values of α

and β would seem to be much less important.

USE OF STABILITY THEORY WITH LINEAR FLOW

Symmetry makes it possible to treat many reservoir problems and laboratory core flood problems as if the flow were one-dimensional. For this reason we will discuss in some detail an example long-core flood. The discussion shows how stability theory can be used to optimize solvent recovery of oil. It leads to results applicable to a variety of practical problems. Later discussion will cover the more complex multi-dimensional cases.

STABILITY IN A LONG-CORE FLOOD

The fluid and rock properties to be used in example calculations are given in Table 1. Density and viscosity depend on the composition of the single hydrocarbon phase. The relationships are conveniently given as empirical equations. Fractional solvent concentration is $\bar{c}$, while fractional concentration of dissolved gas is denoted by $\bar{c}_g$. By difference, the remaining material is oil. Values for the dispersion coefficients based on experiment are given in Table 1. Other materials and other flow conditions could require different values.

As an example problem, we consider flow through a long, square-cut core about 2 in. on a side and positioned with a 10° dip. The core has been flooded with solvent for 40 days at a frontal advance rate of about 1 ft/day. The flood is also assumed to have been started by an abrupt change to solvent, as shown by the input curve in Fig. 1 (Curve A). If flow is linear and stable so that no fingering occurs, concentrations will be uniform across any section of the core. Thus, it is convenient to picture the result by means of a solvent concentration profile, as if solvent could be separately observed within the system. For this case, the concentration profile should look like Curve B in Fig. 1 after traveling 40 ft. This profile is defined by the equation,

$$\bar{c} = \tfrac{1}{2}\,\mathrm{erfc}\left[\frac{x - u_0 t}{2\sqrt{D_1 t}}\right] \qquad (6)$$

in which a negligible term has been dropped.[1]

The first question to be answered is whether or not such a flood should be stable. Using solvent concentration data from Fig. 1, dimensionless stability coefficient values such as those from Eq. 3

TABLE 1 – PROPERTIES FOR EXAMPLE CALCULATIONS

Linear Flow

t for $\bar{c} = 3.46 \times 10^6$ seconds	($t \approx 40$ days)
D_1	$= 0.375\ u_0$ cm²/sec
D_3	$= 0.0375\ u_0$ cm²/sec
u_0	$= 3.47 \times 10^{-4}$ cm/sec ($u_0 \approx 1$ ft/day)
L	= 5 cm ($L \approx 2$ in.)
k	= 0.87 darcies
μ	$= 10 \exp(-3\bar{c} - 6.3\bar{c}_g)$ cp
ρg	$= (8 - 2.9\bar{c} - 7.3\bar{c}_g) \times 10^{-4}$ atm/cm
θ	$= -10^0$
ϕ	= 0.25

Two-Dimensional Flow

As Above Except:

t	$= 1.38 \times 10^8$ sec ($t \approx 1{,}600$ days)
L	= 305 cm ($L \approx 10$ ft)

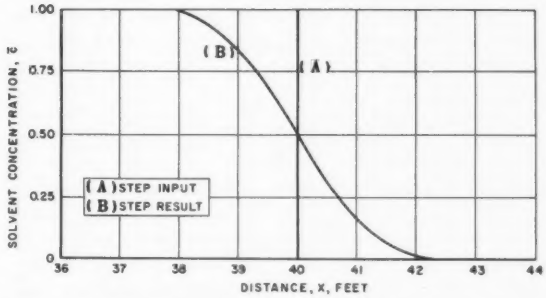

FIG. 1 – CONCENTRATION PROFILE, LONG-CORE EXAMPLE.

are plotted in Fig. 2 for three different, long wavelength disturbances. Instability is indicated over a considerable concentration range in each case, as shown by negative values of the coefficient γ. The results imply a substantial space region within which such disturbances can grow. Because natural core properties always are such as to initiate small disturbances, it is doubtful that displacement could have occurred as shown by Fig. 1. A more likely sequence would be initial instability followed by viscous fingering and, finally, a larger mixing zone than that shown.

GRAVITY STABILIZED MINIMUM SOLVENT SLUG

The hypothetical core flood just described can be modified to make use of gravity stabilization. Suppose conditions are maintained such that the function g_1 (Eq. 4) is positive. Then by Eq. 5, the concentration gradient can be made as steep as we like. To see what is required to accomplish this, Fig. 3 shows g_1 as a function of concentration $\bar{c}$ for possible flood rates u_0.

Since gravity stabilization requires that g_1 be positive for all $\bar{c}$, the limiting value is obtained at $\bar{c} = 0$ where fluid viscosity is greatest and the response to gravity is least. Thus, a critical rate for gravity stabilization is defined by setting $g_1 = 0$ and maximizing $\bar{\mu}$. The result is

$$u_g^* = -\frac{k}{\bar{\mu}}\frac{d\rho}{dc}\left[\frac{d\ \ln\ \mu}{dc}\right]^{-1}\frac{g\ \sin\ \theta}{\phi} \qquad (7)$$

For the example data, u_g^* (Curve 4 of Fig. 3) corresponds to 0.017 ft/day. At or below this very low rate, complete gravity stabilization is possible with no reliance on dispersion. The rate is low enough for the dispersion mechanism to become molecular diffusion, but a result similar to Curve B of Fig. 1 would be obtained.

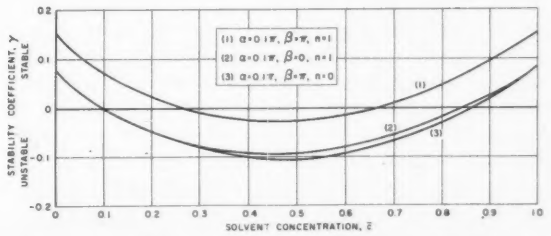

FIG. 2 – EXAMPLE STABILITY COEFFICIENTS (γ) FOR LONG-CORE FLOOD.

An elementary treatment of this kind of problem considers the entire mixing zone as a kind of "interface" region. This suggests as a condition for stability

$$u = -k \frac{\Delta(\rho g)}{\Delta \mu} \frac{\sin \theta}{\phi} \quad \ldots\ldots\ldots\ldots\ldots\ldots (8)$$

where Δ represents total change in the quantity across the interface. Eq. 8 is the limiting finite-difference form of Eq. 7 and represents a kind of average behavior through the interface. Used with the example data, Eq. 8 suggests a limiting rate of 0.053 ft/day. Unfortunately, correct use of Eq. 8 requires that mixing-zone thickness be negligible. Because a mixed region forms almost immediately, only the more restrictive Eq. 7 is appropriate.

FORMATION OF A MINIMUM-SOLVENT SLUG

The preceding discussion showed how gravity could be used to stabilize displacement. Because such low flow rates are required, the process is unlikely to prove practical. The present section will show how to form a slug containing minimum solvent, yet in such a manner that flow will be stable at some pre-selected rate. The results apply to linear flow. To do this requires a somewhat novel approach – the use of a gradual change in properties of the injected fluid rather than an abrupt change from one fluid to another.[6] In addition, it is necessary to consider the complete problem in which gas displaces solvent, which in turn recovers oil. Thus, the complete definitions of viscosity and density in Table 1 are required. The symbol $\bar{c}_g$ is used for fractional gas concentration.

The principles are as follows. Flow behavior is single-phase and the mixing mechanism is dispersion provided (1) all fluid compositions remain in the miscible region, and (2) stability conditions are satisfied. Formation of a solvent slug which will satisfy these criteria involves three steps: (1) finding the maximum rates of change of solvent concentration consistent with stability for the specified conditions and, thus, the way in which solvent-oil and gas-solvent transition zones are to be injected; (2) finding how much pure solvent must be injected between transition zones to make certain that dispersion mixing does not lead to immiscibility; and (3) finding out how much the rate can be increased as the solvent slug travels and stability criteria become less restrictive. These steps are illustrated by an example.

Step 1

The first step is to establish maximum concentration gradients consistent with stability. This can be done by applying Eq. 5 separately to solvent-oil and gas-solvent transition zones. The results specify just what the "shape" of the injected concentration profile must be. We use the core and fluid properties in Table 1 and a displacement rate of 1 ft/day. To obtain the required data, note the following equivalence.

$$\frac{\partial \bar{c}^*}{\partial x} = -\frac{1}{u_0} \frac{\partial \bar{c}^*}{\partial t} \quad \ldots\ldots\ldots\ldots\ldots\ldots\ldots\ldots (9)$$

which, combined with Eq. 5, gives on integration

$$t^* = -\int_{\bar{c}_i^*}^{\bar{c}^*} \frac{L^2 g_1 d\bar{c}}{(\beta^2 + n^2\pi^2)D_3} + t_i^* \quad \ldots\ldots (10)$$

If a concentration $\bar{c}_i^*$ is being injected at the initial time t_i^*, Eq. 10 tells what concentration $\bar{c}^*$ must be injected at any subsequent time t^* to keep the solvent slug stable but as small as possible.

Eq. 10 is used first to construct the leading transition zone by which solvent is to displace oil. The conservative values $\beta = 0$ and $n = 1$ can be used for the perturbation properties. Eq. 4 defines the function g_1 which depends on both density and viscosity. To compute these functions, note that $\bar{c}_g = 0$ at this leading part of the transition zone. It is convenient to measure time t^* relative to a time $t_i^* = 0$ for which $\bar{c}_i^* = 0$. In this way we arrive at the solvent-oil injection profile $\bar{c}_a^*$ shown in Fig. 4 as a function of time. A backward time scale is used, listing time after start of injection. Thus, the profile appears the same as it would if we were able to observe it within the core.

Construction of the trailing transition zone where gas displaces solvent is handled similarly. In this case $\bar{c}_g = 1 - \bar{c}$, a condition which denotes no oil present. Thus, the function g_1 has different numerical values at the trailing edge. Using Eq. 10 once again but with the new data, the shape of the gas-solvent transition zone $\bar{c}_c^*$ is as shown in Fig. 5. A convenient starting point for the calculation is $\bar{c}_i^* = 1$ at $t_i^* = 0$.

The curve calculated from Eq. 10 at the trailing edge of the slug gives the same t^* value for two different concentrations. This occurs because the permissible gradient becomes infinite at a concentration just below $\bar{c}_c^* = 0.8$. When solvent concentrations fall below this point, the mixture becomes gravity stabilized. Solvent is minimized by abrupt termination of the slug, following the solid curve. The dashed extension giving double values in Fig. 5 merely shows what the limiting behavior would be if the gas-solvent positions in the system were reversed.

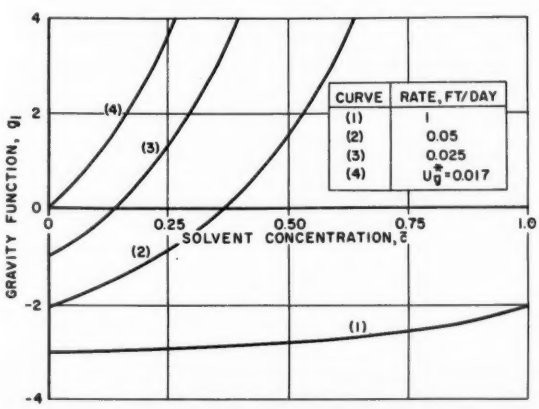

FIG. 3 – GRAVITY FUNCTION (g_1) FOR LONG-CORE FLOOD.

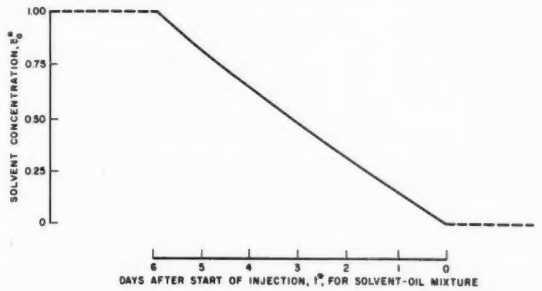

FIG. 4 – STABLE SOLVENT-OIL TRANSITION ZONE, LONG-CORE FLOOD.

Step 2

The second step is to find a way to form a slug that includes the stable transition zones, and that will not separate into two fluid phases at some later stage. The method is trial-and-error solution of a dispersion problem. Phase behavior is assumed to be known as a function of $\bar{c}$ and $\bar{c}_g$. (Note that the flow equations were written in terms of volume fractions, not mole fractions).

We start by visualizing the two transition zones separated by an unknown amount of gas- and oil-free solvent. The transition zones are shaped as noted under Step 1. These zones are conveniently labelled as $\bar{c}_a^*$ for the solvent-oil transition, $\bar{c}_b^*$ for plain solvent and $\bar{c}_c^*$ for the final gas-solvent transition. Each $\bar{c}^*$ will be a function $\bar{c}^*(\tau)$ of time τ. The time t_1 required to inject the solvent-oil transition zone $\bar{c}_a^*$ is known (Fig. 4), as is the time difference $t_3 - t_2$ for the final gas-solvent transition $\bar{c}_c^*$ (Fig. 5). The problem is to find the unknown time interval $t_2 - t_1$, during which plain solvent must be injected to prevent two-phase behavior at some later time.

When these fractions of the total solvent requirement are put together into a single injection program, the solvent concentration at any later time t and a distance x into the system will be given by

$$\bar{c}(x,t) = \int_0^{t_1} \bar{c}_a^*(\tau)F(\tau)d\tau + \int_{t_2}^{t_3} \bar{c}_c^*(\tau - t_2)F(\tau)d\tau + \tfrac{1}{2}\,\mathrm{erfc}\left[\frac{x - u_0(t-t_1)}{2\sqrt{D_1(t-t_1)}}\right] - \tfrac{1}{2}\,\mathrm{erfc}\left[\frac{x - u_0(t-t_2)}{2\sqrt{D_1(t-t_2)}}\right] \quad \ldots\ldots(11)$$

Negligible terms have been dropped from Eq. 11. The functions $\bar{c}_a^*(\tau)$ and $\bar{c}_c^*(\tau - t_2)$ are the transition zones as shown in Figs. 4 and 5. These are given implicitly by Eq. 10 as indicated under Step 1. The time variable τ is a dummy integration variable, and the function $F(\tau)$ is

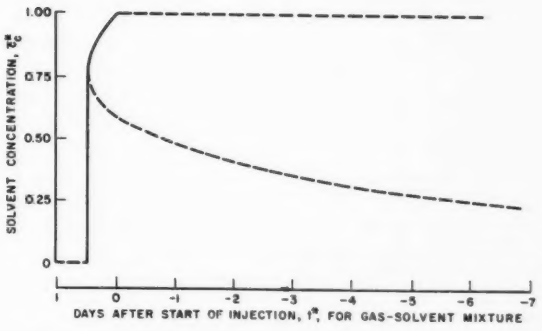

FIG. 5 – STABLE GAS-SOLVENT TRANSITION ZONE, LONG-CORE FLOOD.

$$F(\tau) = \left\{\frac{[x + u_0(t-\tau)]}{4\sqrt{\pi D_1}\,(t-\tau)^{3/2}}\right\} \exp\left\{-\left[\frac{x - u_0(t-\tau)}{2\sqrt{D_1(t-\tau)}}\right]^2\right\} \quad \ldots\ldots(12)$$

In a similar way, gas concentration is given by the following equation.

$$\bar{c}_g(x,t) = \tfrac{1}{2}\,\mathrm{erfc}\left[\frac{x - u_0(t-t_2)}{2\sqrt{D_1(t-t_2)}}\right] - \int_{t_2}^{t_3} \bar{c}_c^*(\tau - t_2)F(\tau)d\tau \quad \ldots\ldots(13)$$

Oil can be obtained by difference because the sum of all fractional concentrations must be one.

Starting with any reasonable estimate for the time t_2, trial-and-error procedures will lead to a solution. For example, let t be the time required for the flood to progress through the entire system. Using a trial value of t_2, compute $\bar{c}$ and $\bar{c}_g$ for a number of positions x. If all $\bar{c}$ and $\bar{c}_g$ values correspond to a single fluid phase, the trial t_2 overestimated the amount of solvent needed. A smaller t_2 should then be used. On the other hand, the data could indicate that two fluid phases would be present at some point in the system. This shows a need for more solvent and a larger value of t_2. The final time difference that proves satisfactory, $t_2 - t_1$, will indicate the shortest time for which plain solvent can be injected between leading and trailing transition zones while maintaining single-phase behavior throughout displacement. The result, $t_2 - t_1 = 0$, can be a correct answer for this problem and often may be a useful starting value for t_2.

Phase behavior for the example system is indicated by the data in Table 2. These data lead to the injection profile of Fig. 6 (Part A) that will remain both stable and in a single fluid phase while traveling 40 ft through the example long-core system. This profile contains less than 8 per cent of a pore volume of solvent. The appearance of the

profile after traveling 40 ft is shown by Part B of Fig. 6. Just a trace of oil in the gas-solvent transition region is enough to reach the miscibility limit. Everywhere except at the single indicated point the mixture is safely within the single-phase region, even though no region of pure solvent remains.

Step 3

The final step is to see how much, if any, flow rate can be increased with time. As the flood progresses, dispersion spreads out the solvent bank. Smaller concentration gradients should permit higher rates. The appropriate generalization of Eq. 7 for the critical rate becomes the minimum positive value of

$$u^* = \left\{ \frac{k}{\bar{\mu}} \frac{g \sin\theta}{\phi} \left[\frac{\partial \rho}{\partial \bar{c}} \frac{\partial \bar{c}}{\partial x} + \frac{\partial \rho}{\partial \bar{c}_g} \frac{\partial \bar{c}_g}{\partial x} \right] \right\} \left\{ \frac{D_3}{u^* L^2} [\beta^2 + n^2\pi^2] - \left[\frac{\partial \ln \mu}{\partial \bar{c}} \frac{\partial \bar{c}}{\partial x} + \frac{\partial \ln \mu}{\partial \bar{c}_g} \frac{\partial \bar{c}_g}{\partial x} \right] \right\}^{-1} \quad \ldots\ldots (14)$$

Eq. 14 includes the assumption that $\alpha = 0$ and is valid for one-dimensional flow. It allows for the effect of dispersion in stabilization, which is an addition to Eq. 7, and also allows for a three-component fluid.

The function u^* from Eq. 14 for the slug profile of Fig. 6 at 40 ft is plotted in Fig. 7. Because u^* is a limit function, Eq. 14 gives the limiting rates (from a possibly large range of rates as shown in Fig. 7) for which the displacement is stable. Thus, the shaded areas represent rates for which the corresponding part of the profile of Fig. 6 (Part B) is stable. As shown in Figs. 6 and 7, the critical rate is determined near the leading edge of the solvent bank. This is the smallest positive value of u^* obtained from Eq. 14, as shown by the data in Fig. 7. Negative rates calculated from Eq. 14 have no meaning. For the example data, the critical rate is about 2 ft/day, and a gradual increase in rate throughout the displacement is possible.

TABLE 2 – LIMITING COMPOSITIONS FOR MISCIBILITY, EXAMPLE THREE-COMPONENT SYSTEM

If $\bar{c}_g$ Is	$\bar{c}$ Must Be ≥	$(1-\bar{c}-\bar{c}_g)$ Must Be ≤
1.00	0	0
0.97	0.0291	0.0009
0.94	0.0582	0.0018
0.92	0.0774	0.0026
0.90	0.0966	0.0034
0.89	0.1062	0.0038
0.88	0.1157	0.0043
0.87	0.1251	0.0049
0.86	0.1344	0.0056
0.85	0.1435	0.0065
0.84	0.1524	0.0076
0.83	0.1611	0.0089
0.82	0.1695	0.0105
0.81	0.1777	0.0123
0.80	0.1854	0.0146

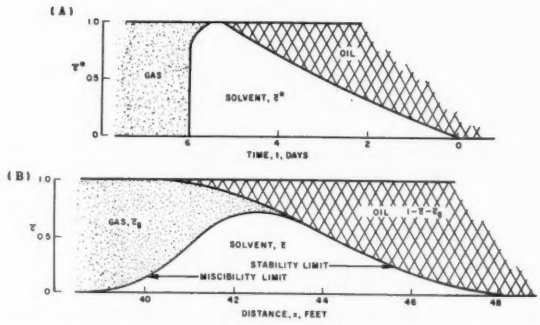

FIG. 6 – (A) MINIMUM SLUG INJECTION PROFILE AND (B) RESULTING PROFILE AT 40 FT, LONG-CORE FLOOD.

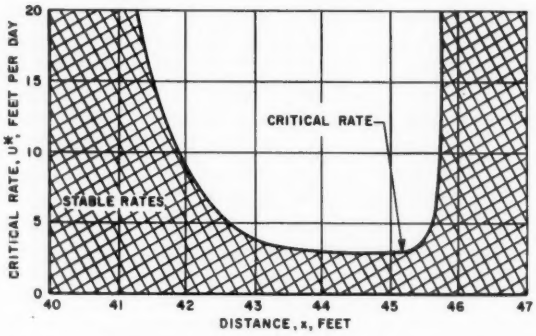

FIG. 7 – CRITICAL RATES FOR THE PROFILE OF FIG. 6 (PART B).

USE OF STABILITY THEORY WITH TWO-DIMENSIONAL FLOW

A mathematical solution to the problem of two-dimensional, stable displacement behavior has been obtained [1] for a set of reasonable assumptions. The present section of this paper shows an example result which makes use of this solution. The example reservoir is linear, 10-ft thick and has a 10° dip. The flood rate is 1 ft/day. Other properties are given in Table 1. While profiles are useful in depicting one-dimensional flow behavior, two-dimensional flow is best illustrated as a solvent concentration "wave". Any cross section through the wave then gives a concentration profile. If fingering did not occur, therefore, the advancing solvent can be pictured as the wave shown in Fig. 8. Fig. 8 is an oblique view illustrating the shape of the wave after it travels 1,600 ft. Concentration is plotted along the vertical axis. The positive x-direction is to the right and the positive z-direction into the page; thus, the view is the same as if the reservoir were tipped on its side. For clarity, z-distances are also magnified relative to x-distances. Concentration profiles parallel to the direction of flow are given for distances of 0, 2.5, 5, 7.5 and 10 ft above the lower reservoir boundary.

Similar calculations reveal that, at the short distance of 100 ft, lateral dispersion has had almost no effect at all. The effect gradually increases, until at 6,400 ft the solvent wave is completely

smeared out in the (vertical) z-direction. As shown in Fig. 8, some segregation persists at 1,600 ft. The regions stable to a $\cos \pi y \cos \pi z$ disturbance are cross-hatched in Fig. 8. These exclude large regions of intermediate concentration with high concentration gradients in the x-direction. The steepest gradients in the z-direction occur near the center of the system. Here the stabilizing influence of gravity is felt most strongly, and the thickness of the unstable region is reduced to a minimum.

It is unlikely that displacement could occur without fingering when unstable regions persist as shown by Fig. 8. The perturbation considered has a wave length of 2 ft. This is equivalent to considering the example 10-ft section of reservoir as if it were made up from a stack of similar 2-ft thick sections. Within this stack, similar inhomogeneities would be (at most) 2-ft apart. Although each geologic formation must have its own pattern of variability, such values would seem to be reasonable for many natural oil-reservoir rocks. We conclude that, for stability and for maximum efficiency, the flood described above should have been conducted under more restrictive conditions. A relatively high oil viscosity of 10 cp was included in the assumptions for this example, however. A more suitable reservoir would contain lower viscosity oil. For example, with 2-cp oil and no change in the other properties, displacement would be stable except during an early period of high concentration gradients. Provided initial problems could be overcome, efficient displacement would become practical.

SIMPLIFIED METHODS FOR USE OF THEORETICAL RESULTS

The principles outlined in the preceding sections can be applied to any reservoir problem, no matter how complex the flow pattern may be. A more exact theory could have been developed by starting from a more detailed mathematical picture of flow within an imperfect system. This would add complexity, however, and does not at present appear justified. Economics will usually dictate just how detailed a useful theory should be. For some purposes it would seem that even simpler methods than those presented could be adopted; therefore, we will discuss several useful simplifications.

EQUIVALENT LINEAR SYSTEM

Whatever the detailed pattern of a field-scale flood, a useful approximation is as an equivalent rectangular system in which flow is linear. That is, rows of injection wells and production wells are replaced by lines drawn to connect members of a row across the system. The distance between injection and production lines drawn in this way then is chosen to represent the path length along which dispersion mixing will occur. Thus, the mathematical problem is reduced in crude fashion by one dimension, and the methods presented herein become applicable. Growth of the transition zone during stable flow is related approximately to the square root of the distance traveled. Thus, to minimize solvent requirement, a single slug should be made to travel the entire length of a long and narrow system.

EXTENDED "RECTANGULAR" SLUG

Although the concept of the injection of a solvent gradient is sound, many practical problems are involved. These may make further consideration of abrupt injection of solvent worthwhile. Fingering is almost certain to follow such an abrupt change and

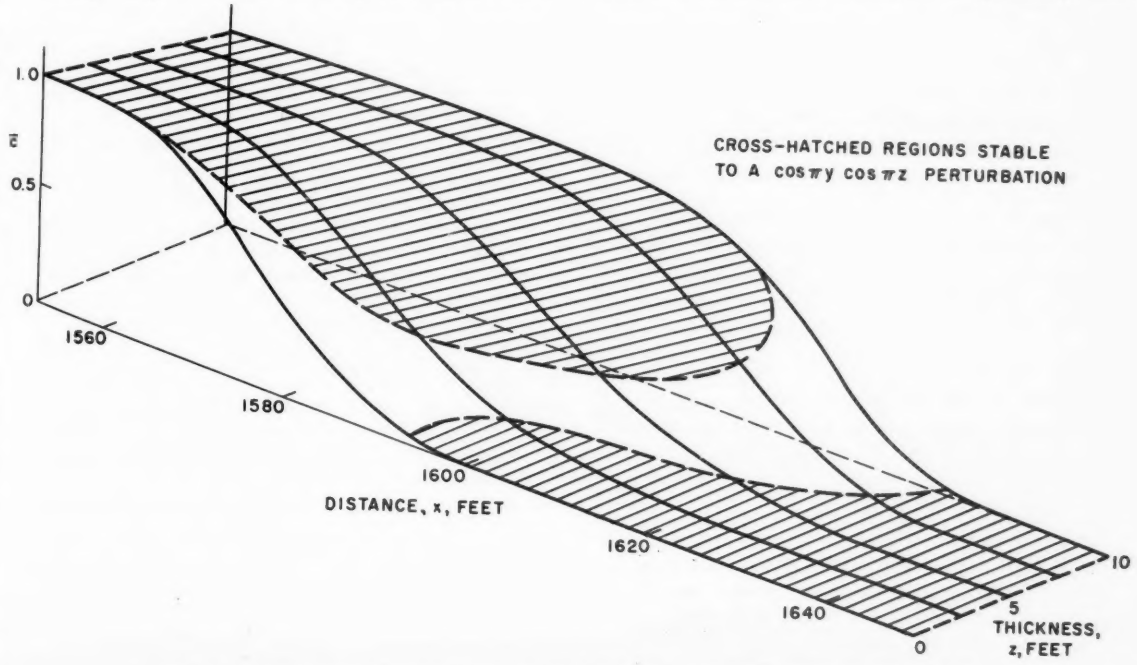

FIG. 8 – CONCENTRATION PROFILES AT 1,600 FT, TWO-DIMENSIONAL EXAMPLE.

will increase the solvent requirement. The question is, how much should such an excess be?

The first step toward a useful approximate answer is to compute the time required to inject a minimum-solvent transition zone, as given by Eq. 10. In place of the gradient, however, plain solvent is to be injected for the same total length of time. Thus, the solvent injection profile becomes rectangular in shape and contains a solvent excess that depends in an appropriate way on the degree of instability. This makes a reasonable allowance for instability. Miscibility calculations for a rectangular slug with stable flow become particularly simple. If fingering ensues, however, the computed results could be in serious error. The excess solvent injected because of instability will be lost. A proper way to approximate the extended slug requirement is as follows.

Step 1

When the injected concentration profile is rectangular in shape and dispersion is the mixing mechanism, solvent and gas concentration equations reduce to

$$\bar{c} = \tfrac{1}{2}\,\mathrm{erfc}\left[\frac{x-u_0 t}{2\sqrt{D_1\, t}}\right] - \tfrac{1}{2}\,\mathrm{erfc}\left[\frac{x-u_0(t-t')}{2\sqrt{D_1\,(t-t')}}\right] \quad \ldots\ldots\ldots (15)$$

$$\bar{c}_g = \tfrac{1}{2}\,\mathrm{erfc}\left[\frac{x-u_0(t-t')}{2\sqrt{D_1\,(t-t')}}\right] \quad \ldots\ldots\ldots (16)$$

The first step is to compute $\bar{c}$ and $\bar{c}_g$ using Eqs. 15 and 16 for various positions x within the transition zone. The time t' is the time for which plain solvent is assumed to have been injected. Trial-and-error procedures are used to find the smallest time t' for which all portions of the solvent slug will remain miscible until it has reached the end of the system.

Step 2

Compute from Eq. 10 the total time required to inject a stable solvent-oil transition zone. Repeat the computation to find the time to inject a gas-solvent transition zone. The function g_1 will differ for the two computations.

Step 3

Take one-half the sum of the transition-zone times from Step 2 and add this to the minimum time t' found under Step 1. The total is the estimated time during which solvent alone should be injected to form an extended rectangular slug. It includes an allowance for instability.

GRAVITY SEGREGATION

The two-dimensional result in Fig. 8 shows the behavior of a stable concentration wave after it has traveled a substantial distance. During earlier stages, a large amount of "extra" solvent appears necessary because of gravity segregation. For the example data at a distance of 6,400 ft, however, the profile proved nearly uniform in cross section. In addition, it was spread out in the direction of flow little more than it would have been had true one-dimensional flow and dispersion prevailed.

We conclude that no allowance for gravity segregation is required when a solvent bank is to travel as much as 1,000 times the bed thickness. In such cases the problem can be reduced to one dimension. This does not apply to shorter, thicker systems for which solvent may tend to override the oil. These require detailed study.

CONCLUSIONS

A theory of stability in miscible displacement of oil by a solvent has been presented. Application of the theory leads to the definition of limiting conditions for stable miscible displacement, such as a minimum slug size. The criteria that must be satisfied are miscibility and stability. Stability means that no viscous fingering will occur and that mixing will be caused only by dispersion. Miscibility means that complete recovery in the swept regions will be obtained. Thus, for any specified set of reservoir conditions an optimum use of solvent is defined.

ACKNOWLEDGMENT

This paper is an outgrowth of a paper[2] presented in 1959 at the AIChE-SPE Joint Symposium in San Francisco. The author prepared the Symposium paper while associated with the California Research Corp., La Habra, Calif.

REFERENCES

1. Perrine, R. L.: "The Development of Stability Theory for Miscible Liquid-Liquid Displacement", *Soc. Pet. Eng. Jour.* (March, 1961) 17.
2. Perrine, R. L.: "Conditional Instability in Miscible Liquid-Liquid Displacement", Preprint No. 42 presented at the AIChE-SPE Joint Symposium in San Francisco (Dec. 6-9, 1959).
3. Blackwell, R. J.: "Laboratory Studies of Microscopic Dispersion Phenomena in Porous Media", Preprint No. 29 presented at the AIChE-SPE Joint Symposium in San Francisco (Dec. 6-9, 1959).
4. de Jong, G. de Josselin: *Trans.*, Am. Geophys. Union (Feb., 1958) Vol. 39, 67.
5. Saffman, P. G.: *Jour. Fluid Mech.* (Oct. 1959) Vol. 6, 321.
6. Weinaug, C. F. and Ling, D.: U. S. Patent No. 2,867,277 (Jan. 6, 1959).
7. von Rosenberg, D. U.: *AIChE Jour.* (March, 1956) Vol. 2, 55.
8. Day, P. R.: *Trans.*, Am. Geophys. Union (1956) Vol. 37, 595.
9. Blackwell, R. J., Rayne, J. R. and Terry, W. M.: "Factors Influencing the Efficiency of Miscible Displacement", *Trans.*, AIME (1959) Vol. 216, 1. ***

The Development of Stability Theory for Miscible Liquid-Liquid Displacement

RICHARD L. PERRINE
MEMBER AIME

U. OF CALIFORNIA AT LOS ANGELES
LOS ANGELES, CALIF.

ABSTRACT

A stability theory is developed for miscible liquid-liquid displacement within a porous medium. In the usual case considered, a high-density high-viscosity "oil" is displaced downdip by a low-density low-viscosity "solvent". Perturbation methods are used to find the conditions under which the spreading mechanism changes from the stable dispersion process to unstable viscous fingering. We find that instability is conditional, that there is a dependence on the shape of a disturbance leading to a "diameter" effect and that very difficult experimental scaling problems may result. A useful consequence is the definition of a minimum "slug size" for stable miscible displacement. This should make possible optimum use of the solvent process for oil recovery. The results may apply to many situations in which one fluid displaces another of somewhat different fluid properties within a porous medium.

INTRODUCTION

The process of miscible liquid-liquid displacement looked very favorable when it first received serious consideration as a means to increase petroleum recovery. Some early laboratory results were interpreted to mean that only a small "slug" of solvent was needed, perhaps 2 to 3 per cent of a hydrocarbon pore volume. This "slug" could recover the oil in an entire reservoir provided the fluids remained miscible.[1,2] Only a slow growth of the "mixing zone", or gradual transition from oil to solvent, should occur. This would follow naturally from mixing by a dispersion mechanism such as that described by Scheidegger.[3] And, indeed, laboratory cores have shown this kind of behavior provided solvent viscosity was at least as great as that of the oil.[2,4-6] The same kind of behavior has also been observed with solvent viscosity lower than that of the oil after the distance traversed became large. Not all laboratory results have been this favorable, however.[7-9] Mixing zone growth may become proportional to the distance traveled rather than the square root of this quantity. Such behavior accompanies high rates in short systems of large diameter, provided the viscosity ratio is adverse. If this more rapid spreading were to persist in a reservoir, the solvent requirement for miscible "slug" displacement could exceed 30 per cent of a pore volume. There is considerable economic importance in the difference between 3 and 30 per cent solvent.

A logical conclusion is that two different kinds of flow behavior are possible, with each kind leading to a different result. One kind gives efficient displacement, the other does not. In the efficient case, the solvent bank spreads out only by the mechanism we have termed dispersion. Under these conditions, displacement is as near piston-like as possible. In the second kind of flow, found only with adverse viscosity ratios, viscous fingering occurs. That is, permeability variations cause a small finger of low-viscosity solvent-rich fluid to move ahead of its average position within the mixing zone. This creates a path of low resistance to flow, and an even greater amount of solvent-rich fluid follows. Thus, the process is autocatalytic. Once started, the fingering mechanism rapidly becomes dominant.

The question to be answered is this. Under what conditions will each of these two different kinds of flow occur? In particular, what conditions denote the transition from dispersion to viscous fingering as the solvent spreading mechanism? The answer may tell us whether or not the desirable, near piston-like miscible displacement process is practical. An answer to this problem can be obtained from theory by the use of perturbation methods. The procedure is as follows. We first formulate a mathematical representation of the system. Then a small disturbance (or perturbation) in solvent concentration profile is introduced and observed to see what happens. Unstable flow is indicated when a small disturbance will grow larger. This will lead to eventual viscous fingering. If on the other hand the disturbance dies out, the displacement is stable. In this latter case, with dispersion as the spreading mechanism, near piston-like displacement is possible.

Thus, this paper presents the development of a stability theory for miscible liquid-liquid displace-

Original manuscript received in Society of Petroleum Engineers office May 23, 1960. Revised manuscript received Oct. 27, 1960.

[1]References given at end of paper.

ment. The problem differs from immiscible displacement theory[10] in that no interface between fluids is involved. The results are important because they state the limiting conditions required for efficient, stable miscible displacement of oil by a solvent. Thus, they determine a minimum "slug" size. The results are optimistic to the extent that only small disturbances in an otherwise ideal system are considered. A less ideal system could only lead to less favorable results such as the requirement of additional solvent. When the required conditions prove impractical, the reservoir is not suited to the miscible "slug" process. An alternative recovery method should then be used.

APPLICATION OF PERTURBATION METHODS

Mathematical description of stable miscible displacement involves two transport mechanisms – flow, and what we will term "hydrodynamic dispersion".[3,11-16] While such concepts as flow and diffusion are well understood, dispersion is relatively new. Thus, a brief description is included. The reader is urged to consult the references for thorough, rigorous development.

We consider a system that is semi-infinite in the x-direction, infinite in the y-direction, and bounded at $z' = 0$ and $z' = L$ in the z-direction. The x-axis is rotated to a negative angle θ below the horizontal. Flow is one-dimensional in the positive x-direction, and the respective dispersion coefficients are assumed constant. Fluid density is a linear function of solvent concentration, while viscosity dependence is exponential. Although not necessary, these assumptions give simplicity with little loss in generality. The fluids are assumed incompressible, and the system homogeneous in its properties.

We will use the following notation, where primes indicate actual variables and unprimed quantities their dimensionless equivalents.

$$x = x'/L - u_0 t'/L,\ x_s = x'/L,\ y = y'/L$$

$$z = z'/L,\ t = u_0 t'/L,\ u = u'/u_0,$$

$$v = v'/u_0,\ w = w'/u_0,\ p = kp'/Lu_0\mu_0\phi,$$

$$D_1 = D_1'/Lu_0,\ D_3 = D_2'/Lu_0 = D_3'/Lu_0$$

$$\eta_q = \frac{\partial \eta}{\partial q}\ ,\ \text{etc.}$$

The space co-ordinates, thus, are x, y and z, and t is the time. The linear displacement velocity for stable displacement is u_0, while μ_0 is the fluid viscosity at zero concentration and c is the fractional solvent concentration. Velocities in the x, y and z directions are u, v and w. These velocities are volumetric flow rates per unit cross-sectional area and per unit porosity. P is pressure, k permeability, ρ density, g the acceleration of gravity and ϕ porosity. Dispersion coefficients are denoted by D, and letter subscripts are used to denote partial derivatives.

To help visualize the way in which fluid moves through porous rock, it is convenient to think of the fluid as if it existed in many separate fluid "elements", each bounded by an imaginary surface. Thus, it is possible to discuss the motion of a single element much as if it moved independently of all others. Thinking this way and recognizing that porous materials are homogeneous only in a gross sense, at any time some elements will be moving faster than others. The relative speed will vary with local pore geometry. Thus, of many possible paths leading downstream, some will prove to be much faster on the average than others. An element entering a fast path will travel further in a given period of time than the average of all such elements. But there must also be some slower than average paths. The net result is that a cloud of fluid elements starting out together will become spread out, or dispersed, both in the direction of flow and to the side. A few will end up far downstream, a few will move very little and most will travel at nearly the average rate. This spreading is what is termed dispersion.

The several theoretical treatments of dispersion that have been given[3,11-16] lead to a common result: to a good approximation, the dispersion process is mathematically described by the diffusion equation with constant dispersion coefficients (units of a diffusion coefficient). Dispersion coefficients in the direction of flow (axial) and at right angles (lateral) may differ substantially.[15-17] At some low rate, the dispersion process necessarily reduces to molecular diffusion. Thus, the description of stable miscible displacement requires a diffusion-type equation for solvent continuity, an equation for continuity of velocity and Darcy's law for the equations of motion. In terms of the stationary dimensionless co-ordinates (x_s), these become

$$c_t - D_1 c_{xx} - D_3 c_{yy} - D_3 c_{zz} + uc_x + vc_y + wc_z = 0 \quad \text{.....(1.1)}$$

$$u_x + v_y + w_z = 0 \quad \text{.....(1.2)}$$

$$u + (\mu_0/\mu)p_x + (k\rho g \sin\theta)/u_0\mu\phi = 0 \quad \text{..... (1.3)}$$

$$v + (\mu_0/\mu)p_y = 0 \quad \text{..... (1.4)}$$

$$w + (\mu_0/\mu)p_z + (k\rho g \cos\theta)/u_0\mu\phi = 0 \quad \text{..... (1.5)}$$

DEVELOPMENT OF PERTURBATION EQUATIONS

There are two kinds of displacement – stable and unstable – so that we are led to ask the following question. Which kind of flow is more likely to occur, and under what conditions? Mathematically, the problem can be stated this way. Suppose there is a quantity $\bar{c}$ which represents solvent concentration for stable flow. It is a solution of Eqs. 1.1 through 1.5. Suppose also that the actual sol-

vent concentration c differs just slightly from the barred quantity. Will c then change toward $\bar{c}$ or away from it?

This problem can be pictured for a hypothetical system by drawing contours along which concentration remains constant. Fig. 1 shows such a visualization for a two-dimensional system. Initially, all contours parallel the z-axis in an ideal system, as shown in Part A. This corresponds to stable behavior. A more natural kind of behavior is shown in Part B of Fig. 1. Rather than being straight, the contours contain small disturbances, or perturbations, such as would result from the normal variation of properties within a real system. When instability occurs, any small disturbances (as in Part B) may grow and acquire a finger-like shape. This result is what is shown in Part C.

Thus, the dependent variables in a real system (including small perturbations) are denoted by a set of equations of the form given by Eq. 2.[18]

$$\eta = \bar{\eta} + \epsilon\eta^{(1)} + \epsilon^2\eta^{(2)} + \cdots,$$

$$\eta = c,\ u,\ v,\ w,\ p \qquad \text{..... (2.0)}$$

Each barred quantity represents a stable displacement result, such as is shown in Part A of Fig. 1. These are solutions of Eq. 1.1 through 1.5. The remainder of Eq. 2 represents the perturbation. If Eq. 2 is also to be a solution of the equations of Eq. 1 with an arbitrary small ϵ, after substitution the coefficients of ϵ^n must vanish separately for each n. Thus, from the coefficients of $\epsilon^1 = \epsilon$, we obtain the first-order perturbation equations.

$$c_t^{(1)} - D_1 c_{xx}^{(1)} - D_3 c_{yy}^{(1)} - D_3 c_{zz}^{(1)} + \bar{u}c_x^{(1)} + \bar{v}c_y^{(1)} + \bar{w}c_z^{(1)} + \bar{c}_x u^{(1)} + \bar{c}_y v^{(1)} + \bar{c}_z w^{(1)} = 0 \qquad \text{.....(3.1)}$$

$$u_x^{(1)} + v_y^{(1)} + w_z^{(1)} = 0 \qquad \text{.....(3.2)}$$

$$u^{(1)} + \frac{\mu_0}{\bar{\mu}} p_x^{(1)} + \left[\frac{kg}{\bar{\mu}u_0} \frac{d\rho}{dc} \frac{\sin\theta}{\phi} + \bar{u} \frac{d \ln \mu}{dc} \right] c^{(1)} = 0 \qquad \text{.....(3.3)}$$

$$v^{(1)} + \frac{\mu_0}{\bar{\mu}} p_y^{(1)} + \left[\bar{v} \frac{d \ln \mu}{dc} \right] c^{(1)} = 0 \qquad \text{..... (3.4)}$$

$$w^{(1)} + \frac{\mu_0}{\bar{\mu}} p_z^{(1)} + \left[\frac{kg}{\bar{\mu}u_0} \frac{d\rho}{dc} \frac{\cos\theta}{\phi} + \bar{w} \frac{d \ln \mu}{dc} \right] c^{(1)} = 0 \qquad \text{.....(3.5)}$$

The dispersion coefficients D_1 and D_3 are considered to be unaffected by the perturbation. This is not strictly correct because they depend on the displacement velocity. For cases of interest, however, flux by dispersion is a small fraction of the total. We considerably simplify the problem by this neglect of a second-order effect.

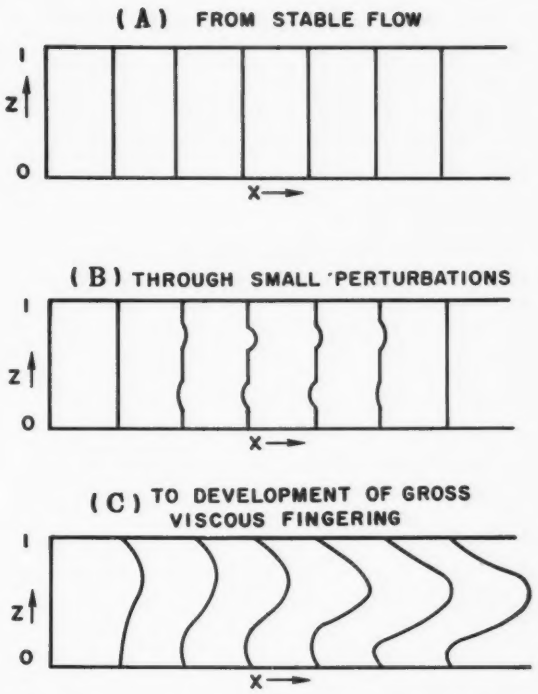

FIG. 1 – GROWTH OF FINGERING AS SHOWN BY CONTOURS.

So long as discussion is restricted to the first-order theory, the superscripts (1) for the perturbation variables can be dropped. The bar is retained to designate the properties of the stable displacement. At this point, we also make use of several assumed properties of the linear stable flow: $\bar{u} = 1$, $\bar{v} = \bar{w} = 0$, $\bar{c}_y = 0$. Transforming to moving space co-ordinates $x = x_s - t$, we obtain as the perturbation equations

$$c_t - D_1 c_{xx} - D_3 c_{yy} - D_3 c_{zz} + \bar{c}_x u + \bar{c}_z w = 0 \qquad \text{.....(4.1)}$$

$$u_x + v_y + w_z = 0 \qquad \text{.....(4.2)}$$

$$u + (\mu_0/\bar{\mu}) p_x + g_1 c = 0 \qquad \text{.....(4.3)}$$

$$v + (\mu_0/\bar{\mu}) p_y = 0 \qquad \text{.....(4.4)}$$

$$w + (\mu_0/\bar{\mu}) p_z + g_3 c = 0 \qquad \text{.....(4.5)}$$

where the functions g (of $\bar{c}$) are defined by

$$g_1 = \frac{d \ln \mu}{dc} + \frac{kg}{\bar{\mu}u_0} \frac{d\rho}{dc} \frac{\sin\theta}{\phi} \qquad \text{.....(5.1)}$$

$$g_3 = \frac{kg}{\bar{\mu}u_0} \frac{d\rho}{dc} \frac{\cos\theta}{\phi} \qquad \text{.....(5.2)}$$

Because the set of equations of Eq. 4 are linear, an arbitrary initial perturbation is readily expressed as the sum of its Fourier components. This assumes that conditions of convergence and differentiability

are met. The equations of Eq. 4 describe the deviation of a small perturbation from stable behavior. Higher-order perturbation theory can be applied for larger disturbances by also considering variables with superscripts of two or higher.

SOLUTION OF THE PERTURBATION EQUATIONS

Linearity of the equations of Eq. 4 also means that the solution for an arbitrary perturbation will be the sum of solutions for the individual Fourier components. Thus, we need only study separately the behavior of particular complex Fourier terms. One such follows.

$$\eta = \tilde{\eta} \exp\,[if(x,y,z,t)],$$

$$\eta = c, u, v, w, p \quad \ldots\ldots(6.0)$$

where

$$f(x,y,z,0) = \alpha x + \beta y + n\pi z \quad \ldots\ldots(7.0)$$

It is understood that the physical quantities represented by Eq. 6 are real. Substituting in the equations of Eq. 4 from Eq. 6,

$$\left[if_t - iD_1 f_{xx} - iD_3 f_{yy} - iD_3 f_{zz} + D_1 f_x^2 + D_3 f_y^2 + D_3 f_z^2 \right] \tilde{c} + \bar{c}_x \tilde{u} + \bar{c}_z \tilde{w} = 0 \quad \ldots\ldots(8.1)$$

$$if_x \tilde{u} + if_y \tilde{v} + if_z \tilde{w} = 0 \quad \ldots\ldots(8.2)$$

$$g_1 \tilde{c} + \tilde{u} + i(\mu_0/\bar{\mu}) f_x \tilde{p} = 0 \quad \ldots\ldots(8.3)$$

$$\tilde{v} + i(\mu_0/\bar{\mu})\, f_y \tilde{p} = 0 \quad \ldots\ldots(8.4)$$

$$g_3 \tilde{c} + \tilde{w} + i(\mu_0/\bar{\mu})\, f_z \tilde{p} = 0 \quad \ldots\ldots(8.5)$$

In matrix notation, these equations are of the form, $A\tilde{y} = 0$, which requires either that the column vector $\tilde{y}$ is zero or that $|A| = 0$. Thus, we obtain

$$\{[if_t - iD_1 f_{xx} - iD_3 f_{yy} - iD_3 f_{zz} + D_1 f_x^2 + D_3 f_y^2 + D_3 f_z^2][f_x^2 + f_y^2 + f_z^2]\} + Ef_x^2 + Ff_x f_z + Gf_z^2 + (E+G) f_y^2 = 0 \quad \ldots\ldots(9.0)$$

where the functions E, F and G are defined as

$$E = -g_3 \bar{c}_z \quad \ldots\ldots(10.1)$$

$$F = g_3 \bar{c}_x + g_1 \bar{c}_z \quad \ldots\ldots(10.2)$$

$$G = -g_1 \bar{c}_x \quad \ldots\ldots(10.3)$$

The solution $f(x,y,z,t)$ to Eq. 9 must satisfy the initial condition, Eq. 7, and also the boundary conditions

$$\left.\begin{array}{l} \text{Real } c_z = 0 \\ \text{Real } w = 0 \end{array}\right\} \; z = 0,\ z = 1 \quad \ldots\ldots(11.0)$$

To solve Eq. 9, we assume that the function can be expanded as a Taylor series. This requires that the complex variable f be an analytic function. If f is also to satisfy Eq. 7,

$$f(x,y,z,t) = \alpha x + \beta y + n\pi z + f_t^\circ t + (2!)^{-1}[f_{tt}^\circ t^2 + 2f_{xt}^\circ (x-x_o)t + 2f_{yt}^\circ (y-y_o)t + 2f_{zt}^\circ (z-z_o)t] + \cdots \quad \ldots\ldots(12.0)$$

The superscripts o indicate that the coefficients are to be evaluated at the point $(x_o, y_o, z_o, 0)$. We can similarly expand the known functions E, F and G of the stable solution. For example,

$$E = E^\circ + E_x^\circ (x-x_o) + E_z^\circ (z-z_o) + E_t^\circ t + (2!)^{-1}[E_{xx}^\circ (x-x_o)^2 + E_{zz}^\circ (z-z_o)^2 + E_{tt}^\circ t^2 + 2E_{xz}^\circ (x-x_o)(z-z_o) + 2E_{xt}^\circ (x-x_o)t + 2E_{zt}^\circ (z-z_o)t] + \cdots \quad \ldots\ldots(13.0)$$

After taking the indicated derivatives, the results are substituted in Eq. 9. For f to be a solution, the coefficients of each term in $(x-x_o)$, $(x-x_o)t$, t^2, etc., must vanish. This leads to an infinite sequence of algebraic equations. In terms of the functions,

$$\delta^{-2} = (\alpha^2 + \beta^2 + n^2\pi^2)^{-1} \quad \ldots\ldots(14.1)$$

$$H^\circ(x,z,t) = (\alpha^2 + \beta^2)E^\circ + \alpha n\pi F^\circ + (\beta^2 + n^2\pi^2)G^\circ \quad \ldots\ldots(14.2)$$

$$H_x^\circ = (\alpha^2 + \beta^2)E_x^\circ + \alpha n\pi F_x^\circ + (\beta^2 + n^2\pi^2)G_x^\circ, \text{ etc.} \quad \ldots\ldots(14.3)$$

The first of these equations are

$$if_t^\circ = -\alpha^2 D_1 - (\beta^2 + n^2\pi^2) D_3 - \delta^{-2} H^\circ \quad \ldots\ldots(15.1)$$

$$if_{xt}^\circ = -\delta^{-2} H_x^\circ \quad \ldots\ldots(15.2)$$

$$if_{yt}^\circ = 0 \quad \ldots\ldots(15.3)$$

$$if_{zt}^\circ = -\delta^{-2} H_z^\circ \quad \ldots\ldots(15.4)$$

$$if_{tt}^\circ = -\delta^{-2}(H_t^\circ + D_1 H_{xx}^\circ + D_3 H_{zz}^\circ) - i\delta^{-2}\{H_x^\circ [2\alpha D_1 + \delta^{-2}(2\alpha E^\circ + n\pi F^\circ) - \delta^{-4}(2\alpha H^\circ)] + H_z^\circ [2n\pi D_3 + \delta^{-2}(\alpha F^\circ + 2n\pi G^\circ) - \delta^{-4}(2n\pi H^\circ)]\} \quad \ldots\ldots(15.5)$$

$$if_{xxt}^\circ = -\delta^{-2} H_{xx}^\circ \quad \ldots\ldots(15.6)$$

$$if^{\circ}_{yyt} = 0 \quad \text{.....(15.7)}$$

$$if^{\circ}_{zzt} = -\delta^{-2}H^{\circ}_{zz} \quad \text{.....(15.8)}$$

Before proceeding further, it is worthwhile to note several facts. First, if perturbation growth requires that the higher-order theory be considered, these higher-order terms will contribute a higher growth rate. For example, if a term in the first-order solution grows initially at the rate exp (bt), there will be a corresponding part of the second-order solution initially proportional to exp ($2bt$). Thus, any growth implies rapid growth, and it is sufficient to follow the behavior of the system for a short time. The behavior must be known at every position, however. Because we know the functions H for every position (x_o, y_o, z_o), the results are conveniently expressed as the family of particular solutions $f(x_o, y_o, z_o, t)$. The Taylor series then simplifies to a series in time t only, from which we need at most a few terms.

$$f(x_o, y_o, z_o, t) = \alpha x_o + \beta y_o + n\pi z_o + f^{\circ}_t t + (2!)^{-1} f^{\circ}_{tt} t^2 + (3!)^{-1} f^{\circ}_{ttt} t^3 + \cdots \quad \text{.....(16.0)}$$

The first two coefficients of t are given by Eqs. 15.1 and 15.5.

Thus, the first-order perturbation solution can be expressed in the following form, as for concentration.

$$c = \tilde{c} \exp(i\alpha x + i\beta y + in\pi z + i\gamma_I t) \exp(-\gamma_R t) \quad \text{.....(17.0)}$$

in which the "phase shift" coefficient γ_I is given by

$$\gamma_I = \text{Real}\left[\sum_{m=1}^{\infty} (m!)^{-1} f^{\circ}_{mt} t^{m-1}\right] \quad \text{....(18.1)}$$

and the "stability" coefficient γ_R is given by

$$i\gamma_R = \text{Imaginary}\left[\sum_{m=1}^{\infty} (m!)^{-1} f^{\circ}_{mt} t^{m-1}\right] \quad \text{.....(18.2)}$$

In terms of the function values given in Eqs. 15.1 and 15.5, these are

$$\gamma_I = -\tfrac{1}{2}t\delta^{-2}\{H^{\circ}_x[2\alpha D_1 + (2\alpha E^{\circ} + n\pi F^{\circ})\delta^{-2} - 2\alpha H^{\circ}\delta^{-4}] + H^{\circ}_z[2n\pi D_3 + (\alpha F^{\circ} + 2n\pi G^{\circ})\delta^{-2} - 2n\pi H^{\circ}\delta^{-4}]\} + \cdots \quad \text{.....(19.1)}$$

$$\gamma_R = [\alpha^2 D_1 + (\beta^2 + n^2\pi^2)D_3 + \delta^{-2}H^{\circ}] + \tfrac{1}{2}t\delta^{-2}[H^{\circ}_t + D_1 H^{\circ}_{xx} + D_3 H^{\circ}_{zz}] + \cdots \quad \text{.....(19.2)}$$

The parameters α, β and n characterize the initial perturbation, as do the functions E°, F° and G° the initial state of the corresponding stable displacement.

We wish to find from Eq. 17 the conditions under which the perturbation becomes smaller in time. Because $\tilde{c}$ is constant and the complex exponential is limited in magnitude to one, stability does not depend on them at all. The important factor in determining growth is the exponential term that remains and which, in turn, depends on the stability coefficient γ_R. For stability to be assured, each such coefficient of time in the Fourier series must be positive. This will guarantee that each term grows smaller with time. If so much as a single value of γ_R were negative, a small disturbance could grow at an exponential rate and eventually lead to viscous fingering. This means that only the least stable term of the original, complete Fourier series need be considered. If this one term with minimum γ_R grows smaller, all other terms will do the same.

A study of the functions involved will show that stability can arise from several sources. For example, gravitational forces can offset viscous forces under some conditions and provide gravity stabilization. In other cases gravity may not be quite sufficient, but the additional effect of dispersion may keep γ_R positive. This second case is dispersion stabilization. Stability is determined by the interplay of forces so that behavior changes with different displacement conditions. However, even the most general problem can be reduced to determining the sign of the coefficient of time in an exponent.

To repeat the reasoning we have followed, suppose we are given an arbitrary initial disturbance. A complete description of flow behavior would require solution of nonlinear partial differential equations in which coefficients (such as the flow rate) depend on the solvent concentration answer. In fact, for some conditions we may even be uncertain as to what equations will eventually be required to describe the behavior. But before it can die out, any disturbance must first become small enough for our linearized theory to apply. Giving this small disturbance a Fourier series representation, any unstable terms with negative γ would grow rather than die out, although there would be deviations from the predicted growth for moderately large amplitudes. The limiting conditions for stable miscible displacement can be specified after consideration of all possible modes of disturbance.

It is possible to have borderline instability without viscous fingering. If growth is slow enough, a return to stable displacement is possible before any macroscopic fingers are formed. Substantial growth will accelerate divergence, however. Perhaps the true condition for prevention of viscous fingering in a natural system is that the disturbance must die out before it travels past a second perturbation source. However fingering is defined, it is experimentally easy to show that, once formed, fingers cause a radically different displacement mechanism.[6] This less efficient mechanism is like immiscible displacement with no interfacial ten-

sion[7,8] so that, given enough solvent, almost all oil can be recovered.

SOLUTION FOR STABLE DISPLACEMENT

The perturbation parameters γ_I and γ_R defined in the preceding section are functions of the stable behavior $\bar{c}$ through their dependence on the functions E°, F°, G° and H°. Thus, we anticipate that any criteria for stability will depend strongly on the appropriate kind of stable behavior. To interpret the result implicit in Eq. 17 will require a reasonably general form of the solution $\bar{c}$ for stable behavior.

In most cases of stable displacement, gravity will be very important. Coupled with the effect of dispersion, gravity must prevent viscous fingering. The flow will then be very nearly parallel and there will be a nearly horizontal "mixing zone" between the solvent and the displaced fluid. This will be broadened from an "interface" by the effects of dispersion. Thus, in the mathematical description we assume parallel flow, or flow in the x-direction only. Dispersion occurs in both x and z directions, with the behavior independent of y position.

Any boundary condition that may be suggested for the inlet end of the system, $x=-t$, can be questioned. We select one which in the absence of dispersion would result in a horizontal interface, stationary in a moving co-ordinate system. Thus the equation to be solved and its boundary conditions are

$$\bar{c}_t - D_1 \bar{c}_{xx} - D_3 \bar{c}_{zz} = 0 \quad \text{.....(20.1)}$$

$$\bar{c}(x,z,0) = 0, \quad x > 0;$$

$$\lim_{x \to \infty} \bar{c}(x,z,t) = 0 \quad \text{.....(20.2)}$$

$$\bar{c}_z(x,0,t) = \bar{c}_z(x,1,t) = 0 \quad \text{.....(20.3)}$$

For $0 \leq t \leq -\cot\theta$:

$$\lim_{x \to -t} \bar{c}(x, z>h, t) = 1;$$

$$\lim_{x \to -t} \bar{c}(x, z<h, t) = 0 \quad \text{.....(20.4)}$$

while, for $t \geq -\cot\theta$:

$$\lim_{x \to -t} \bar{c}(x,z,t) = 1 \quad \text{.....(20.5)}$$

where

$$h = 1 + t\tan\theta, \quad -\pi/2 \leq \theta < 0 \quad \text{.....(20.6)}$$

The time t is the time for which displacement at the constant linear velocity u_o has been maintained.

Disregarding the effects of dispersion, these equations describe the kind of behavior illustrated in Fig. 2(A) for a time $t < -\cot\theta$. A similar description is given by Fig. 2(B) for times $t > -\cot\theta$. For the special case where $\theta = -\pi/2$, the system reduces to a one-dimensional problem with step-function input.

This boundary value problem can be solved by construction of an image system that implicitly

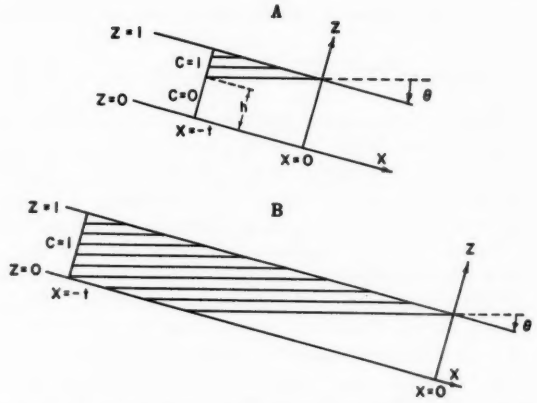

FIG. 2 — STABLE DISPLACEMENT SOLUTION WITH NO DISPERSION — (A) $t < -\cot\theta$, (B) $t > -\cot\theta$. SHADED AREA REPRESENTS SOLVENT.

makes use of the Green's function for the solution[19] and separation of variables. We construct an "extended" system of mirror images of the real system. This implies the extended definition of gravity g and dip angle θ in the equations of Eq. 1 as the following anti-periodic functions.

$$g(z) = g, \quad \theta(z) = \theta, \quad 0 < z < 1 \quad \text{.....(21.1)}$$

$$g(z) = -g, \theta(z) = -\theta, 1 < z < 2 \quad \text{.....(21.2)}$$

$$g(z) = g(z + 2n), \quad \theta(z) = \theta(z + 2n);$$

$$n = \pm 1, 2, \ldots \quad \text{.....(21.3)}$$

A new boundary condition for Eq. 20.1 then replaces Eq. 20.4 so that, for $0 \leq t \leq -\cot\theta$,

$$\lim_{x \to -t} \begin{cases} \bar{c}(x, h<z<2-h, t) = 1 \\ \bar{c}(x, -h<z<h, t) = 0 \\ \bar{c}(x,z,t) = \bar{c}(x, z+2n, t); \\ n = \pm 1, 2, \ldots \end{cases}$$

$$\text{.....(21.4)}$$

The remaining equations apply as before. The extended system is such that its solution automatically satisfies the conditions contained in Eq. 20.3. Summing the point-source contributions throughout the extended system and solvent "reflected" from the $x = -t$ boundary, we obtain as the stable solution

$$\bar{c}(x,z,t) = \int_1^0 Z(z,t,\phi) \exp(-\omega^2) \frac{\partial\omega}{\partial\phi} d\phi$$

$$+ \tfrac{1}{2} \operatorname{erfc}\left[(x - \cot\theta)/2\sqrt{D_1(t + \cot\theta)}\right]$$

$$+ \exp[(x+t)/D_1] \int_1^0 Z(z,t,\phi) \exp(-\lambda^2) \frac{\partial\lambda}{\partial\phi} d\phi$$

$$+ \tfrac{1}{2} \exp[(x + t)/D_1] \operatorname{erfc}\left[(x + 2t + \cot\theta)/2\sqrt{D_1(t + \cot\theta)}\right] \quad \text{..... (22.1)}$$

where

$$\omega(\phi) = [x - (1-\phi)\cot\theta]/2\sqrt{D_1[t + (1-\phi)\cot\theta]} \quad \text{.....(22.2)}$$

$$\lambda(\phi) = [x+2t+(1-\phi)\cot\theta]/2\sqrt{D_1[t+(1-\phi)\cot\theta]} \quad \text{.....(22.3)}$$

$$Z(z,t,\phi) = \sum_m (4\pi)^{-1/2}\left\{ \operatorname{erf}\left[\frac{2m + 2 - \phi - z}{2\sqrt{D_3[t+(1-\phi)\cot\theta]}}\right] - \operatorname{erf}\left[\frac{2m + \phi - z}{2\sqrt{D_3\ [t+(1-\phi)ctn\theta]}}\right]\right\};$$

$$m = -\infty, \ldots -1, 0, 1, \cdots, +\infty \quad \text{.....(22.4)}$$

When $\theta = -\pi/2$, we obtain the important special case corresponding to injection of a step-function, for which the solution reduces to[20]

$$\bar{c}(x,t) = \tfrac{1}{2}\operatorname{erfc}\left[\frac{x}{2\sqrt{D_1\ t}}\right] + \tfrac{1}{2}\exp\left[\frac{x+t}{D_1}\right]\operatorname{erfc}\left[\frac{x+2t}{2\sqrt{D_1\ t}}\right] \quad \text{.....(22.5)}$$

This result can be obtained directly by use of the Laplace transform and arises naturally for a vertical displacement. However, it also applies when the injection rate is high enough for viscous forces to be dominant with any angle θ. In this latter case, dispersion must be the stabilizing mechanism, which may severely restrict the range of applicability.

PROPERTIES OF THE PERTURBATION SOLUTION

At this point it is convenient to note some of the properties of the perturbation solution and their relation to the real initial perturbation. Suppose that we had started with the real disturbance,

$$c(x,y,z,0) = 2\cos\alpha x\cos\beta y\cos n\pi z \quad \text{.....(23.0)}$$

This gives eight complex exponential terms including all combinations of wave numbers $(\pm\alpha, \pm\beta, \pm n\pi)$. The properties of γ_R are such that

$$\gamma_R(+\alpha, \pm\beta, +n\pi) = \gamma_R(-\alpha, \pm\beta, -n\pi) \quad \text{.....(24.1)}$$

$$\gamma_R(+\alpha, \pm\beta, -n\pi) = \gamma_R(-\alpha, \pm\beta, +n\pi) \quad \text{.....(24.2)}$$

Similarly, we can show that for γ_I,

$$\gamma_I(+\alpha\ \pm\beta, +n\pi) = -\gamma_I(-\alpha, \pm\beta, -n\pi) \quad \text{.....(24.3)}$$

$$\gamma_I(+\alpha, \pm\beta, -n\pi) = -\gamma_I(-\alpha, \pm\beta, +n\pi) \quad \text{.....(24.4)}$$

Thus, the complex exponentials resulting from Eq. 23 recombine into two families of cosine terms, in general with different damping and phase shift.

$$c_1 = \cos\beta y\cos[\alpha x + n\pi z + \gamma_I(\alpha, n\pi)t]\exp[-\gamma_R(\alpha, n\pi)t] \quad \text{.....(25.1)}$$

$$c_2 = \cos\beta y\cos[\alpha x - n\pi z + \gamma_I(\alpha, -n\pi)t]\exp[-\gamma_R(\alpha, -n\pi)t] \quad \text{.....(25.2)}$$

The extended system described under "Solution for Stable Displacement" is also useful for studying boundary conditions on the perturbation. Take an initial perturbation from the c_1 family, $\cos\beta y\cos(\alpha x + n\pi z)$. The part of this disturbance lying within the real system, $0 < z < 1$, has as its mirror image in the right-hand adjacent strip $1 < z < 2$ a member of the c_2 family, given by Eq. 25.2. That is, for any point z_1 and its geometrical image $z_2 = 2 - z_1$,

$$\begin{aligned}\cos(\alpha x - n\pi z_2) &= \cos[\alpha x - n\pi(2 - z_1)] \\ &= \cos(\alpha x + n\pi z_1 - 2n\pi) \\ &= \cos(\alpha x + n\pi z_1)\end{aligned} \quad \text{.....(26.0)}$$

But the stable solution for $\bar{c}$ (Eq. 22) has similar image properties as a consequence of the anti-periodicity of the extended system. These are reflected in the functions E°, F°, G° and H°. Thus we can show that, when an $(\alpha, -n\pi)$ perturbation and the corresponding stable solution from the $1 < z < 2$ strip are mapped into the $0 < z < 1$ strip by reflection, the result is identical to that for an $(\alpha, n\pi)$ perturbation. This requires that the behavior of the superimposed systems remain the same for all time. We always have members of both families in any real solution; thus, perturbation flux into the boundary from the right is always equal in magnitude but oppositely directed to that from the left. This argument is readily extended to any other "boundary" z = integer in the extended system; in this sense, the boundary conditions of Eq. 11 are satisfied.

Thus, the solution to the perturbation problem consists of two families of perturbation waves given by the equations of Eq. 25. Considered in the extended system, these satisfy the first-order perturbation equations of Eq. 3 and the initial and boundary conditions. The effect of a boundary is to reflect the wave back into the system, with an image of the original in the extended anti-periodic system as the source of the reflection.

SUMMARY OF THEORETICAL RESULTS

We have shown in the preceding sections that there are two families of mathematical solutions for the equations describing growth of an initially small disturbance. Each solution contains an exponential factor, $\exp(-\gamma_R t)$. The coefficient of time γ_R depends on the appropriate stable displacement behavior $\bar{c}$ and also on the parameters α, β and n of the real initial perturbation term, $\cos\alpha x$

cos βy cos $n\pi z$. For a displacement to be stable, the coefficient γ_R in each such exponent must be positive. Thus, it is sufficient to consider the particular term with minimum γ_R. No doubt the most important part of this particular term is the time-independent element, which determines the initial behavior of the disturbance. This is given by

$$\gamma_R = [\alpha^2 D_1 + (\beta^2 + n^2\pi^2)D_3 + \delta^{-2}H°] \quad \ldots\ldots (27.0)$$

a special case of Eq. 19.2 for which the terms are defined by Eqs. 6, 7 and 14. The functions used are to be evaluated at any point of interest (x_o, y_o, z_o) and at the initial time with respect to perturbation behavior, $t = 0$.

In terms of the stability coefficient γ_R, we can define a surface of neutral stability on which such a coefficient vanishes. When present, this surface divides the system into two parts – an exterior region where all γ_R are positive, and an interior region of higher concentration gradients within which at least one γ_R is negative. Thus, given an appropriate perturbation source, unstable fingers can grow from the interior region to dominate displacement behavior. For true stability, this interior region must be absent, in which case the surface $\gamma_R = 0$ does not exist. With time, the enclosed unstable concentration range will shrink. This leads to the first of several important generalizations.

CONDITIONAL INSTABILITY

The first term in γ_R is a positive constant representing the stabilizing effect of dispersion. All other terms depend on concentration gradients which must eventually become very small. This means that the only instability observed is a conditional instability—one which will disappear after a sufficiently long time.

"WAVE LENGTH" DEPENDENCE

The numbers α, β and n characterize the initial disturbance as the sum of a series of sinusoidal concentration waves. One effect of the constant term in γ_R is to make long "wave lengths" the least stable modes. Thus, stability is determined by the "fundamental" Fourier mode of an arbitrary initial perturbation, a term with small α, β and n. Provided the smallest of these numbers are large enough, the particular perturbation can be stable even though displacement is not stable in the general sense.

"DIAMETER" EFFECT

Wave-length dependence is most important in laboratory-size systems. In laboratory cores, the longest wave length (which determines stability) is likely to reflect the size of the system rather than characteristics of the formation material. The importance of dispersion as a stabilizing mechanism is enhanced many-fold by such a reduction in maximum wave length. This is shown when dimensions are introduced into Eq. 27 and the first terms acquire an inverse proportionality to L^2, with L the width of the system. Experimental results showing the indicated "diameter" effect have been obtained.[9]

GRAVITY STABILIZATION

We assume a normal case in which a low-density low-viscosity solvent displaces oil downdip. The function g_1 (from the equations of Eq. 5) then becomes positive when gravity is dominant, and negative when gravity is subordinate to viscous forces. The second function of the pair g_3 is always negative. If we consider a case in which both α and n are positive and g_1 is positive, gravity effectively stabilizes the mode. This can be shown through the defining equations (Eqs. 5, 10 and 14).

Gravity dominance will not always lead to stability, however, as can be shown for some combinations of parameters. In particular, gravity dominance naturally leads toward instability when the less-dense fluid displaces updip.

MINIMUM SLUG SIZE

The condition for neutral stability, $\gamma_R = 0$, also defines the minimum size of a solvent "slug" for stable displacement of oil. As an example, consider the simplified case for which the stable flow is one-dimensional, $\bar{c}_z = 0$, and α for the perturbation is negligible. This latter corresponds to a perturbation extending almost indefinitely in the direction of flow, as could follow if it neither grew nor died out. With all other properties specified, we wish to define the maximum permissible solvent concentration gradient, $\bar{c}_x^*$. In magnitude this is given by

$$|\bar{c}_x^*| = |(\delta^2 D_3)(g_1)^{-1}| \quad \ldots\ldots (28.0)$$

Maximum gradients occur at injection before any dispersion has occurred. Thus, Eq. 28 defines the steepest solvent concentration profile consistent with stability that can be injected under the prescribed conditions.

Optimum use of solvent requires the smallest "mixing zones" possible. This implies the construction of a stable solvent slug by: (1) formation of a transition zone from oil to solvent, such as would be defined by Eq. 28 for example; (2) addition of enough pure solvent to prevent later immiscibility as a result of dispersion mixing; and, finally, (3) formation of a second transition zone from solvent to gas. This final transition requires re-application of Eq. 28. The total quantity of solvent required can be obtained by integration over such a contour, thus defining a minimum slug size.

SCALING OF LABORATORY EXPERIMENTS

Scaling rules for laboratory miscible displacement experiments have been presented by previous authors.[6,21] Stability phenomena impose additional requirements that must be met if a laboratory flood is to represent particular reservoir conditions. For stable displacement, only the dispersion and flow relationships between systems need be scaled. We expect a similar simplification for a high degree of instability. Unpublished experimental data tend to verify this view. Near the limits of stability, however, both the degree and source of instability must be matched in scaled experiments.

Inclusion of the very difficult requirement of scaled perturbation sources is a condition which may well make exact scaling impossible.

ACKNOWLEDGMENT

This paper is an outgrowth of "Conditional Instability in Miscible Liquid-Liquid Displacement", presented at the AIChE-SPE Joint Symposium on Fundamental Concepts of Miscible Fluid Displacement: Part II; Fifty-Second Annual Meeting, San Francisco, December 6-9, 1959. The author prepared the Symposium paper while associated with the California Research Corporation, La Habra, Calif.

REFERENCES

1. Hall, H. N. and Geffen, T. M.: "Laboratory Study of Solvent Flooding", *Trans.*, AIME (1957) Vol. 210, 48.
2. Koch, H. A., Jr. and Slobod, R. L.: "Miscible Slug Process", *Trans.*, AIME (1957) Vol. 210, 40.
3. Scheidegger, A. E.: "Theory of Flow of Miscible Phases in Porous Media", presented at International Union of Geodesy and Geophysics in Toronto (Sept., 1957); *Jour. Appl. Phys.* (1954) *25*, 994; *The Physics of Flow Through Porous Media*, U. of Toronto Press (1957).
4. von Rosenberg, D. U.: *AIChE Jour.* (1956) Vol. 2, 55.
5. Day, P. R.: *Trans.*, Am. Geophys. Union (1956) Vol. 37, 595.
6. Blackwell, R. J., Rayne, J. R. and Terry, W. M.: "Factors Influencing the Efficiency of Miscible Displacement", *Trans.*, AIME (1959) Vol. 216, 1.
7. Everett, J. P., Gooch, F. W., Jr. and Calhoun, J. C., Jr.: "Liquid-Liquid Displacement in Porous Media as Affected by the Liquid-Liquid Viscosity Ratio and Liquid-Liquid Miscibility", *Trans.*, AIME (1950) Vol. 189, 215.
8. Griffith, J. D. and Nielsen, R. F.: "Some Studies on Miscible Fluid Displacement", *Bull. No. 68*, Mineral Ind. Exper. Stat., Pennsylvania State U., 71.
9. Lacy, J. W., Draper, A. L. and Binder, G. G.: "Miscible Fluid Displacement in Porous Media", *Trans.*, AIME (1958) Vol. 213, 76.
10. Chuoke, R. L., van Meurs, P. and van der Poel, C.: "The Instability of Slow, Immiscible, Viscous Liquid-Liquid Displacements in Permeable Media", *Trans.*, AIME (1959) Vol. 216, 188.
11. Baron, T.: *Chem. Eng. Prog.* (1952) Vol. 48, 118.
12. McHenry, K. W. and Wilhelm, R. H.: *AIChE Jour.* (1957) Vol. 3, 83.
13. Beran, M. J.: *Jour. Chem. Phys.* (1957) Vol. 27, 270.
14. Rifai, M. N. E., *et al: Dispersion Phenomena in Laminar Flow Through Porous Media*, San. Eng. Res. Lab., U. of California, Berkeley, Report I. E. R., Series 93, Issue 2 (1956).
15. de Jong, G. de Josselin: *Trans.*, Am., Geophys. Union (1958) Vol. 39, 67.
16. Saffman, P. G.: *Jour. Fluid Mech.* (1959) Vol. 6, 321.
17. Blackwell, R. J.: "Laboratory Studies of Microscopic Dispersion Phenomena in Porous Media", Preprint 29 presented at AIChE-SPE Joint Symposium in San Francisco (Dec. 6-9, 1959).
18. Lin, C. C.: *The Theory of Hydrodynamic Stability*, Cambridge U. Press (1955).
19. Sneddon, I.: *Elements of Partial Differential Equations*, McGraw-Hill Book Co., Inc., N. Y. (1957).
20. Aronofsky, J. S. and Heller, J. P.: "Diffusion Model to Explain Mixing of Flowing Miscible Fluids in Porous Media", *Trans.*, AIME (1957) Vol. 210, 345.
21. Offeringa, J. and van der Poel, C.: "Displacement of Oil from Porous Media by Miscible Liquids", *Trans.*, AIME (1954) Vol. 201, 310.

***

Effect of Oil Production Rate on Performance of Wells Producing from More Than One Horizon

W. TEMPELAAR-LIETZ
MEMBER AIME

SHELL OIL CO.
LOS ANGELES, CALIF.

ABSTRACT

The performance of a two-horizon depletion-type reservoir produced through combination wells is analyzed. By introducing some simplifying approximations, it has been possible to obtain formulas which are easy to handle. Only ordinary differential equations are used, and the development of the analysis can be followed without difficulty by the non-specialist. A rigorous analysis has been made of this problem. It has been found that the approximations introduced in the simplified analysis are fully justified and that errors seldom will be more than 2 per cent.

The report shows the effect of the rate of withdrawal upon the relative depletion of the two horizons. Numerical examples are given.

INTRODUCTION

In its simplest form an oil reservoir consists of a continuous, homogeneous body of porous and permeable rock, enclosed at the top and the bottom by impermeable material. The flow of fluid through such a reservoir has been the subject of numerous papers, and the mathematical analysis of well performance, pressure build-up, etc., has reached a high degree of refinement. One of the basic assumptions introduced into these analyses is the homogeneity of the reservoir. In non-homogeneous reservoirs, these computations still can be carried out satisfactorily, provided small irregularities in the physical properties of the rock are distributed in a random fashion.

The flow equations are derived as solutions of the continuity equation, and their solutions are dependent upon the assumption of many constant factors in the reservoir: permeability to oil, compressibility of the reservoir fluid, viscosity saturation, etc. When these are assumed to be constant, the continuity equation can be solved rigorously. When these assumptions do not hold and corrections are introduced, it becomes very difficult and often impossible to solve analytically.

The present analysis is concerned with production from a two-layer depletion-type reservoir in which the layers have different permeabilities. Instead of using the continuity equation, results were derived from some simple physical ideas. In a single-layer reservoir in which the oil is at a pressure above the bubble point, the rate of production often has been assumed to be directly proportional to the pressure drawdown. In the simplified analysis it has also been assumed that the drop in average reservoir pressure is directly proportional with the cumulative withdrawal. These considerations in the past have been the basis of the analysis of reservoir performance and have been applied to a variety of problems, often with marked success. In the problem under investigation these relationships are shown to be compatible with the equation of continuity, but the approach has the advantage of leading to ordinary differential equations in which changes in constants can be introduced without making the analytical solution impossible.

It has the additional advantage that it can be understood more readily by the large group of engineers who are not reservoir specialists. For that reason, detailed steps in the mathematical developments have been shown in full.

SCOPE OF ANALYSIS

The analysis in this paper has been applied to a two-layer depletion-type reservoir in which both horizons are produced simultaneously in the same well. Because of the difference in permeability, it is obvious that the depletion of the two zones will proceed at different rates. For various problems it may be of interest to know the degree of depletion of the two zones at any arbitrary time and to in-

Paper originally published in 1953 as Shell Oil Co. report. At that time a search of the literature revealed no mathematical analysis of the production from a multiple-zone reservoir as herein described. Since then, the report has been referenced in later studies on related subjects.

At the 34th Annual Fall Meeting of SPE in Dallas in 1960, the paper by C. S. Matthews, *et al* (page 43 of this issue of *Soc. Pet. Eng. Jour.*) was presented. A portion of that paper is devoted to a rather detailed analysis of the report, and it was felt that publication of the 1953 report might be desirable.

Consequently, the author submitted this paper—essentially in its original 1953 form — for presentation at the Regional SPE Meeting in Pasadena, Calif. on Oct. 22-23, 1959. Subsequent constructive comments by the Society's Transactions Editorial Committee are gratefully acknowledged and have led to modification of the text to its present form.

vestigate the possibility of affecting this relative depletion by operating practices. One of the main factors under control of the operator is the rate of withdrawal, and the effect of various rates upon the distribution of depletions is demonstrated. In the development of the analysis, some basic assumptions have been introduced which now will be discussed.

BASIC ASSUMPTIONS

The following assumptions have been made.

1. Each of the two layers producing simultaneously in one well has an equal (unit) thickness. The reasoning followed in the computations should not change when layers of different thicknesses are assumed.
2. The two layers have the same initial reservoir pressure.
3. The P-V-T data of the fluids in the two reservoirs are equal.
4. The well under consideration is one in a regular drainage pattern, and surrounding wells are producing at comparable rates.
5. The structure is flat, and gravity effects can be ignored so that radial flow formulas can be applied.
6. The reservoir is the depletion type.
7. The present analysis is mainly concerned with the period in which the producing GOR is equal or close to the original solution GOR, up to the time that free gas starts moving; and, experience has shown that during that period the relationship between pressure and cumulative production can be approximated closely by a straight line. In this analysis, it has been assumed that such a straight-line relationship does exist.
8. Although the permeabilities of the two layers may differ widely, it often is found that the porosities show a random scattering. It has been assumed for this analysis that the average porosities of the layers are equal.

This assumption will lead to a simplification of the formulas. For the case of different porosities, adjustments in the analysis easily can be made.

9. The instantaneous rate of production is directly proportionate with the difference between the average pressure of the reservoir and the producing pressure in the well. This assumption will be discussed in detail in the Appendix.
10. The drainage reservoirs of the individual wells are approximated by circles with radii equal to one-half the distance between the wells.

MATHEMATICAL ANALYSIS

Let it be assumed that a well is producing from two zones simultaneously, and let the two zones be referred to as Zone I and Zone II.

The recovery per psi pressure drop for each of the zones will be represented by A barrels (Assumptions 7 and 8).

The proportionality factor according to Assumption 9 will be referred to as the productivity index and will be represented by i_1 for Zone I and i_2 for Zone II. The nature of these i-values will be discussed further in the Appendix.

The instantaneous rate of production from the two zones combined will be denoted by q B/D, and in this analysis it has been assumed that this rate is constant throughout the period under consideration.

The original reservoir pressure is represented by P_o; and at a time t the average reservoir pressure in Zone I will be $\bar{p}_1$; the average pressure in Zone II will be represented by $\bar{p}_2$, and the back pressure in the producing well by p_w, all expressed in pounds per square inch.

At that time the cumulative production from Zone I will be equal to

$$Q_1 = A(P_o - \bar{p}_1).$$

Similarly, for Zone II,

$$Q_2 = A(P_o - \bar{p}_2).$$

Therefore, the cumulative recovery from both zones at time t can be represented by

$$Q = Q_1 + Q_2 = 2AP_o - A(\bar{p}_1 + \bar{p}_2).$$

Since it has been assumed that the well has produced at a constant rate of q B/D,

$$2AP_o - A(\bar{p}_1 + \bar{p}_2) = qt. \quad \ldots\ldots\ldots\ldots \quad (1)$$

The rate of production from Zone I at the time t will be equal to

$$\frac{dQ_1}{dt} = i_1(\bar{p}_1 - p_w),$$

and because of Assumptions 6 and 8

$$\frac{dQ_1}{dt} = i_1(\bar{p}_1 - p_w) = -A\frac{d\bar{p}_1}{dt} \quad \ldots\ldots\ldots\ldots \quad (2)$$

Similarly, for Zone II,

$$\frac{dQ_2}{dt} = i_2(\bar{p}_2 - p_w) = -A\frac{d\bar{p}_2}{dt} \quad \ldots\ldots\ldots\ldots \quad (3)$$

Therefore,

$$\frac{dQ_1}{dt} + \frac{dQ_2}{dt} = \frac{dQ}{dt} = q,$$

or

$$i_1\bar{p}_1 + i_2\bar{p}_2 - (i_1 + i_2)p_w = q,$$

so that

$$p_w = \frac{i_1\bar{p}_1 + i_2\bar{p}_2 - q}{i_1 + i_2}. \quad \ldots\ldots\ldots\ldots \quad (4)$$

Substituting Eq. 4 in Eq. 2,

$$-A\frac{d\bar{p}_1}{dt} = i_1\bar{p}_1 - \frac{i_1}{i_1 + i_2}(i_1\bar{p}_1 + i_2\bar{p}_2 - q) \ldots\ldots \quad (5)$$

From Eq. 1,

$$2P_o - (\bar{p}_1 + \bar{p}_2) = \frac{q}{A}t,$$

or

$$\bar{p}_2 = 2P_o - \bar{p}_1 - \frac{q}{A}t. \quad \ldots\ldots\ldots\ldots \quad (6)$$

Substituting Eq. 6 in Eq. 5,

$$-A\frac{d\bar{p}_1}{dt} = i_1\bar{p}_1 - \frac{i_1^2}{i_1+i_2}\bar{p}_1 - \frac{i_1 i_2}{i_1+i_2}(2P_o - \bar{p}_1 - \frac{q}{A}t) + \frac{i_1}{i_1+i_2}q,$$

or

$$\frac{dp_1}{dt} + \frac{2\,i_1\,i_2}{A\,(i_1+i_2)}p_1 + \frac{q\,i_1\,i_2}{A^2(i_1+i_2)}t + \frac{q\,i_1 - 2\,i_1\,i_2\,P_o}{A\,(i_1+i_2)} = 0 \quad \ldots\ldots\ldots\ldots \quad (7)$$

Let

$$\frac{2\,i_1\,i_2}{A\,(i_1+i_2)} = C_1$$

$$\frac{q\,i_1\,i_2}{A^2\,(i_1+i_2)} = C_2$$

$$\frac{q\,i_1 - 2\,i_1\,i_2\,P_o}{A\,(i_1+i_2)} = C_3$$

Then,

$$\frac{d\bar{p}_1}{dt} + C_1\,\bar{p}_1 + C_2 t + C_3 = 0. \quad \ldots\ldots\ldots \quad (8)$$

This equation is linear and can be solved as follows. Assume $\bar{p}_1 = uv$.

Then, $$\frac{d\bar{p}_1}{dt} = u\frac{dv}{dt} + v\frac{du}{dt} \quad \ldots\ldots\ldots\ldots \quad (9)$$

Substituting Eq. 9 in Eq. 8,

$$u\frac{dv}{dt} + v\frac{du}{dt} + C_1 uv + C_2\,t + C_3 = 0,$$

or

$$u\left(\frac{dv}{dt} + C_1 v\right) + \left(v\frac{du}{dt} + C_2 t + C_3\right) = 0 \quad \ldots \quad (10)$$

One now can assume one relationship between u and v.

$$u\left(\frac{dv}{dt} + C_1 v\right) = 0. \quad \ldots\ldots\ldots\ldots \quad (11)$$

Eq. 10 now can be written

$$v\frac{du}{dt} + C_2 t + C_3 = 0. \quad \ldots\ldots \quad (12)$$

From Eq. 11,

$$\frac{dv}{dt} = -C_1 v$$

$$v = e^{-C_1 t} \quad \ldots\ldots\ldots\ldots \quad (13)$$

Substitution of Eq. 13 into Eq. 12 gives

$$e^{-C_1 t}\frac{du}{dt} + C_2 t + C_3 = 0,$$

or

$$\frac{du}{dt} = -C_2 t\ e^{C_1 t} - C_3\ e^{C_1 t},$$

so that

$$u = -\frac{C_2}{C_1^2}(C_1 t - 1)\ e^{C_1 t} - \frac{C_3}{C_1}\ e^{C_1 t} + C_4, \quad (14)$$

in which C_4 = constant of integration.

With $\bar{p}_1 = uv$ and $v = e^{-C_1 t}$ Eq. 14 can be transformed to

$$\bar{p}_1 = -\frac{C_2}{C_1^2}(C_1 t - 1) - \frac{C_3}{C_1} + C_4 e^{C_1 t}. \quad \ldots \quad (15)$$

For $t = o$ is $\bar{p}_1 = P_o$ or

$$C_4 = P_o - \frac{C_2}{C_1^2} + \frac{C_3}{C_1}.$$

Substituting the values for C_1, C_2 and C_3,

$$C_4 = \frac{q\,(i_1 - i_2)}{4\,i_1\,i_2}. \quad \ldots\ldots\ldots\ldots \quad (16)$$

Substituting the value of p_1 in Eq. 6,

$$\bar{p}_2 = 2\,P_o - \bar{p}_1 - \frac{q}{A}t$$

using the proper values,

$$\bar{p}_2 = P_o - \frac{qt}{2A} + \frac{q(i_1 - i_2)}{4\,i_1\,i_2}\left[1 - e^{\frac{-2\,i_1\,i_2\,t}{A(i_1+i_2)}}\right]. \quad (17)$$

Eq. 17 gives the value of the average pressure in Zone II = $\bar{p}_2$ at any given time t, and substitution of this value into Eq. 6 gives the corresponding value for $\bar{p}_1$.

$$\bar{p}_1 = P_o - \frac{qt}{2A} - \frac{q(i_1 - i_2)}{4\,i_1\,i_2}\left[1 - e^{\frac{-2\,i_1\,i_2\,t}{A(i_1+i_2)}}\right].$$

NUMERICAL EXAMPLES

To illustrate the theory, numerical examples have been worked out. The following basic data were used. Porosity of reservoir rock = 0.200; water saturation S_w = 0.300; oil saturation S_o = 0.700; compressibility of water $C_w = 2.5 \times 10^{-6}$ vol/vol/psi; and compressibility of oil $C_o = 10 \times 10^{-6}$ vol/vol/psi.

Therefore, effective compressibility referred to oil $= C_o + \frac{S_w}{S_o} \times S_w = 11.09 \times 10^{-6}$ vol/vol/psi.

In the first example it is assumed that the original reservoir pressure was P_o = 6,000 psi while the bubble point of the oil was P_b = 3,000 psi. Further assumptions include: zonal thickness h = 100 ft;

drainage radius r_b = 500 ft; well radius r_w = 0.25 ft; permeability Zone I k_1 = 100 md; and permeability Zone II k_2 = 10 md.

Considering the period in which the reservoir pressure is still above 3,000 psi, Fig. 1 was constructed. For this plot, the value of 11.09×10^{-6} vol/vol/psi was used. It will be observed that, while in the early stages the rate of production from Zone I represents the bulk of the well's production, gradually the production from Zone II increases while that from Zone I decreases.

After having produced about 30,000 bbl from the well, each zone is contributing half the production of the well. It also will be observed that from that time the lines run practically parallel. Theoretically, the lines should come together after an infinite time. At the time Zone I reaches the bubble point, it will have produced a cumulative production of 65,000 bbl. If the well had been producing at a rate of 100 B/D, Zone II would have produced about 63,000 bbl, while at a rate of 500 B/D this recovery would be only 55,000 bbl.

To demonstrate the effect of changes in one of the controlling factors, an expansion factor of 50×10^{-6} vol/vol/psi has been used. From about 100 P-V-T analyses carried out by Shell, this figure represents a good average value for the expansion of oil in the first period after it passes the bubble point.

Fig. 2, therefore, represents the performance of an oil reservoir that has the same properties as the one considered in the first case, with the exception that the oil has a bubble point equal to the original reservoir pressure. Again considering the time that 65,000 bbl have been withdrawn from Zone I (maximum expansion oil of Case 1) it now will be seen that, if the well had been producing at a rate of 500 B/D, Zone II would have produced 27,000 bbl or less than half of Zone I (Point Z of Fig. 2).

No corrections have been made for the gradual change in relative permeability because both are changing downward and the magnitude of these changes for 100 and 10 md may affect the difference in depletion one way or the other. In those cases where relative permeability data are available, corrections in the permeability can be made if considered necessary.

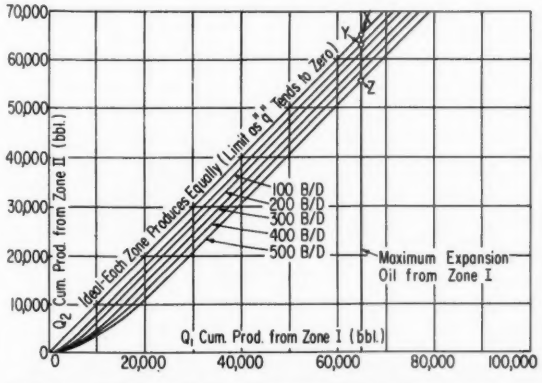

FIG. 1 – CUMULATIVE PRODUCTION FROM ZONE II VS CUMULATIVE PRODUCTION FROM ZONE I. A = 21.7 BBL/PSI; i_1 = 5.17 B/D-PSI; i_2 = .517 B/D-PSI.

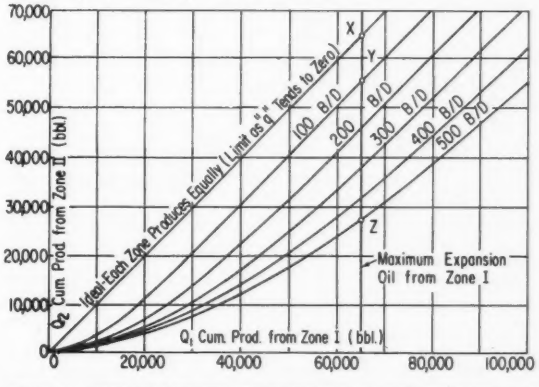

FIG. 2 – CUMULATIVE PRODUCTION FROM ZONE II VS CUMULATIVE PRODUCTION FROM ZONE I. A = 108.5 BBL/PSI; i_1 = 5.17 B/D-PSI; i_2 = .517 B/D-PSI.

GENERAL REMARKS

The analysis carried out in this paper essentially is based on steady-state flow. As such, it should find application in depletion-type reservoirs, i.e., in reservoirs with closed boundaries and in which no edge water encroaches. To verify the validity of this approach for the problem under consideration in which the relative rates of production from the two zones are controlled by continuously changing pressure conditions, the same problem has been solved rigorously. It has been found that, with the exception of the first few hours of production, errors of less than 2 per cent are introduced by the steady-state approach.

CONCLUSIONS

1. An analysis has been made of the performance of a depletion-type reservoir consisting of two horizons of different permeabilities, producing through wells penetrating both horizons.

2. It has been found that simple formulas, based on steady-state conditions, lead to answers that are within a few per cent from the results of computations based upon transient conditions.

3. It is demonstrated that the relative depletion of the two horizons can be affected to a large extent by adjusting the rate of production from the well.

NOMENCLATURE

- A = recovery in bbl per psi pressure drop for each zone
- c_w = compressibility of water, vol/vol/psi
- c_o = compressibility of oil, vol/vol/psi
- f = porosity of reservoir rock, fraction of bulk volume
- h = zonal thickness, ft
- i_1 = productivity index Zone I

i_2 = productivity index Zone II
k = permeability, md
k_1 = permeability, Zone I, md
k_2 = permeability, Zone II, md
P_o = original reservoir pressure, psi
P_b = bubble point of oil, psi
$\bar{p}_1$ = average reservoir pressure Zone I, psi
$\bar{p}_2$ = average reservoir pressure Zone II, psi
p_w = pressure in production well, psi
Q = cumulative production from well, bbl
Q_1 = cumulative production Zone I, bbl
Q_2 = cumulative production Zone II, bbl
q = rate of production of well, B/D
r_b = drainage radius, ft
r_w = radius borehole, ft
S_w = water saturation, fraction of porosity
S_o = oil saturation, fraction of porosity
t = time
ρ = viscosity of fluid
μ = density of fluid

ACKNOWLEDGMENT

The author wishes to express his appreciation to the Shell Oil Co. for permission to publish this paper.

APPENDIX

In the preceding analysis, some assumptions have been made which call for further investigation. In the development of the formulas, it has been assumed that the productivity-indexes i_1 and i_2 can be considered as constant multiplication factors.

It will be shown first that, if the flow pattern at any time can be considered as one of steady state, this assumption is justified.

Under steady-state conditions the pressures throughout the drainage-area are falling equally; i.e., $\frac{dp}{dt}$ is not a function of position.

The density of the fluid can be expressed as

$$\rho = \rho_o e^{-c(P_o - p)} \quad \ldots\ldots\ldots\ldots\ldots\ldots \quad (18)$$

for $p < P_o$. The initial pressure and density will be taken for the reference state (P_o, ρ_o). The compressibility c is assumed constant and sufficiently small for the approximation:

$$\rho = \rho_o [1 - c(P_o - p)]. \quad \ldots\ldots\ldots\ldots\ldots \quad (19)$$

In the steady state, the mass rate at the wellbore face can be expressed by close approximation as

$$m = r_b^2 \, bf \left(\frac{dp}{dt}\right), \quad \ldots\ldots\ldots\ldots\ldots\ldots \quad (20)$$

in which r_b = boundary radius, in this case the drainage radius of the well, f = porosity of the rock and b = thickness of the zone. From Eq. 19 one finds

$$\frac{d\rho}{dt} = \rho_o c \frac{dp}{dt}.$$

Therefore,

$$m = \pi r_b^2 bf \left(c\rho_o \frac{dp}{dt}\right),$$

or

$$\frac{m}{\rho_o} = q = \pi r_b^2 bfc \frac{dp}{dt}, \quad \ldots\ldots\ldots\ldots\ldots\ldots \quad (21)$$

in which q is now expressed as a volume rate and equal to the rate in volumes of original oil per unit time.

The rate past some circular boundary of arbitrary radius r will be

$$q_r = q \frac{(r_b^2 - r^2)}{r_b^2}. \quad \ldots\ldots\ldots\ldots \quad (22)$$

The rate of production past a radius r can be expressed, according to Darcy's law, as

$$q_r = \frac{q(r_b^2 - r^2)}{r_b^2} = 2\pi rb \frac{k}{\mu} \left(\frac{\partial p}{\partial r}\right) \quad \ldots\ldots\ldots \quad (23)$$

in which k is permeability and μ is viscosity, so that

$$\frac{\partial P}{\partial r} = \frac{q\mu}{2\pi kb} \cdot \frac{1}{r}\left(1 - \frac{r^2}{r_b^2}\right),$$

By integration the following expression is obtained for P_r.

$$P_r = \frac{q\mu}{2\pi kb}\left(\ln r - \frac{r^2}{2r_b^2}\right) + C, \quad \ldots\ldots\ldots \quad (24)$$

for $r = r_w$, $P_r = P_w$.

$$P_w = \frac{q\mu}{2\pi kb}\left(\ln r_w - \frac{r_w^2}{2r_b^2}\right) + C. \quad \ldots\ldots\ldots \quad (25)$$

Subtracting Eq. 25 from Eq. 24,

$$P_r - P_w = \frac{q\mu}{2\pi kb}\left(\ln \frac{r}{r_w} - \frac{r^2 - r_w^2}{2r_b^2}\right). \quad \ldots\ldots \quad (26)$$

Introducing a volume average pressure $\bar{P}_r$ for any radius r defined by

$$\bar{P}_r = \frac{1}{V_r} \int_{r_w}^{r} P_r \, dV, \quad \ldots\ldots\ldots \quad (27)$$

in which V_r is the volume of the drainage area from the wellbore to the radius r, the following equation can be written.

$$\bar{P}_r = \frac{1}{\pi(r^2 - r_w^2)bf}\left\{\frac{q\mu}{2\pi kb}\int_{r_w}^{r}\left(\ln \frac{r}{r_w} - \frac{r^2 - r_w^2}{2r_b^2}\right)(2\pi rbf\,dr) + \int_{r_w}^{r} P_w (2\pi rbf\,dr)\right\} \quad \ldots\ldots\ldots\ldots \quad (28)$$

or

$$\bar{P}_r = p_w + \frac{q\mu}{2\pi kb}\left\{\frac{r^2}{r^2 - r_w^2}\ln \frac{r}{r_w} - \frac{1}{2} - \frac{r^2 - r_w^2}{4r_b^2}\right\}. \quad (29)$$

Substituting $r = r_b$ and realizing that under normal conditions $r_w^2 \ll r_b^2$, this formula can be written with close approximation as

$$\bar{P}_r = p_w + \frac{q\mu}{2\pi kb}\left(\ln \frac{r_b}{r_w} - \frac{3}{4}\right), \quad \ldots\ldots\ldots \quad (30)$$

Comparing

$$\bar{P}_{r_b} - P_w = \frac{q\mu}{2\pi kb}\left\{\ln \frac{r_b}{r_w} - \frac{3}{4}\right\}, \quad \ldots \quad (31)$$

with Eq. 26,

$$P_{r_b} - P_w = \frac{q\mu}{2\pi kh}\left\{\ln\frac{r_b}{r_w} - \frac{1}{2}\right\}, \quad \ldots\ldots\ldots \quad (32)$$

it appears that the difference between using $\overline{P}_{r_b}$ and P_{r_b} when substituting normal values for $\frac{r_b}{r_w}$ is of secondary importance.

Eq. 31 may now be written

$$q = i(\overline{P}_{r_b} - p_w), \quad \ldots\ldots\ldots\ldots\ldots \quad (33)$$

in which

$$i = \frac{2\pi kh}{\mu(\ln\frac{r_b}{r_w} - \frac{3}{4})}. \quad \ldots\ldots\ldots\ldots\ldots \quad (34)$$

It appears that the value of i is not a function of time and, therefore, is constant for the reservoir so long as k and μ do not change.

The mass in the reservoir at any time t can be derived from Eq. 19.

$$\int_{r_w}^{r_b} \rho dV = \rho_o \int_{r_w}^{r_b} dV - C\ \rho_o P_o \int_{r_w}^{r_b} dV +$$

$$C\ \rho_o \int_{r_w}^{r_b} P_r\, dV. \quad \ldots\ldots\ldots\ldots\ldots \quad (35)$$

Using the definition of Eq. 27 for P_r, Eq. 35 can be rewritten. Let m represent the mass in the reservoir at time t and m_o the original mass; then,

$$m = m_o - C\rho_o P_o V_{r_b} + C\rho_o \overline{P}_{r_b} V_{r_b},$$

or

$$\frac{m_o - m}{\rho_o} = C\, V_{r_b}\, (P_o - \overline{P}_{r_b}),$$

and with

$$V_{r_b} = \pi bf\,(r_b^2 - r_w^2) - Q = C\pi bf\,(r_b^2 - r_w^2)\,(P_o - P_{r_b}),$$

$$Q = A(P_o - \overline{P}_{r_b})$$

in which Q = cumulative production in volumes of original reservoir oil and A is a constant. $\overline{P}_{r_b}$ is the same pressure appearing in Eq. 33.

Hence, if we can assume that, if the formulas developed for steady-state conditions can be applied to the problem under consideration, the following main equations can be written.

$$Q = A(P_o - \overline{P})$$

$$q = \frac{dQ}{dt} = i\,(\overline{P} - p_w)$$

These equations are essentially the same as those used in the main body of the report.

***

Linear Water Flood with Gravity and Capillary Effects

S. A. HOVANESSIAN
MEMBER AIME
F. J. FAYERS*
JUNIOR MEMBER AIME

CALIFORNIA RESEARCH CORP.
LA HABRA, CALIF.

ABSTRACT

The one-dimensional displacement equation for a homogeneous porous medium, including the effects of gravity and capillary forces, has been solved by a numerical method. A finite-difference scheme is developed for obtaining saturation, pressure and fractional flow profiles in waterflood recovery problems. From the numerical examples given, it is concluded that the gravitational forces have a pronounced effect on the saturation profiles and the pressure distribution curves of the system.

INTRODUCTION

Within the past 20 years, a number of papers have appeared in the literature dealing with the quantitative treatment of waterflood recovery problems. In their celebrated paper, Buckley and Leverett [1] described a method for calculating saturation profiles when the effects of capillary pressure and gravity are excluded. Terwilliger, *et al*,[2] included the effect of gravity in their theoretical and experimental investigation of oil recovery problems and obtained close correlation between experiment and theory. Welge[3] described a simplified method for obtaining the average saturation and the oil recovery from an oil reservoir. The effect of gravity can be included in this calculation.

More recently (1958) Douglas, *et al*,[4] presented a method for calculating saturation profiles which includes the effect of capillary pressure. The authors start with the one-dimensional displacement equation (which is nonlinear in the derivative) and, by a change of variable, transform this equation to a semi-linear partial differential equation. This equation is then solved by a finite-difference method on a high-speed digital computer. Fayers and Sheldon[5] obtained the solution of the one-dimensional displacement equation by directly replacing the differential equation by a finite-difference equation. The effects of capillary pressure and gravity were included in their solution. Here, since the movement of the foot of the saturation front is governed by a separate equation, the elapsed time in attaining a particular saturation profile cannot be obtained. The results of these two papers indicate that the inclusion of capillary forces eliminates the triple-valued Buckley-Leverett saturation profiles.

In the present paper, the one-dimensional displacement equation for a homogeneous permeable medium, including the effects of capillary and gravity forces, is solved.

The method of solution resembles that described in the paper by Douglas, *et al*, since it involves a similar transformation of variable. However, it extends their work in that the effect of gravity is included and, in addition, pressure profiles may be calculated. Also, the functions of saturation [$k_{ro}(S)$, $k_{rw}(S)$ and $P_c(S)$] required are entered in tabular form rather than as low-order polynomials. This simplifies data preparation and permits the use of a greater range of function types.

Unlike the method of Fayers and Sheldon, the corresponding elapsed time required for the development of each saturation profile is calculated and, also, saturation profiles may be calculated after breakthrough.

THEORETICAL CONSIDERATIONS

The dimensionless form of the one-dimensional displacement equation for a homogeneous porous medium as obtained from Darcy's law and material balance relations can be written as follows.[5]

$$\frac{\partial S}{\partial T}+\frac{dG(S)}{dS}\frac{\partial S}{\partial X}+N_c\frac{\partial}{\partial X}\left[C(S)\frac{\partial S}{\partial X}\right]=0 \quad \ldots\ldots\ldots\ldots (1)$$

where S = water saturation,

T = dimensionless time = $\frac{qt}{L\phi}$,

$G(S)$ = gravity function = $F_w(1-N_G k_{ro})$,

F_w = fractional water flow = $\left(1+\frac{k_{ro}}{k_{rw}}\frac{\mu_w}{\mu_o}\right)^{-1}$,

N_G = gravity constant = $[(\rho_w-\rho_o)gk\sin\theta]/\mu_o q$,

X = dimensionless distance = x/L,

Original manuscript received in Society of Petroleum Engineers office June 6, 1960. Revised manuscript received Oct. 14, 1960.

[1]References given at end of paper.

*Now with English Electric Co., Atomic Power Div., Leicester, England.

N_c = capillary pressure constant = $\frac{k\bar{p}_c}{\mu_o q L}$,

$C(S)$ = capillary function = $F_w k_{ro} \frac{dP_c}{dS}$,

$p_c = p_w - p_o$, and

f_w = actual fractional water flow = $G(S) - N_c C(S) \frac{\partial S}{\partial X}$.

The solution of Eq. 1 will give the values of saturation S as a function of time T and position X. This equation is a second-order nonlinear partial differential equation and it cannot be solved by the present classical techniques. However, it is possible to remove the "nonlinearity in the derivative" from the equation by introducing the following transformation.[4,6]

$$r(S) = \frac{1}{Z} \int_{S_i}^{S} C(S)\, dS \qquad \ldots\ldots\ldots\ldots\ldots (2)$$

where $Z = \int_{S_i}^{1-S_{or}} C(S)\, dS$,

S_i = initial water saturation, and

S_{or} = residual water saturation.

The introduction of transformation Eq. 2 into Eq. 1 yields

$$\frac{1}{C(r)} \frac{\partial r}{\partial T} + \frac{1}{Z} \frac{dG(r)}{dr} \frac{\partial r}{\partial X} + N_c \frac{\partial^2 r}{\partial X^2} = 0 \qquad \ldots\ldots\ldots\ldots\ldots (3)$$

In Eq. 3, the capillary pressure and gravity functions are both expressed as functions of the transformed variable r. This equation is nonlinear but not in the derivative.

The partial differential equation (Eq. 3) can be approximated by the finite-difference equation,[7,8]

$$-\frac{\bar{r}_n - r'_n}{\Delta T} = A(r_n^*) \left[\frac{\bar{r}_{n+1} - \bar{r}_{n-1}}{2\Delta X}\right] + B(r_n^*) \left[\frac{\bar{r}_{n+1} - 2\bar{r}_n + \bar{r}_{n-1}}{(\Delta X)^2}\right] \qquad \ldots\ldots\ldots\ldots\ldots (4)$$

The space subscript is n. Primed and unprimed quantities denote, respectively, values at the beginning and end of the time step ΔT. Also,

$$r_n^* = r'_n + \left(\frac{\partial r_n}{\partial T}\right)' a\Delta T \qquad \ldots\ldots\ldots\ldots\ldots (5)$$

$$\bar{r}_n = a r_n + (1-a) r'_n \qquad \ldots\ldots\ldots\ldots\ldots (6)$$

where a = time centering parameter, $0 < a \leqslant 1$ (usually set at 0.5) and

$$A(r^*) = \frac{C(r^*)}{Z} \frac{dG(r^*)}{dr^*} \quad \text{and} \quad B(r^*) = N_c C(r^*)$$

Using Eq. 4 to approximate $(\partial r_n / \partial T)'$ in Eq. 5, Eqs. 4 and 5 combine to give

$$a\Delta T \left[\frac{B(r_n^*)}{(\Delta X)^2} - \frac{A(r_n^*)}{2\Delta X}\right] \bar{r}_{n-1} - \left[\frac{2B(r_n^*)\, a\Delta T}{(\Delta X)^2} - 1\right] \bar{r}_n + a\Delta T \left[\frac{B(r_n^*)}{(\Delta X)^2} + \frac{A(r_n^*)}{2\Delta X}\right] \bar{r}_{n+1} = r'_n \qquad \ldots\ldots\ldots\ldots\ldots (7)$$

Denoting the coefficients of $\bar{r}_{n-1}$, $\bar{r}_n$ and $\bar{r}_{n+1}$ by a_n, b_n and c_n, respectively, and setting $d_n = r'_n$, we can write Eq. 7 as

$$a_n \bar{r}_{n-1} + b_n \bar{r}_n + c_n \bar{r}_{n+1} = d_n, \quad n = 1, \cdots, n \qquad \ldots\ldots\ldots\ldots\ldots (8)$$

The boundary conditions are fixed as follows: (1) the fractional flow of water f_w is always unity at the inflow boundary; and (2) the saturation at the outflow boundary must build up to a value S_{out} before water will flow out of the system, thereafter being calculated.

The solution of the finite-difference equations (Eq. 8), together with Eq. 6, will give the values of r as a function of time T and distance X. These values are in turn transformed back to saturation values by means of Eq. 2. Since the numerical procedure involves a great number of algebraic calculations, an electronic digital computer was used for obtaining solutions. Equations also are written for obtaining the fractional water flow and the pressure distribution across the system.

DISCUSSION OF RESULTS

Saturation, fractional-flow and pressure-distribution curves are obtained for oil-wet and for water-wet systems, with angle of inclination and injection flow rate as parameters. The relative permeability and capillary pressure data of the two systems are the same as given in Ref. 5.

Figs. 1 through 3 illustrate the effect of gravity

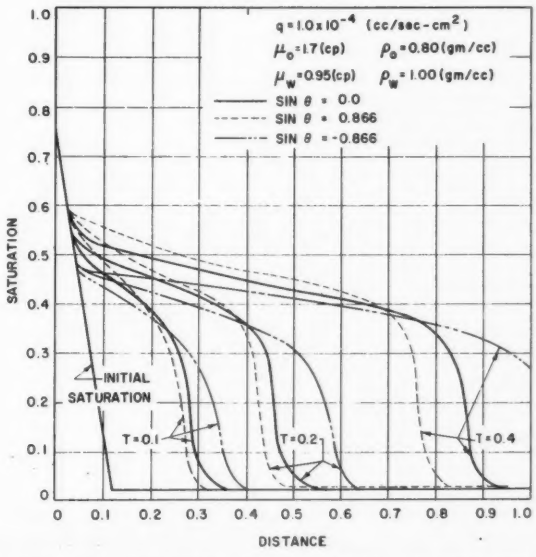

FIG. 1 – SATURATION VS DISTANCE, OIL-WET SYSTEM.

on the saturation, pressure and fractional flow profiles of an oil-wet system. From Fig. 1 it is noted that, for a constant injection rate $q = 10^{-4}$, the saturation profiles move slower for an upward angle of inclination ($\theta = 60°$) than for a horizontal or declined system. The areas under the saturation curves for the same value of T are equal, since T represents the pore volume of water injected. The initial saturation line starts from maximum saturation ($1-S_{or}$) at the input face and drops to a value slightly greater than the connate-water saturation and maintains this value for the remainder of the system.* Fig. 2 gives pressure distribution curves for the same system. It may be seen from this figure that the greatest pressure drop occurs for an inclination angle of +60°. Note the slight dip in the pressure curves at a distance of about 0.4 and 0.8 for T = 0.2 and 0.4, respectively, corresponding to the position of the saturation fronts at the times indicated (Fig. 1). Note also that almost no pressure drop occurs for a dipping angle of 60° below the horizontal, indicating that the pressure difference required to maintain the specified flow rate is approximately offset by gravity forces. Fig. 3 gives the actual fractional flow-vs-saturation curves for the cases illustrated by the previous figures. From Fig. 3, using Welge's method of calculation, we observe that the breakthrough saturation increases as the dip angle increases (from −60° below horizontal to +60° above). This is intuitively reasonable because, in general, the greater the slope of the test section, the greater the tendency for the injected water to accumulate and, thus, to increase the water saturation rather than to move the saturation front forward.

*The finite-difference scheme employed requires that all saturation values be at least slightly greater than the connate-water saturation. This can be seen from Eq. 4, which represents the rate of change of r($r \approx$ saturation). This rate depends on the values of $A(r^*_n)$ and $B(r^*_n)$ which, in turn, depend on the value of r at the beginning of the time step and, hence, are zero for connate-water saturation.

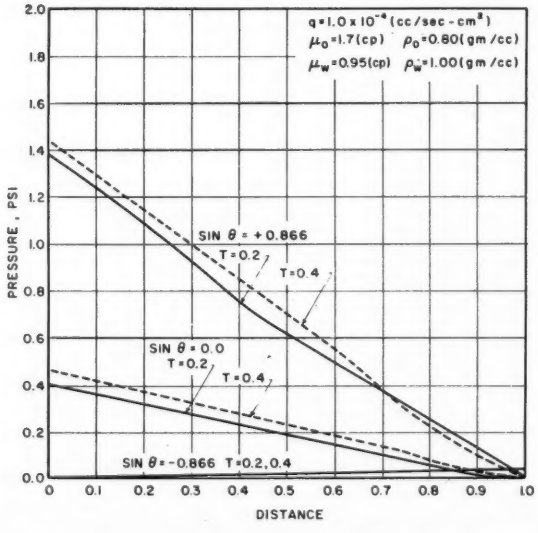

FIG. 2 – PRESSURE VS DISTANCE, OIL-WET SYSTEM.

Figs. 4 and 5 give the saturation and pressure profiles for a horizontal section at two flow rates. Comparison of Figs. 4 and 1 reveals that, as the flow rate increases, the breakthrough saturation increases. This effect has also been observed by Perkins[9] in his experimental investigations. Fig. 5 represents the pressure distribution across the test section for the same input conditions illustrated in Fig. 4. Observe that the greatest pressure drop occurs for the highest flow rate, and note the dips on the two pressure curves corresponding to the flow rate of $q = 10^{-2}$. It may be observed (Fig. 4) that these dips occur at the location of the saturation front at the times indicated.

Figs. 6 and 7 represent the saturation and pres-

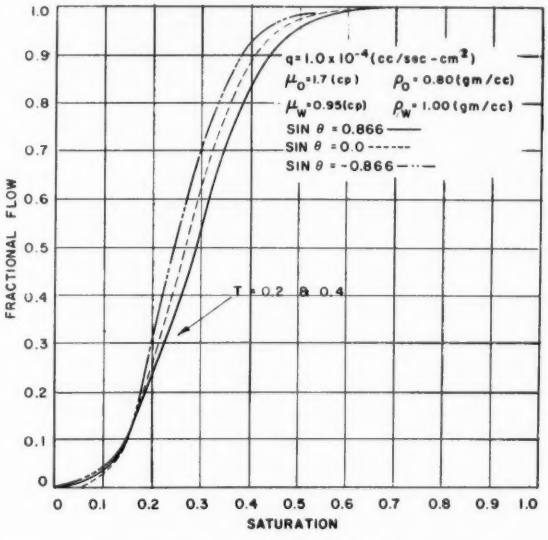

FIG. 3 – FRACTIONAL FLOW VS SATURATION, OIL-WET SYSTEM.

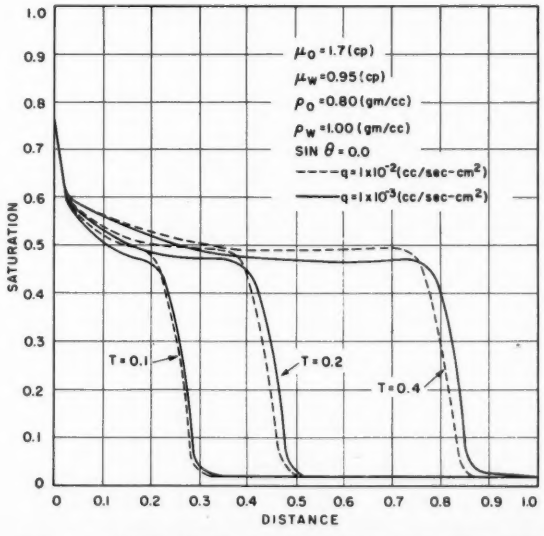

FIG. 4 – SATURATION VS DISTANCE, OIL-WET SYSTEM.

sure profiles for a water-wet system. From Fig. 6 it is noted that the saturation profile for the higher flow rate (dashed line) is steeper than that of the lower flow rate. Comparing Figs. 6 and 4, note that the saturation distribution lines of the former have a greater slope than those of the latter. This comes mainly from the capillary pressure curve because the capillary pressure curves of water-wet and oil-wet systems differ greatly, while the relative permeability curves of the two systems have substantially the same shape. Fig. 7 represents the pressure distribution across the system. Here again, the higher pressure drop occurs in the case of higher flow rate, and the dips in the pressure curves correspond to the location of saturation fronts. The effects of gravity forces were investigated for water-wet systems and no significant change was observed in the saturation, pressure or fractional-flow profiles.

In obtaining these solutions, ΔX was set at 0.04 and ΔT was set at 0.01. The material balance error, using these space and time increments, was less than 1 per cent.

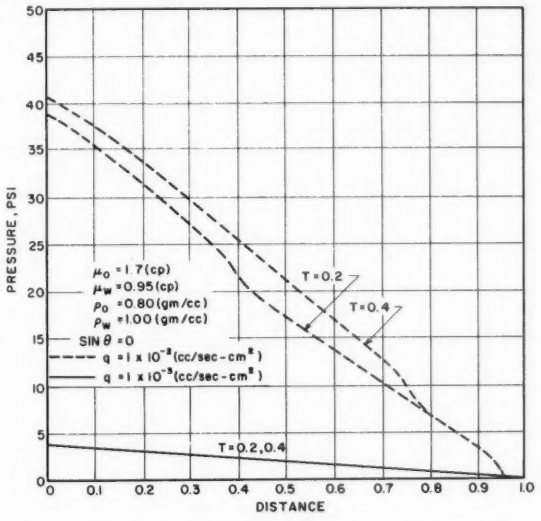

FIG. 5 – PRESSURE VS DISTANCE, OIL-WET SYSTEM.

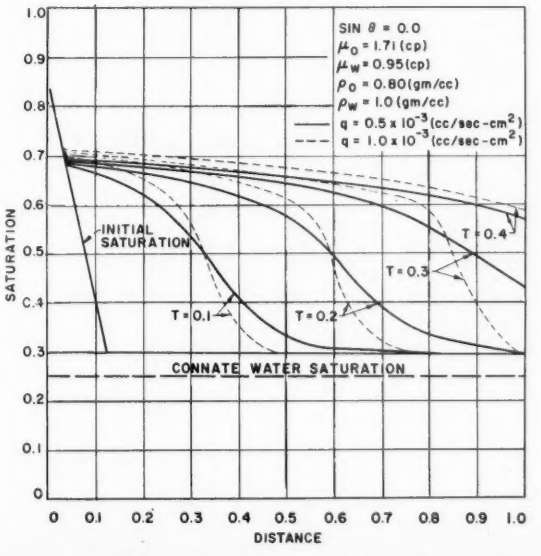

FIG. 6 – SATURATION VS DISTANCE, WATER-WET SYSTEM.

CONCLUSIONS

From the results of this study, the following conclusions can be made.

1. The inclusion of capillarity eliminates the triple-valued Buckley-Leverett saturation profiles.
2. The inclusion of gravity significantly affects the rate of movement of saturation profiles for a certain range of injection flow rates.
3. Gravity forces have a pronounced effect on pressure distribution curves for a certain range of injection flow rates.
4. Injection flow rates have a pronounced effect on saturation profiles and pressure distribution curves.
5. The initial saturation distribution had little effect on the computed results [$S(X)$, $P(X)$, $f_w(X)$] when the initial water in place was small compared to the water in place at the time under consideration.

NOMENCLATURE

a = centering parameter
$C(S)$ = capillary function
F_w = fractional water flow
f_w = actual fractional water flow
$G(S)$ = gravity function
g = gravitational constant (cm/sec^2)
k_o, k_w = permeability to oil and water (darcy)
k_{ro}, k_{rw} = relative permeability to oil and water
k = absolute permeability (darcy)
L = length of system (cm)
N_c = capillary pressure constant

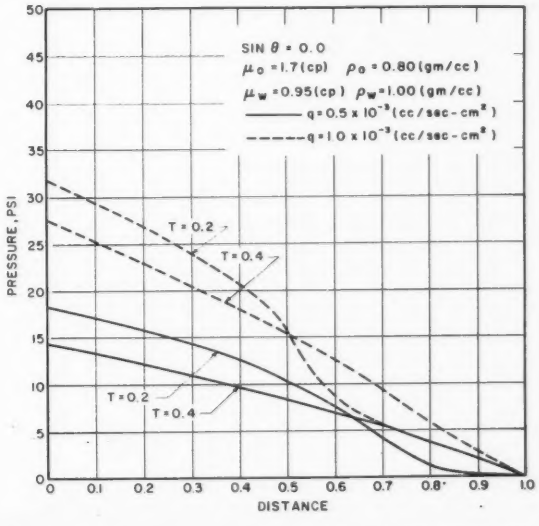

FIG. 7 – PRESSURE VS DISTANCE, WATER-WET SYSTEM.

N_g = gravity constant

P_o, P_w = pressure in oil and water phases (dyne/cm^2)

$\bar{p}_c$ = capillary pressure normalization constant (dyne/cm^2)

P_c = dimensionless capillary pressure

q_o, q_w = volumetric oil and water flow rates (cc/cm^2)/(sec)

$r(S)$ = transformed variable

S = water saturation

S_i = initial water saturation

S_{or} = residual oil saturation

S_{out} = saturation at the outflow boundary

t = time (sec)

T = dimensionless time (pore volume of water injected)

x = distance (cm)

X = dimensionless distance

Z = constant of transformation $= \int_{S_i}^{1-S_{or}} C(S)\,dS$

μ_o, μ_w = viscosity of oil and water (cp)

θ = angle of inclination

ϕ = porosity

ρ_o, ρ_w = density of oil and water (gm/cc)

REFERENCES

1. Buckley, L. E. and Leverett, M. C.: "Mechanism of Fluid Displacement in Sands", *Trans.*, AIME (1942) Vol. 46, 107.
2. Terwilliger, P. L., Wilsey, L. E., Hall, H. N., Bridges, P. M. and Morse, R. A.: "An Experimental and Theoretical Investigation of Gravity Drainage Performance", *Trans.*, AIME (1951) Vol. 192, 258.
3. Welge, H. J.: "Simplified Method for Computing Oil Recovery by Gas or Water Drive", *Trans.*, AIME (1952) Vol. 195, 91.
4. Douglas, Jim, Jr., Blair, P. M. and Wagner, R. J.: "Calculation of Linear Waterflood Behavior Including the Effects of Capillary Pressure", *Trans.*, AIME (1958) Vol. 213, 96.
5. Fayers, F. J. and Sheldon, J. W.: "The Effect of Capillary Pressure and Gravity on Two-Phase Fluid Flow in a Porous Medium", *Trans.*, AIME (1959) Vol. 216, 147.
6. Carslaw, H. S. and Jaeger, J. E.: *Conduction of Heat in Solids*, Oxford U. Press (1959) 10.
7. Richtmyer, R. D.: *Difference Methods for Initial Value Problems*, Interscience Publishers, Inc., N. Y. (1957).
8. Kunz, K. S.: *Numerical Analysis*, McGraw-Hill Book Co., Inc., N. Y. (1957).
9. Perkins, F. M.: "An Investigation of the Role of Capillary Forces in Laboratory Water Floods", *Trans.*, AIME (1957) Vol. 210, 409.

***

Thermal Conductivities of Porous Rocks Filled with Stagnant Fluid

D. KUNII — U. OF TOKYO, TOKYO, JAPAN

J. M. SMITH — NORTHWESTERN U., EVANSTON, ILL.

ABSTRACT

Effective thermal conductivities of sandstones filled with stagnant fluids were measured using a steady-state technique. Data were obtained for seven sandstone samples, taken from four different locations and ranging in permeability from 18 to 590 md. The measurements with gases (helium, nitrogen, air and carbon dioxide) covered a pressure range from 0.039 psia to 400 psig. Data were taken for four liquids — n-heptane, methyl alcohol, 79.8 weight per cent glycerol-water solution and pure water at atmospheric pressure.

The experimental results were used to evaluate the theoretical equations for predicting stagnant conductivities developed earlier.[4] The low-pressure measurements permitted evaluation of the consolidation parameter $h_p D_p/k_s$ (necessary to utilize the theory) for the various types of sandstones. Using these characteristic values, the theoretical equations correlated well with the experimental conductivity data for the several fluids and rock samples.

INTRODUCTION

An aspect of heat transfer in solid-fluid systems of considerable current interest is the effective thermal conductivity of porous media. The stimulus for study of the subject arises from the need for sound procedures for designing thermal methods of petroleum production. The general system occurs when there exists a flow of fluid through the pores of the solid material. However, a logical starting point in developing a theory for predicting the effective thermal conductivity in the general system is to attack the special case when the porous solid is filled with stagnant fluid. Since the flow rates anticipated in thermal production processes are very low, such stagnant conductivities k_e° are also of practical significance.

Original manuscript received in Society of Petroleum Engineers Office Aug. 2, 1960. Revised manuscript received Nov. 4, 1960. Paper presented at Joint AIChE-SPE Symposium, Sept. 22-25, 1960, in Tulsa.

[4]References given at end of paper.

Kunii and Smith[4] recently reviewed the existing data for stagnant conductivities and proposed a theory for heat transfer in porous rocks. This leads to equations for predicting the stagnant conductivity as a function of the properties of the fluid and solid phases. The existing experimental information[1-3,5,7,8] covered a range of porosities and agreed well with the theory. However, the available data were insufficient to examine critically the effects of two important properties on k_e° — the thermal conductivity of the fluid and the pressure. The objectives of the present study are twofold: (1) to measure the effect on k_e° of (a) the pressure for gases, and (b) the thermal conductivity of the fluid k_g for both gases and liquids; and (2) to determine for rocks of different porosities and permeabilities the apparent solid conductivity k_s and the consolidation parameter $h_p D_p/k_s$ required in applying the theoretical equations.

Measurements extrapolated to zero pressure are helpful in evaluating k_s and the consolidation parameter. However, the extrapolations must be based upon data obtained at low pressures because in small pores the molecular conductivity of the fluid may be unusually depressed. This occurs when the mean free path of the molecules is of the same order of magnitude as the pore diameter, that is, in small-diameter pores at low pressures. The phenomenon has been studied recently by Schotte[6] in beds of unconsolidated fine particles. With particles in the size range of 45 to 200 microns, a significant reduction of k_g with pressure was found even at absolute pressures greater than 1 atm. In the sandstones employed in the present investigation, pore diameters lower than those experienced by Schotte are likely, so that the effect would presumably be greater.

SCOPE OF MEASUREMENTS

Stagnant conductivities were measured for four types of sandstones using a total of seven samples. The characteristics of the samples, including porosity and permeability values, are given in Table

1.

Four gases were employed, data being obtained with nitrogen, helium and carbon dioxide at pressures above atmospheric; all sub-atmospheric data were determined using air. To provide a reasonably wide range of fluid thermal conductivity, measurements also were made using four fluids – normal heptane, methyl alcohol, a solution of 79.8 weight per cent glycerol and 20.2 weight per cent water, and pure water. The range of k_g values obtained with these seven fluids is approximately 0.01 to 0.36 Btu/(hr ft °F).

The mean temperatures existing in the rock samples during the runs are given in Table 2 for each fluid.

EXPERIMENTAL

The apparatus for measuring the stagnant conductivity is shown in Fig. 1. The test section consisted of two cylindrical cores, each 1 in. in diameter and about 1 3/8 in. in length. To reduce longitudinal heat transfer, one additional core sample of the same dimensions was used on each end of the test section. The conductivity was determined in the radial direction of the cylindrical cores, that is, in the direction parallel to the plane of the sandstone formation.

To introduce a radial temperature gradient, an electric heater was made by winding 30-gauge nichrome wire around a flexible rod. This rod was inserted into holes 0.093 in. in diameter drilled through the central axis of the core samples. The power input in the test section was determined with a Weston Wattmeter (Model #432) with an accuracy of 0.5 w. The measurement was made by attaching electrical leads to the heater wire across the length of the test section (approximately 2 3/4 in.) Fine sand was used between the test cores and the inner wall surface to adjust the position of the cores, as illustrated in Fig. 1. Cooling water was passed through a jacket surrounding the sample when runs were made with gases.

Copper-constantan thermocouples (30 B. and S. gauge) were used to measure the radial temperature gradient. The thermocouples were inserted in holes drilled in the end surface of the separate core sample as illustrated in Fig. 1. The holes, 0.027 in. in diameter, were drilled to a depth of 0.17 in. Three or four thermocouples were used across each of several radii, and their radial location was measured carefully to the nearest 0.1 mm.

For runs made with gases as the stagnant fluid, the temperatures were measured using a recorder with an expected accuracy of 0.5°F. The fluid was alternately added and evacuated from the test section several times before making thermal measurements. Fluid pressures on the sample at atmospheric pressure and above were measured with a mercury manometer or a Heisse gauge. Sub-atmospheric pressures were determined with a vacuum gauge.

A somewhat different procedure was employed with liquids. The solid cores, dried completely with an infra-red lamp, were first placed in a container half-filled with the required liquid. The remaining gas in the pores of the core was removed with a vacuum pump. Upon removal from the container, the samples were covered with scotch tape to prevent evaporation of fluid. Then, as quickly as possible, the thermocouples were inserted. The

TABLE 1 – POROUS ROCK SAMPLES USED

Boise Sandstone from Idaho Outcrop

Yellowish gray, medium-grained, argillaceous sandstone; micaceous, feldspathic, "pepper and salt" appearance; massive.
BO-1: porosity 0.248, permeability 590 md
BO-2: porosity 0.256

Bartlesville Sandstone from an Oklahoma Outcrop

Moderate yellowish brown, fine-grained, argillaceous sandstone; minor muscovite flakes, altered iron minerals, massive.
BA-2: porosity 0.203, permeability 28 md
BA-5: porosity 0.220

Berea Sandstone from Ohio Outcrop

Very light gray, fine-grained, clean, well sorted sandstone; massive.
BE-1: porosity 0.189, permeability 170 md
BE-2: porosity 0.185

Rangely (Colorado) Reservoir Rock

Olive gray, fine-grained, clean, well compacted sandstone.
RA: porosity 0.117, permeability 18 md

TABLE 2 – RANGE OF MEAN TEMPERATURES OF SANDSTONE SAMPLES DURING RUNS

	°F
Carbon Dioxide	140 to 200
Nitrogen	140 to 190
Helium	90 to 100
Normal Heptane	110 to 140
Methyl Alcohol	90 to 110
Glycerol*	130 to 160
Water	100 to 140

*79.8 wt. per cent glycerol and 20.2 wt. per cent water

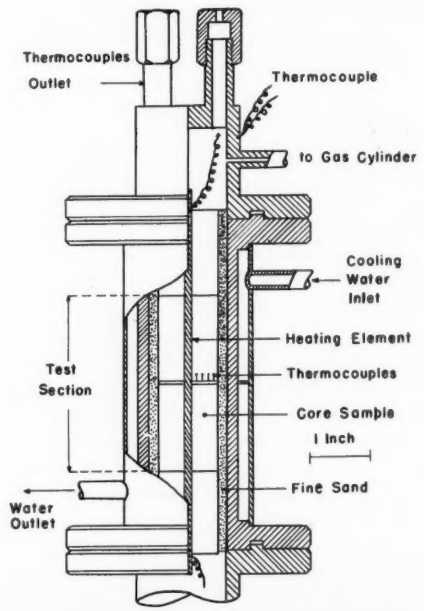

FIG. 1 – EXPERIMENTAL APPARATUS FOR GASES.

test element was then placed in a container filled with the required liquid. The entire unit was inserted in an ice-water, constant-temperature bath. Temperatures were determined for the runs with liquids using a precision portable potentiometer.

EVALUATION OF EXPERIMENTAL PROCEDURE

If longitudinal heat transfer in the core samples is negligible, the stagnant conductivity can be calculated from the measured radial temperature profile by the expression,

$$k^{\circ}_e = -\frac{Q}{2\pi L}\frac{d(\ln r)}{dT} \quad \ldots\ldots\ldots\ldots \quad (1)$$

Typical measurements for several fluids in Core Sample BE-1 are shown in Fig. 2. Within the precision of the data, a straight line relationship is observed. This suggests, according to Eq. 1, that the variation of k°_e with temperature across the radius of the sample is not sufficient to be measured by the experimental procedure used. Hence, a single mean value for k°_e is calculated from Eq. 1 using the slope of the line obtained from plots similar to those illustrated in Fig. 2.

To test the assumption of negligible longitudinal heat transfer, several preliminary measurements were made using Sample BA-5 with air. First, radial temperature profiles were observed and compared at the three contact surfaces (the ends of the cylindrical core samples) of the four core samples mounted in the apparatus (Fig. 1). These results indicated that approximately 0.4 per cent of the total energy input from the heater flowed out in the longitudinal direction.

As the energy input from the heater decreases, a point is ultimately reached when longitudinal heat losses will be significant. Preliminary measurements indicated that this energy level was about 10 w. All the runs were made at values of Q greater than this limiting value.

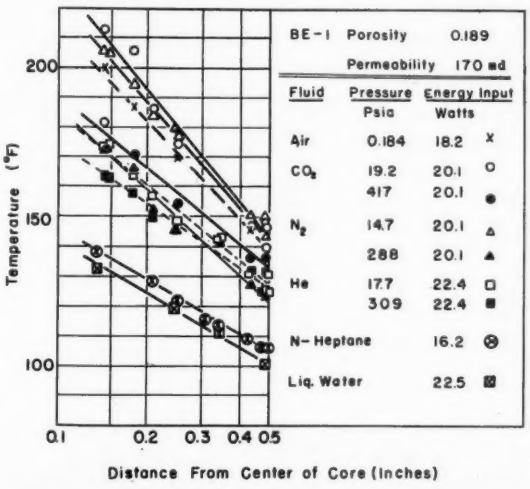

FIG. 2 – EXAMPLES-TEMPERATURE DISTRIBUTION IN CORE SAMPLE.

To test further the significance of longitudinal heat transfer, measurements were carried out when the ends of the apparatus were maintained at different temperatures with nichrome wire heaters. The energy input to the central heater was maintained at 15 w, leading to a mean core temperature of about 150°F. Under these conditions, varying the temperature of the ends of the apparatus from 70° to 200° F did not affect the stagnant conductivity.

From these preliminary tests it appeared that the equipment was satisfactory for measuring reasonably accurate values of k°_e. Considering errors in energy input, temperature and position measurements, and errors in applying Eq. 1, it is believed that the maximum uncertainty was less than 10 per cent.

RESULTS

EFFECT OF PRESSURE ON k°_e

The data showing the effect of pressure on k°_e for gases are plotted in Figs. 5 and 6 for pressures greater than 1 atm. Fig. 5 demonstrates that different core samples from the same sandstone formation (Bartlesville sandstone) do not exhibit significant differences in stagnant conductivity. On the other hand, the thermal conductivity of the gas is a significant factor; i.e., the results for helium are appreciably higher than those for nitrogen and carbon dioxide. In Fig. 6, data are plotted for three different types of sandstones, and here large differences are observed.

The small increase in k°_e with pressure at high pressures, shown in Figs. 3 and 4, is probably due to the small increase in the normal thermal conductivity of the gas with pressure. However, the more rapid change in k°_e with pressure at low values of P must be the result of another factor because the normal thermal conductivity is essentially constant at these pressures. This effect is more pronounced at sub-atmospheric pressures as demonstrated by the curves in Fig. 5 for air. The decrease in k°_e with pressure is most pronounced for the sample with the lowest porosity, Rangely sandstone (RA). This suggests that the fluid conductivity is being reduced by the small-diameter pores in the core samples. Schotte[6] has adapted equations based upon kinetic theory to show the effect of pressure on the apparent value of k_g in packed beds of fine particles (45 to 200 microns). One of his equations can be reduced to the following form to illustrate the effect of pressure P and pore size b.

$$k_g = \frac{k^{*}_g}{1 + C\,(T/pb)} \quad \ldots\ldots\ldots\ldots \quad (2)$$

Here, k^{*}_g is the normal thermal conductivity of the gas. For a given core sample at a fixed temperature, Eq. 2 indicates that k_g approaches the normal conductivity as P approaches a large value and that k_g approaches zero as P tends toward zero. This suggests that the stagnant thermal conductivity of the core (k°_e) would approach a constant value, equal to the contribution of the solid phase, as the pressure approaches zero. The S-shaped

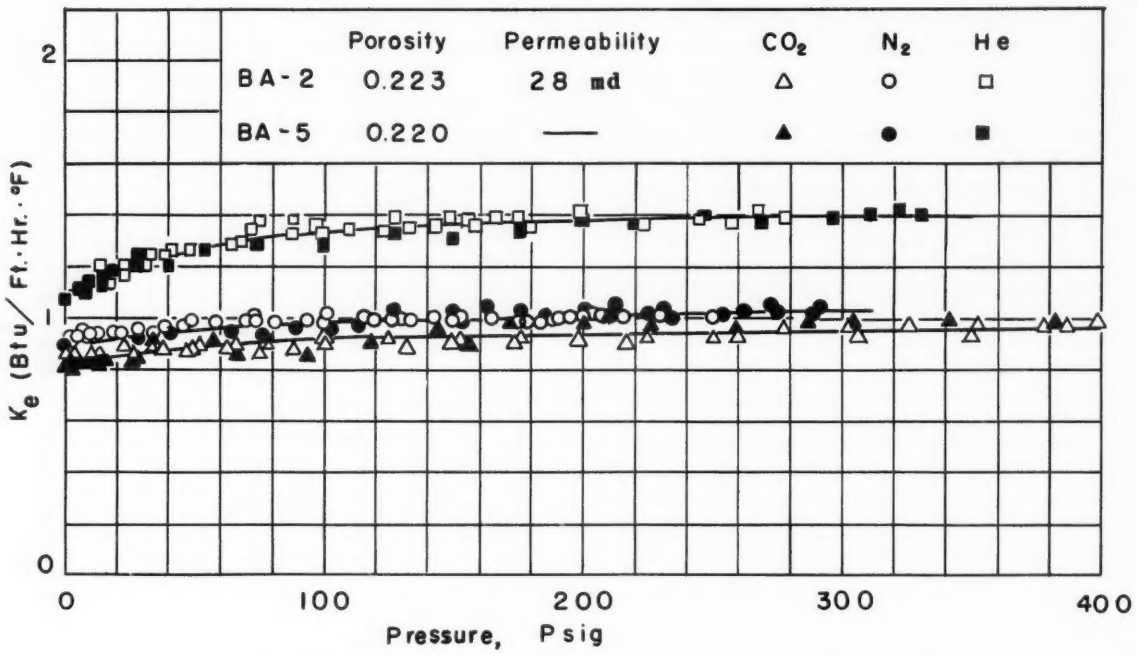

FIG. 3 – STAGNANT CONDUCTIVITIES OF BARTLESVILLE SANDSTONE.

behavior of the curves in Fig. 5 is in agreement with this reasoning. The significant conclusion here is that the solid contribution to the stagnant conductivity $(k^o_e)_o$ cannot be obtained by extrapolating to $P = 0$ data at above atmospheric pressure, such as shown in Figs. 3 and 4. Rather, measurements must be made under vacuum conditions to obtain $(k^o_e)_o$ by extrapolation. The values of this parameter, as determined from Fig. 5 for the four types of sandstone, are given in Table 3.

EVALUATION OF CONSOLIDATION PARAMETER

In Ref. 4, the following equation was proposed to predict the stagnant conductivity of porous rocks (radiation negligible).

$$\frac{k^o_e}{k_s} = \phi'\left(\frac{k_g}{k_s}\right) + \frac{(1-\phi')\left(1+\frac{\phi'}{\phi}a\right)}{1+\frac{\phi'/\phi}{\frac{1}{a}\left(\frac{k_g}{k_s}\right)+\frac{D_p b_p}{k_s}}} \quad \ldots \quad (3)$$

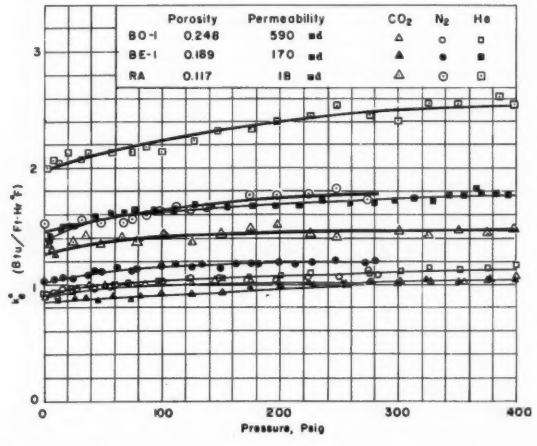

FIG. 4 – STAGNANT CONDUCTIVITIES OF SANDSTONES.

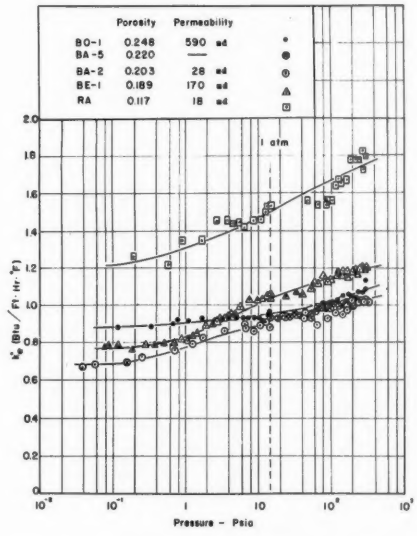

FIG. 5 – EFFECT OF PRESSURE ON STAGNANT CONDUCTIVITIES OF SANDSTONE DATA TAKEN BELOW ATMOSPHERIC WITH AIR AND DATA TAKEN ABOVE ATMOSPHERIC WITH NITROGEN.

The objective here is to use this expression and the experimental values of $(k^o_e)_o$ in Table 3 to determine the relationship between the apparent thermal conductivity of the solid phase k_s and the consolidation parameter $h_p D_p/k_s$. Both are characteristic properties of the sandstone sample. This is accomplished by considering Eq. 3 at zero pressure where k_g approaches zero. From the equations in Ref. 4, the following limiting results are readily obtained.

$$\lim_{k_g \to 0} \left(\frac{1}{a} \frac{k_g}{k_s} \right) = 0 \quad \ldots\ldots\ldots\ldots (4)$$

and

$$\lim_{k_g \to 0} a = 0 \quad \ldots\ldots\ldots\ldots (5)$$

The value of ϵ, the void fraction of the original bed of unconsolidated particles prior to consolidation, is suggested in Ref. 4 to be 0.476. This is the maximum void fraction in a uniform arrangement of spherical particles in contact. Using this result and Eqs. 4 and 5, the general expression (Eq. 3) for k^o_e/k_s reduces at zero pressure to the form,

$$(k^o_e)_o/k_s = \frac{1 - \phi'}{1 + \frac{\phi'}{\phi} \Big/ \left(\frac{D_p h_p}{k_s} \right)} \quad \ldots\ldots (6)$$

This equation provides a relationship between k_s and $D_p h_p/k_s$. If k_s were known, $D_p h_p/k_s$ could be determined from $(k^o_e)_o$ and Eq. 6. However, k_s is not necessarily the thermal conductivity of the pure solid phase (for example, quartz for sandstone cores). It may differ from this due to the non-uniform geometry of the solid phase and due to impurities between the grains of solid particles and the cementing material holding the grains together.

This problem is avoided by utilizing the experimental data for the effect of k_g on k^o_e, along with Eq. 6, to ascertain separate values for k_s and $D_p h_p/k_s$. The experimental data for the several fluids and sandstone samples are shown in Figs. 6 through 8. The curves on the figures represent Eq. 3 plotted for certain values of k_s and $D_p h_p/k_s$. These specific values were obtained in the following way.

1. Sets of consistent numbers for k_s and $D_p h_p/k_s$ were first determined from Eq. 6.

2. The most appropriate set was then obtained for each type of sandstone by comparison with the experimental data in Figs. 6 through 8.

Figs. 6 and 7 include calculated curves for three sets of k_s and $h_p D_p/k_s$, designated on the curves by the numerical value for k_s. These results indicate that it is not possible to determine k_s more closely than approximately ± 0.2 Btu/(hr ft °F).

TABLE 3 – THERMAL PROPERTIES OF SANDSTONE

Sandstone Sample	$(k^o_e)_o$ Btu/ft hr °F	k_s Btu/ft hr °F	$\frac{D_p h_p}{k_s}$
BO	0.88	1.8	0.965
BA	0.69	3.2	0.159
BE	0.77	4.6	0.103
RA	1.22	4.6	0.105

The values of the two parameters so evaluated are shown in the last two columns of Table 3.

It is interesting to note that these parameters are essentially the same for the BE and RA sandstones. The difference in stagnant conductivity between the two types of rock must be due primarily to the difference in porosities. Visual examination of the Boise (BO) sandstone suggests that it has a markedly different structure from the other types. It seems to be well consolidated with somewhat larger pore diameters than those associated with the other sandstones. This micaceous and feldspathic structure is probably responsible for the low value of k_s (Table 3) determined for the Boise sample.

CORRELATION AND PREDICTION OF STAGNANT CONDUCTIVITIES

For Eq. 3 to be a useful prediction method for k^o_e, it is necessary that values of k_s and $D_p h_p/k_s$ be available. At present these values cannot be obtained except by experimental means. Until data such as that shown in Table 3 are available for a large variety of rock samples, the method is not valuable for prediction purposes. However, the agreement in Figs. 6 through 8 between experimental

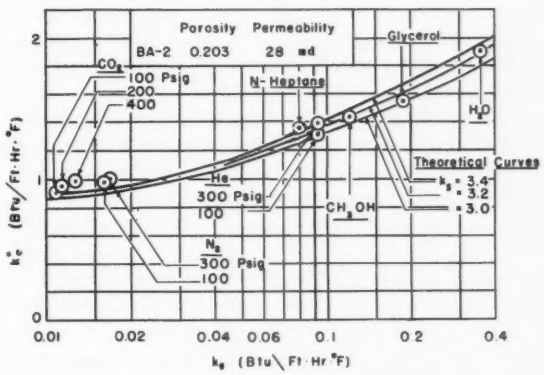

FIG. 6 – STAGNANT CONDUCTIVITIES VS CONDUCTIVITIES OF FLUIDS, BARTLESVILLE SANDSTONE.

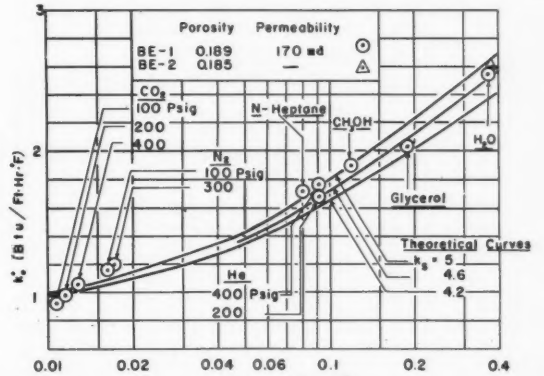

FIG. 7 – STAGNANT CONDUCTIVITIES VS CONDUCTIVITIES OF FLUIDS, BEREA SANDSTONE.

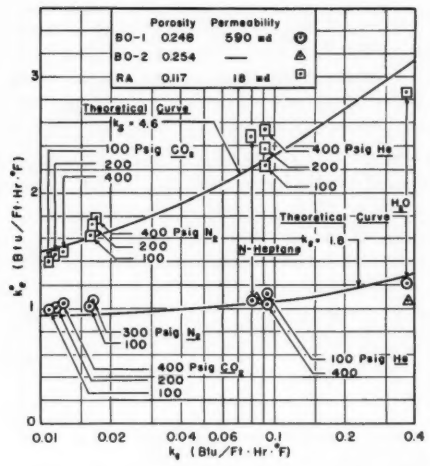

FIG. 8 – STAGNANT CONDUCTIVITIES VS CONDUCTIVITIES OF FLUIDS, BOISE AND RANGELY SANDSTONES.

data and Eq. 3 suggests that the procedure correctly accounts for the effects of properties of the rock and fluid, such as void fraction and fluid conductivity k_g. Hence Eq. 3 is useful now as a means of predicting the effect of these properties on k_e and requires no experimental data for this use. The method is also valuable for correlating experimental k_e information.

Of the data in the literature, only that of Zierfuss and Vliet[8] included information on the effect of different fluid conductivities. Their conductivity results for air and liquid water showed increases in k^o_e with k_g of the same magnitude as indicated in Figs. 6 through 8. Data were presented for only these two fluids with known thermal conductivities, and no information was given at low pressures. Hence, it was not possible to evaluate $(k^o_e)_o$ and make a quantitative analysis of their results according to Eq. 3.

NOMENCLATURE

b = distance over which conduction takes place (i.e., pore diameter), ft
C = constant, (psi)(ft)(1/°R)
$D_p b_p / k_s$ = dimensionless consolidation parameter for expressing the heat transfer in the solid phase (see Ref. 4)
k^o_e = stagnant conductivity, Btu/(ft)(hr)(°F)
$(k^o_e)_o$ = asymptotic value of stagnant conductivity corresponding to zero thermal conductivity of gas phase (i.e., zero pressure), Btu/(ft)(hr)(°F)
k_g = apparent thermal conductivity of gas, Btu/(ft)(hr)(°F)
k^*_g = normal thermal conductivity of gas, Btu/(ft)(hr)(°F)
k_s = apparent thermal conductivity of solid phase, Btu/(ft)(hr)(°F)
L = length of test section, ft (approximately 2 3/4 in.)
p = absolute pressure, lb/sq ft
r = radial distance, measured from center of core, ft
Q = energy input in the test section, Btu/hr
T = absolute temperature, °R
a = ratio of effective thickness of the fluid film adjacent to the contact surface of two solid particles in the original packed bed (prediction of ϕ is described in Ref. 4)
ϕ = void fraction of original packed bed of unconsolidated particles
ϕ' = porosity of sandstone
$\frac{d \ln r}{d T}$ = slope of temperature vs radial distance line plotted as $\ln r$ vs T (Fig. 2), °R^{-1}

ACKNOWLEDGMENT

The authors wish to express their appreciation for the financial assistance of the California Research Corp., Petroleum Research Fund (American Chemical Society) and the Socony-Mobil Oil Co. J. P. Mason assisted in some of the experimental work.

REFERENCES

1. Asaad, T.: Ph.D. Thesis, U. of California, Berkeley (June, 1955).
2. Birch, F. and Clark, H.: *Am. Jour. Sci.* (1940) Vol. 238, 529.
3. Clark, H.: *Trans.*, Am. Geophys. Union (1940) 543.
4. Kunii, D. and Smith, J. M.: *AIChE Jour.* (1960) Vol. 6, 71.
5. Niven, C. D.: *Can. Jour. Research* (1940) Vol. 18, 132.
6. Schotte, W.: *AIChE Jour.* (1960) Vol. 6, 63.
7. Somerton, W. H.: "A Laboratory Study of Rock Breakage by Rotary Drilling", *Trans.*, AIME (1958) Vol. 213, 375.
8. Zierfuss, H. and Vliet, G.: *Bull.*, AAPG (1958) Vol. 40, No. 10, 2475.

***

A Study of the Behavior of Bounded Reservoirs Composed of Stratified Layers

H. C. LEFKOVITS
P. HAZEBROEK
E. E. ALLEN
C. S. MATTHEWS
MEMBER AIME

SHELL DEVELOPMENT CO.
HOUSTON, TEX.

ABSTRACT

A rigorous study was made of the behavior of reservoirs composed of horizontal layers, unconnected except at the well and filled with a compressible fluid. The report is presented in two parts. Part I deals with the practical implications of the results obtained; Part II contains the mathematical derivation of the solution. The main portion of Part I is concerned with application of the results to reservoirs composed of two layers. Relative rates of depletion of the layers are studied, and it is shown that differential depletion between layers exists in the transient stage of the reservoir, which generally is of an order of magnitude longer than the transient stage in a single-layer reservoir. In the transient stage, the more permeable layer is depleted faster than the less permeable. However, the reservoir approaches a steady-state situation where both layers contribute equally to production. Theoretical build-up curves from such reservoirs are presented, and the influence of a skin effect and flow into casing and tubing are also evaluated. The build-up curves are predicted to have, first, the familiar logarithmic straight-line section and, subsequently, a rising and flattened section. The results found are compared with an extension of an approximate theory, and it is found that this simplified theory is applicable over most of the life of the reservoir. Extensions to reservoirs containing more than two layers are indicated, and examples of the performance and build-up curves for three-layered reservoirs are presented. The theoretical results on build-up curves were applied to field examples of such reservoirs, and satisfactory results were obtained. From the build-up curve, the permeability-thickness product, the wellbore damage and the static pressure are obtained. However, it apparently is not possible to determine the properties of the individual layers from the combined build-up curve.

Original manuscript received in Society of Petroleum Engineers office July 9, 1959. Revised manuscript received March 2, 1960. Paper presented at 34th Annual Fall Meeting of SPE, Oct. 4-7, 1959, in Dallas.

PART I — PRACTICAL APPLICATIONS

INTRODUCTION

A large number of reservoirs have been found where the producing formation is composed of two or more layers of differing physical characteristics, such as permeability and porosity, and where also the thicknesses of the layers differ. Since in general a differential depletion should exist between the layers of such reservoirs, it would be advantageous to know the amount of the differential depletion under a given production history. It also would be valuable to know the pressure behavior, because it could be undesirable to produce a reservoir in such a manner that the pressure in one of the layers would have fallen below the bubble point of the oil at a time when another layer might still be virtually undepleted.

The determination of static pressures in shut-in wells with slow build-up is another feature of importance in layered reservoirs. If the behavior of the reservoir differs appreciably from the predicted behavior of a single-layer reservoir, the type of analysis for build-up curves suggested for single-layer reservoirs is not applicable.

Several authors have treated the problem of finding the pressure and production characteristics of multilayer reservoirs. Horner[1] treated the problem of n layers in an infinite field, the layers being connected only at the well. Tempelaar-Lietz[2] has presented an approximate treatment of the characteristics of a bounded reservoir composed of two layers of different permeabilities and equal thicknesses. Horner gave no information on differential depletion between layers, and the treatment of Tempelaar-Lietz was not applicable for prediction of pressure build-up behavior. In addition, it was thought that a more rigorous treatment than the one by Tempelaar-Lietz would be valuable in determining the range of validity of this solution. The present study, therefore, was made of a bounded reservoir composed of two or more layers,

[1]References given at end of paper.

these layers being unconnected except at the well.

BASIC ASSUMPTIONS

The reservoir to be studied is shown in Fig. 1. Each layer of the reservoir is assumed to be homogeneous and isotropic, and filled with a fluid of small and constant compressibility c. The permeability k, oil-filled porosity ϕ and thickness h of each layer are designated by the corresponding symbol with the subscript 1, 2, ..., n, depending on which layer is referenced. The viscosity of the oil is assumed to be constant and is denoted by μ. The reservoir is initially at a uniform pressure p_o; and at all times $t > 0$, the fluid is produced in such a manner that the production rate q_T, measured at initial reservoir conditions, is held constant.

Under these assumptions, the pressure at any point must satisfy the well known equation for flow of a fluid of small but constant compressibility given in Part II. The solution of this equation for the proper boundary conditions is obtained with the aid of the Laplace transform.

DISCUSSION OF RESULTS

FLOWING-WELL PERFORMANCE

For all but very small times, the solution to the differential equation leads to the following results:

$$p_i - p_w(t) = \frac{q_T}{2\pi}\left[\frac{2t}{\sum_{j=1}^{n} h_j \phi_j r_e^2 c} + \frac{\sum_{j=1}^{n} \frac{\phi_j^2 h_j \mu}{k_j}\left(\ln\frac{r_e}{r_w} - \frac{3}{4}\right)}{\left(\sum_{j=1}^{n} \phi_j h_j\right)^2}\right] + Y(t) \quad \ldots\ldots\ldots\ldots\ldots\ldots\ldots\ldots (1)$$

and

$$q_j(t) = q_T \frac{\phi_j h_j}{\sum_{j=1}^{n} \phi_j h_j} + Z_j(t) , \quad \ldots\ldots\ldots\ldots\ldots\ldots\ldots\ldots (2)$$

where $Y(t)$ and $Z_j(t)$ are transients which approach zero with increasing time. Both of these functions are directly proportional to q_T.

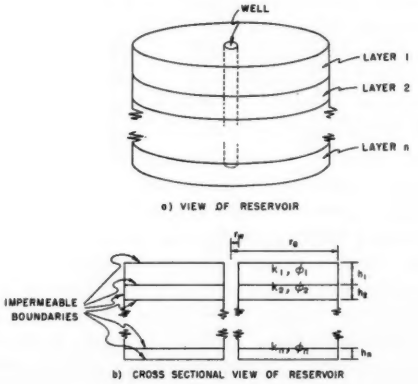

FIG. 1 – THE RESERVOIR.

For the case of two layers, these equations can be rewritten as

$$\frac{p_i - p_w(t)}{q_T\mu/4\pi\bar{k}\bar{h}} = 4\frac{r_w^2}{r_e^2}\, t_D + 2\left(\ln\frac{r_e}{r_w} - \frac{3}{4}\right)\frac{\left(1 + \frac{k_2 b_2}{k_1 b_1}\right)\left\{\left(\frac{b_1\phi_1}{b_2\phi_2}\right)^2 + \frac{b_1 k_1}{b_2 k_2}\right\}}{\left(1 + \frac{b_1\phi_1}{b_2\phi_2}\right)^2} + \frac{Y(t)}{q_T\mu/4\pi\bar{k}\bar{h}} \quad \ldots\ldots\ldots\ldots\ldots\ldots (3)$$

and

$$q_1(t) = q_T\frac{\phi_1 b_1}{\phi_1 b_1 + \phi_2 b_2} + Z_1(t) , \quad \ldots\ldots\ldots\ldots\ldots\ldots (4)$$

where $\bar{k} = (k_1 b_1 + k_2 b_2)/(b_1 + b_2)$,

$\bar{\phi} = (\phi_1 b_1 + \phi_2 b_2)/(b_1 + b_2)$,

$\bar{h} = b_1 + b_2$,

$t_D = \bar{k}t/\bar{\phi}\mu c r_w^2$.

For early times at which the influence of the boundary has not been felt, the expression

$$\frac{p_i - p_w(t)}{q_T\mu/4\pi\bar{k}\bar{h}} = \ln t - \ln\gamma - \frac{k_1 b_1 \ln\frac{\phi_1\mu c r_w^2}{4k_1} + k_2 b_2 \ln\frac{\phi_2\mu c r_w^2}{4k_2}}{k_1 b_1 + k_2 b_2} \quad \ldots\ldots (5)$$

gives the correct pressure behavior at the well, γ denoting Euler's constant. The lower limit of the time range of validity of this equation is small enough to include most times of practical interest.

From Eqs. 3 and 4 it can be seen that a steady state is finally attained in the reservoir, during which the rate of change of the well pressure with respect to time (i.e., dp_w/dt) is constant. Furthermore, at this time the production rate from each layer becomes constant, and it then follows that the pressure everywhere within the reservoir varies linearly with time.

Solutions for two sample cases for two sets of parameters are presented in Figs. 2 and 3. The curves labeled I correspond to the parameters

$$\frac{k_1}{k_2} = 10 , \qquad \frac{\phi_1}{\phi_2} = 1 ,$$

$$\frac{b_1}{b_2} = 1 , \qquad \frac{r_e}{r_w} = 2{,}000 ;$$

whereas, the curves labeled II correspond to the parameters

$$\frac{k_1}{k_2} = 1.25 , \qquad \frac{\phi_1}{\phi_2} = 1 ,$$

$$\frac{b_1}{b_2} = 1 , \qquad \frac{r_e}{r_w} = 2{,}000 ;$$

Fig. 2 shows the pressure behavior at the well. Eq. 5 was used in calculating this behavior for $t_D < 10^6$. During this first period, the pressure decreases logarithmically with time. Physically, this

time range corresponds to the time during which the well has not detectably influenced the pressure at the outer drainage boundary. Hence, the pressure decline at the well is identical to the decline of a well draining an infinite reservoir. The time at which the influence of the drainage boundary is first detected at the well is characterized by the break of the pressure curve away from the straight-line portion of the curve. Now the reservoir produces as if it were composed of one bounded layer and one infinite layer because the influence of the boundary has been reflected only in the more permeable layer. After some time, the less permeable layer also feels its boundary. From then on, the reservoir behaves as a fully bounded reservoir. Steady state, where the relation between p_w and t would be a straight line if plotted on a linear scale, is reached some time thereafter. The dotted lines in Fig. 2 are the approximations given by the method of Tempelaar-Lietz and will be discussed in a later section.

The magnitude of the time necessary to reach steady state in a two-layer reservoir can be compared with the corresponding time for a single-layer reservoir. Matthews and Brons[3] have shown that for a cylindrical reservoir steady state is reached at a dimensionless time

$$\frac{kt}{\phi\mu c r_e^2} \simeq 0.3 \ ,$$

If $r_e/r_w = 2{,}000$, then steady state is reached at

$$\frac{kt}{\phi\mu c r_w^2} \simeq 1.2 \times 10^6$$

In a two-layer reservoir, the dimensionless time needed to reach steady state varies with the properties of the two layers; the average of the cases studied in this report is about

$$\frac{\bar{k}t}{\bar{\phi}\mu c r_w^2} \simeq 8 \times 10^7 \ .$$

Hence, the time needed to reach steady state is of the order of 50 times as great as the corresponding time for a single-layer reservoir. The reason for

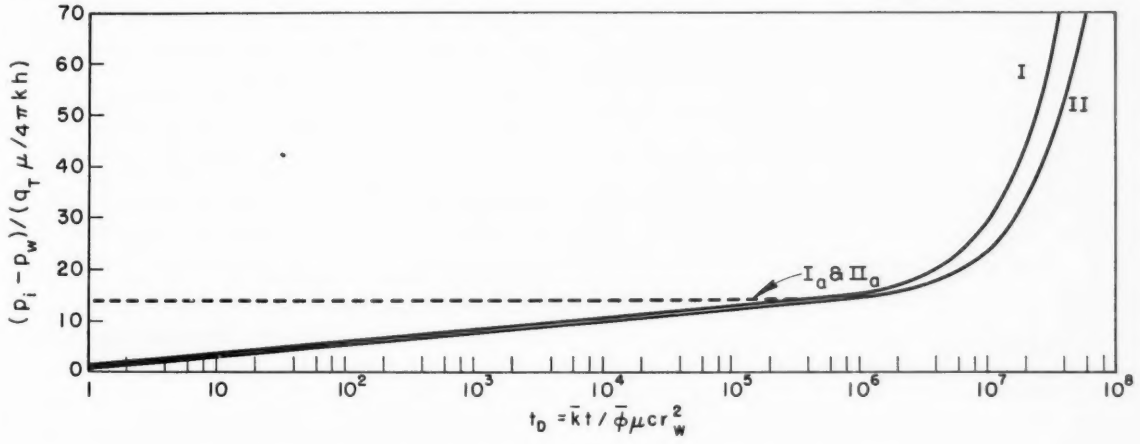

FIG. 2 – WELL PRESSURE-DECLINE CURVES FOR TWO-LAYER RESERVOIRS.

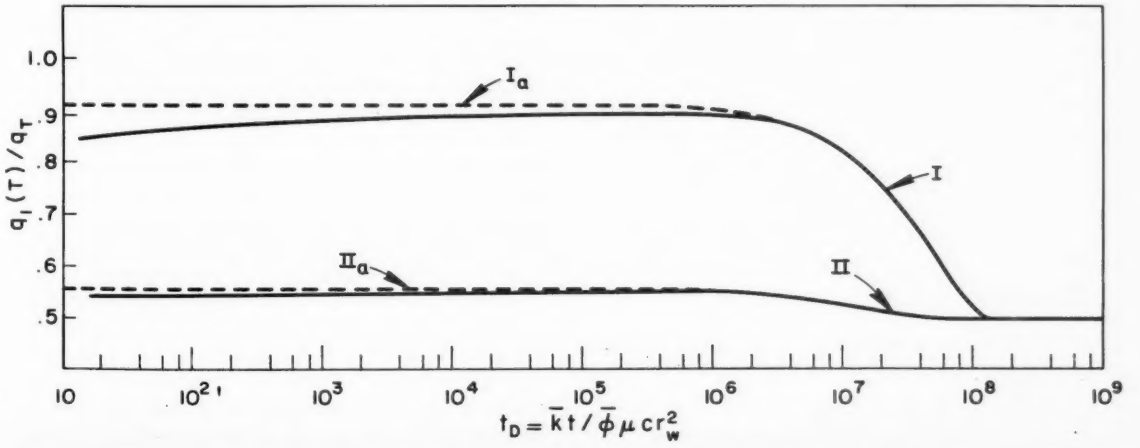

FIG. 3 – FRACTIONAL PRODUCTION RATES FROM THE MORE PERMEABLE LAYER OF TWO 2-LAYER RESERVOIRS.

this lies mainly in the changing rates of production from the layers in the multilayer case.

The behavior of the production rate for these two cases is shown in Fig. 3, in each instance for the more permeable layer. The ordinate in the graph is $q_1(t)/q_T$, the fractional production rate from this layer. The dotted lines again are the approximations of Tempelaar-Lietz. The fractional production rate from the other layer $q_2(t)/q_T$ can be obtained from the relation

$$\frac{q_2(t)}{q_T} = 1 - \frac{q_1(t)}{q_T}.$$

At early times, the production rate from the more permeable layer is increasing; it approaches asymptotically the value $q_1(t)/q_T = k_1b_1/(k_1b_1 + k_2b_2)$, which behavior corresponds to the case of a well draining an infinite reservoir. After the initial increase, the production rate begins to decrease, a phenomenon which corresponds to the physical fact that the influence of the boundary in the more permeable layer has been reflected on the behavior of the reservoir. At some later time, the effect of the boundary is also felt in the less permeable layer; subsequent to this time, the curves are seen to approach asymptotically a constant value, this value being $q_1(t)/q_T = b_1\phi_1/(b_1\phi_1 + b_2\phi_2)$. This value is the fractional production rate of Layer 1 at steady state.

The ratio $b_1\phi_1/(b_1\phi_1 + b_2\phi_2)$ is equal to the ratio of the oil-filled volume of Layer 1 to the oil-filled volume of the entire reservoir; hence, at steady state, each layer produces at a fractional rate equal to the fraction of oil-filled volume it contains.

With regard to fractional depletion between the layers, if each layer always produced at a fractional rate proportional to the oil-filled volume it contains, there would be no differential depletion. Hence, during production of a reservoir, differential depletion takes place previous to the time when steady state is reached.

The total production rate q_T from the reservoir is an important factor in the differential depletion of the reservoir. The time required to reach steady state is essentially independent of q_T, but the cumulative production from each layer is directly proportional to q_T. If $Q_1(t)$ and $Q_2(t)$ denote the cumulative production at the time t from Layers 1 and 2, respectively,

$$\frac{Q_1(t)}{b_1} = \int_0^t \frac{q_1(t)}{b_1}\,dt,$$

$$\frac{Q_2(t)}{b_2} = \int_0^t \frac{q_2(t)}{b_2}\,dt.$$

Also, the differential depletion $\Delta D(t)$ per unit thickness is then defined as

$$\Delta D(t) = \left| \frac{Q_1(t)}{b_1} - \frac{Q_2(t)}{b_2} \right|.$$

But we can also write

$$\frac{Q_j(t)}{b_j} = q_T \int_0^t \frac{q_j(t)}{b_j q_T}\,dt, \qquad j = 1, 2,$$

so that

$$\Delta D(t) = q_T \left| \int_0^t \frac{q_1(t)}{b_1 q_T}\,dt - \int_0^t \frac{q_2(t)}{b_2 q_T}\,dt \right| \quad . \quad . \quad . \quad (6)$$

Since the ratios $q_1(t)/q_T$ and $q_2(t)/q_T$ are independent of q_T, the differential depletion is directly proportional to q_T. For example, if the maximum differential depletion in a reservoir produced at a rate q_T is ΔD and if the reservoir had been produced at a rate $2\,q_T$, the maximum differential depletion would have been $2\Delta D$.

The results from another sample case are presented in Figs. 4 and 5. The properties of the layers are $k_1/k_2 = 4$, $b_1/b_2 = 0.05$ and $\phi_1/\phi_2 = 2$. The results are presented for four different values of r_e/r_w — r_e/r_w = 2,000, 1,000, 100 and 10. Fig. 4 shows the well pressure behavior as a function of production time; the straight-line portion again corresponds to the time range when the influence of the boundary has not been felt at the well, and the deviation from this straight line corresponds to the influence of the boundary.

The times at which the pressure-decline curves deviate from the straight-line portion increase with with the dimensions of the reservoir. This is because the time required (t_r) for the pressure disturbance caused by the opening of the well to reach a certain point (r) away from the well increases with the distance of the point from the well. A good approximation is given by $t_r \propto r^2$.

Fig. 5 shows the fractional production rate from the more permeable layer for several ratios r_e/r_w for the properties just mentioned.

THEORETICAL PRESSURE BUILD-UP CURVES

Since the behavior of the reservoir is described by linear differential equations, the behavior during build-up can be obtained by superposition. Fig. 6 shows a typical theoretical pressure build-up curve obtained from a two-layer reservoir. As in a single-layer reservoir, there is an initial straight-line section, AB. After the straight-line portion, the build-up curve levels off (BC), this leveling off corresponding in a single-layer reservoir to the pressure's having almost reached its average pressure. However, in a multilayer reservoir the pressure again rises (CD) and then finally levels off at the average pressure (DE). The rise in CD is due to the repressuring of the more depleted, permeable layer by the less depleted, less permeable layer.

Several other examples of pressure build-up curves are presented in Figs. 7 through 10, the parameters for each reservoir being indicated on the same page as the graph. Figs. 7 and 8 present pressure build-up curves, plotted both against Δt, the shut-in time and against $\Delta t/(t + \Delta t)$. Figs. 7 and 8 are at a closed-in time when the reservoir is still in the stage where the influence of the boundary has not

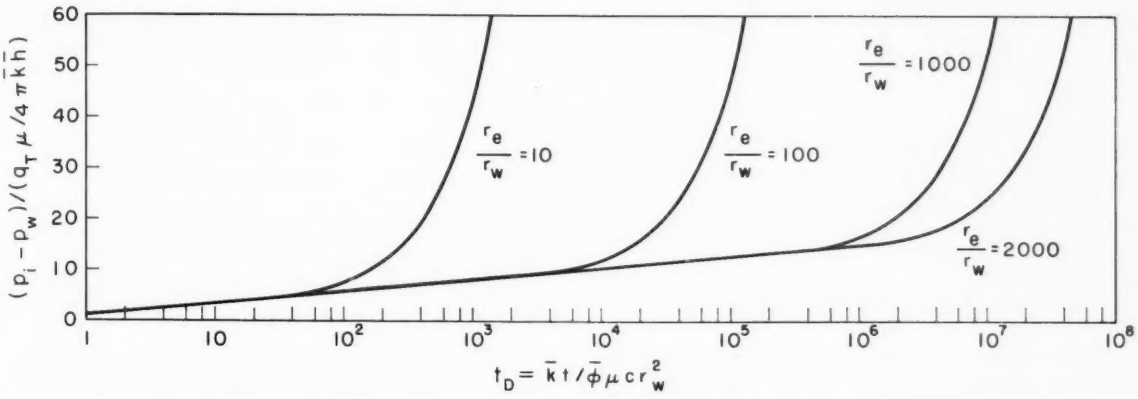

FIG. 4 – WELL PRESSURE-DECLINE CURVES FOR A TWO-LAYER RESERVOIR FOR DIFFERENT RATIOS OF r_e/r_w.

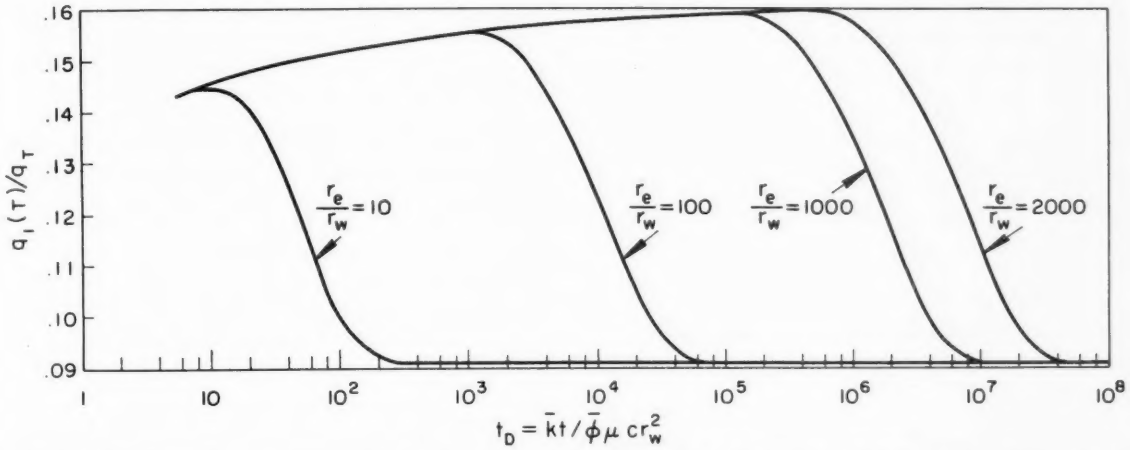

FIG. 5 – FRACTIONAL PRODUCTION RATES FROM MORE PERMEABLE LAYER OF A TWO-LAYER RESERVOIR FOR DIFFERENT RATIOS OF r_e/r_w.

been felt during production. Fig. 9 is a build-up curve for the same reservoir at a closed-in time when the influence of the boundary has been felt. From these curves, it can be seen that the entire portion CDE (as in Fig. 6) expands greatly in vertical scale with increasing production time.

The magnitude of the pressure rise during the portion CDE of the pressure build-up curve depends on the contrast of the properties of the layers. If the two layers are nearly equal in permeability, the pressure rise in this portion will be small (see Fig. 10), whereas if the two layers differ widely in properties, the pressure rise will be considerable (see Fig. 9).

For equivalent information, a well in a multilayer reservoir must remain shut in longer than a well in a single-layer reservoir, the ratio of required shut-in times being roughly equal to the ratio of the times needed to attain steady state in the two reservoirs. It was seen that this latter ratio is large (of the order of 50); it then follows that wells producing from multilayer reservoirs may have to remain shut in for considerable times to provide useful pressure build-up data.

A reason for the difference in type of pressure build-up curves obtained from two-layer and single-layer reservoirs is that in a two-layer reservoir flow occurs from one layer to the other during build-up. There is differential depletion between the layers, the more permeable layer having been depleted more than the less permeable layer; when the well is shut in, there must be flow from the

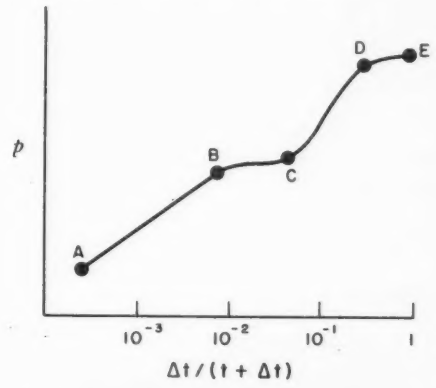

FIG. 6 – THEORETICAL PRESSURE BUILD-UP CURVE FOR TWO-LAYER RESERVOIR.

less permeable layer to the more permeable layer for the pressure to stabilize over the entire reservoir.

SKIN EFFECT

In the study of skin effects, the skin factor S_j in each layer was defined by means of the equations

$$S_j = \frac{p_{fj} - p_w}{q_j(t)\mu/2\pi k_j b_j}, \quad j = 1, 2, \ldots, n \quad . \quad . \quad (7)$$

where p_{fj} denotes the formation pressure in the jth layer.

The mathematical analysis of the problem showed that the effect of the skin could be represented by a fictitious well radius in each layer. Eqs. 1 and 2 were modified to include these characteristics.

The effect of introducing a fictitious well radius can best be illustrated for the case of a single-layer reservoir producing at a constant rate. As shown in Fig. 11, the skin will cause a discontinuity in the pressure at the well. The behavior of the pressure in the vicinity of the well is logarithmic; if the curve is extrapolated logarithmically (the dotted line in Fig. 11), there exists a point r^*_w such that $p(r^*_w) = p_w$. Then r^*_w can be considered the fictitious well radius representing the skin. The relation between r_w and r^*_w is given by

$$r^*_w = r_w e^{-S} \quad . \quad . \quad . \quad . \quad . \quad . \quad . \quad . \quad . \quad . \quad . \quad . \quad . \quad . \quad . \quad (8)$$

Several curves showing the influence of skin effects are presented in Figs. 12 and 13. The characteristics of the reservoir studied are

$$\frac{k_1}{k_2} = 10 \quad , \qquad \frac{\phi_1}{\phi_2} = 1 \quad ,$$

$$\frac{b_1}{b_2} = 10 \quad , \qquad \frac{r_e}{r_w} = 2{,}000 \quad .$$

In each graph, Curve a refers to the case where no skin was present in either layer (i.e., $S_1 = 0$ and $S_2 = 0$); Curve b refers to the case where the skin effects were taken to be $S_1 = 10$ and $S_2 = 1$; and Curve c refers to the case where the skin effects were taken to be $S_1 = 1$ and $S_2 = 10$.

A comparison shows that for Case b there was less differential depletion than for Case a, where the reservoir had no skin, and that for Case c there was more differential depletion than for Case a. These facts are readily explained; if a high resistance to flow is placed in the more permeable layer, it will tend to equalize the flow from the layers and, thus, will reduce differential depletion.

Pressure build-up curves for these cases and for cases with no skin have the same sort of shape. However, the effect of the skin on pressure build-up curves is different for multilayer and single-layer reservoirs. For a reservoir composed of a single layer, the effect vanishes after a short interval of shut-in time; on the other hand, in a multilayer reservoir the effect of the skin is present

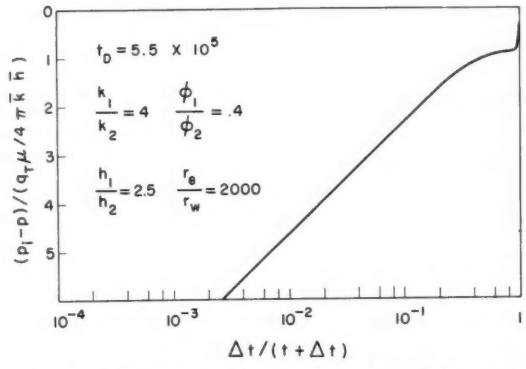

FIG. 7 – PRESSURE BUILD-UP CURVE WITH $\Delta t/(t + \Delta t)$ AS ABSCISSA.

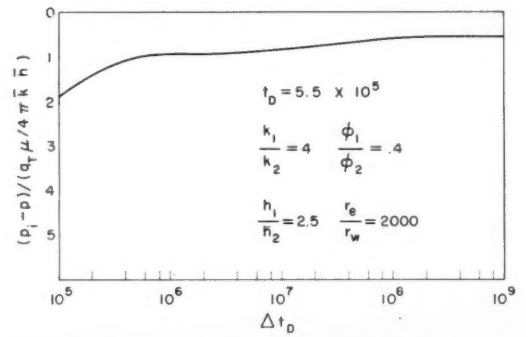

FIG. 8 – PRESSURE BUILD-UP CURVE WITH Δt AS ABSCISSA.

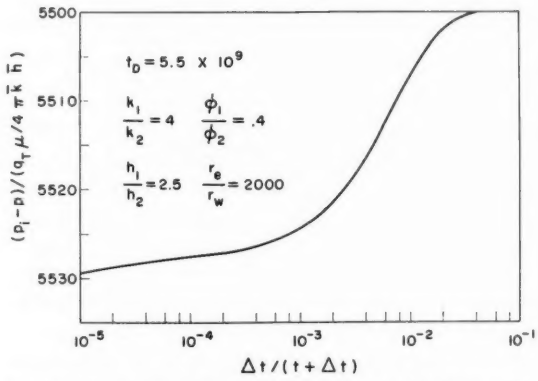

FIG. 9 – PRESSURE BUILD-UP CURVE WITH $\Delta t/(t + \Delta t)$ ABSCISSA.

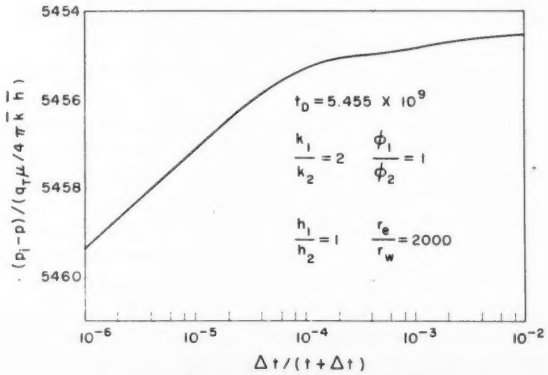

FIG. 10 – PRESSURE BUILD-UP CURVE.

during the entire range of shut-in time. This is true because, at the time the well is closed in, differential depletion exists between the layers; during shut-in, flow must then occur from one layer to another through the wellbore, and the skin acts as a resistance to that flow. Hence, the influence of the skin is felt during the entire pressure build-up.

FLOW INTO CASING AND TUBING DURING BUILD-UP

To evaluate this effect, it was assumed that the flow from the formation did not drop discontinuously to zero at the instant the well was closed in, but that the flow decreased in an exponential fashion; that is,

$$q_c(\Delta t) = q_T e^{-a\Delta t}, \quad \ldots\ldots\ldots \quad (9)$$

as discussed by van Everdingen[4] for the single-layer case.

Results show that after-production deforms the straight-line portion of the pressure build-up curve in the same fashion that it influences the curve for a single-layer reservoir. Fig. 14 shows a build-up curve both with and without after-flow. The two curves overlap for all shut-in times for which the flow due to after-production is essentially zero.

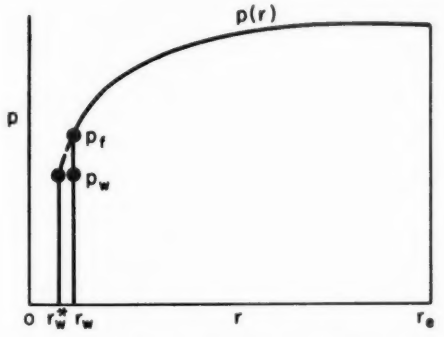

FIG. 11 – FICTITIOUS WELL RADIUS TO REPRESENT SKIN EFFECT.

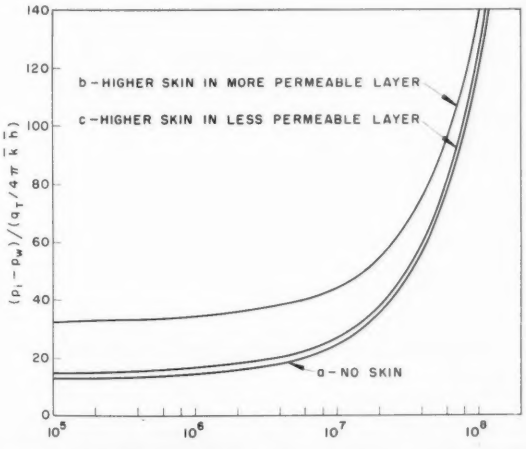

FIG. 12 – PRESSURE-DECLINE CURVES SHOWING INFLUENCE OF SKIN EFFECT.

EXTENSION TO THREE-LAYER RESERVOIRS

Several examples of three-layer reservoirs were studied; results show that, qualitatively, their behavior is like that of a two-layer reservoir. Differential depletion exists between layers, the differential depletion being directly proportional to the total production rate. The shape of the pressure build-up curves is the same as that for two-layer reservoirs. Figs. 15 and 16 give examples of results obtained for three-layer reservoirs.

COMPARISON OF RESULTS WITH THE TEMPELAAR-LIETZ THEORY

The previously mentioned work of Tempelaar-Lietz presents an approximate theory of the behavior of a two-layer reservoir where the layers had different permeabilities, equal thicknesses and equal porosities. The simplifying assumption made by Tempelaar-Lietz in his treatment was that the production rate from each layer was proportional to the difference between average pressure in that layer and the well pressure, the constant of proportionality being a function of the parameters associated with that layer.

The theory presented by Tempelaar-Lietz easily can be extended to include differences between the layers in thicknesses and porosities, as well as in well radii. The formulas obtained from this treatment are given at the end of this section.

The results obtained by the Tempelaar-Lietz theory were compared with the exact solutions obtained in this study. It was found that the Tempelaar-Lietz solutions are very good approximations to the true solutions for pressure decline and rate behavior for all but early production times. To be more exact, the Tempelaar-Lietz solutions do not express the true behavior for early times (when the reservoir can be considered to behave like an infinite reservoir) and for times shortly thereafter. After the influence of the boundary is felt, the Tempelaar-Lietz solutions become applicable with good approximation. A comparison of results is presented in Figs. 2 and 3, where both the true and approximate solutions are presented for one example. The approximate solutions are labeled with the subscript *a*.

The Tempelaar-Lietz pressure-decline equation cannot be used as an approximation to the pressure build-up curves because the pressure values are needed at times at which the Tempelaar-Lietz solution is inapplicable. However, the portion CDE in Fig. 6 can be described by the Tempelaar-Lietz equation, and the method for finding average pressures described later will make use of this fact.

The generalization of the Tempelaar-Lietz theory to the case of unequal properties of the layers gives the following formulas.

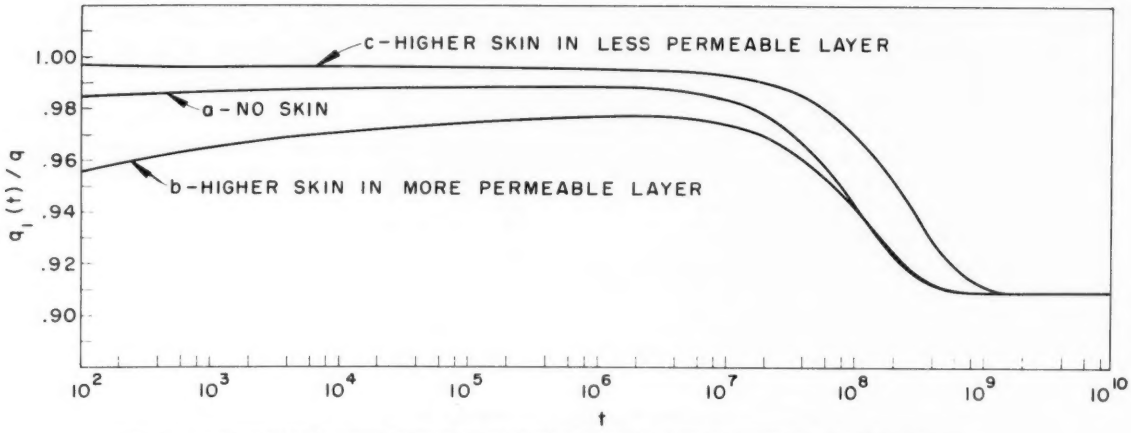

FIG. 13 – FRACTIONAL PRODUCTION RATES SHOWING INFLUENCE OF SKIN EFFECT.

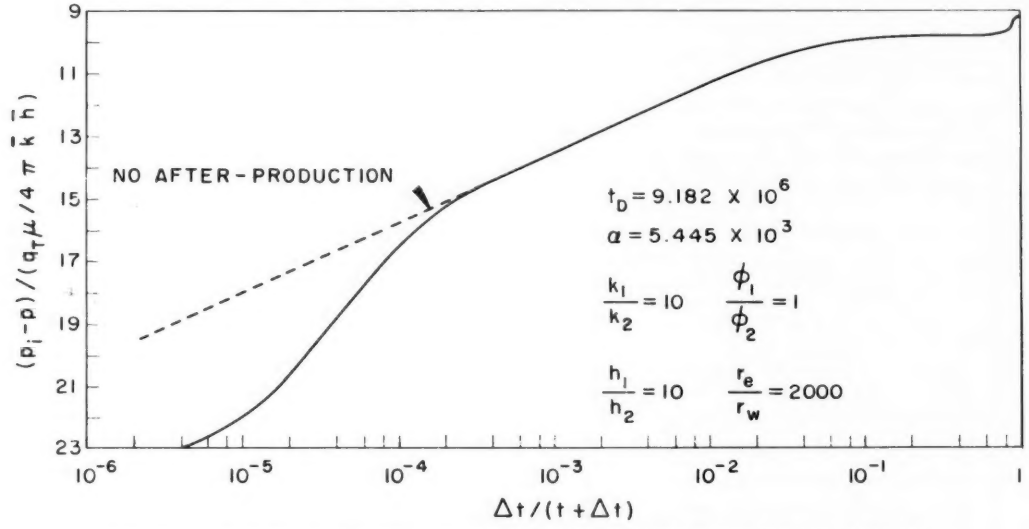

FIG. 14 – PRESSURE BUILD-UP CURVE SHOWING EFFECT OF AFTER-PRODUCTION.

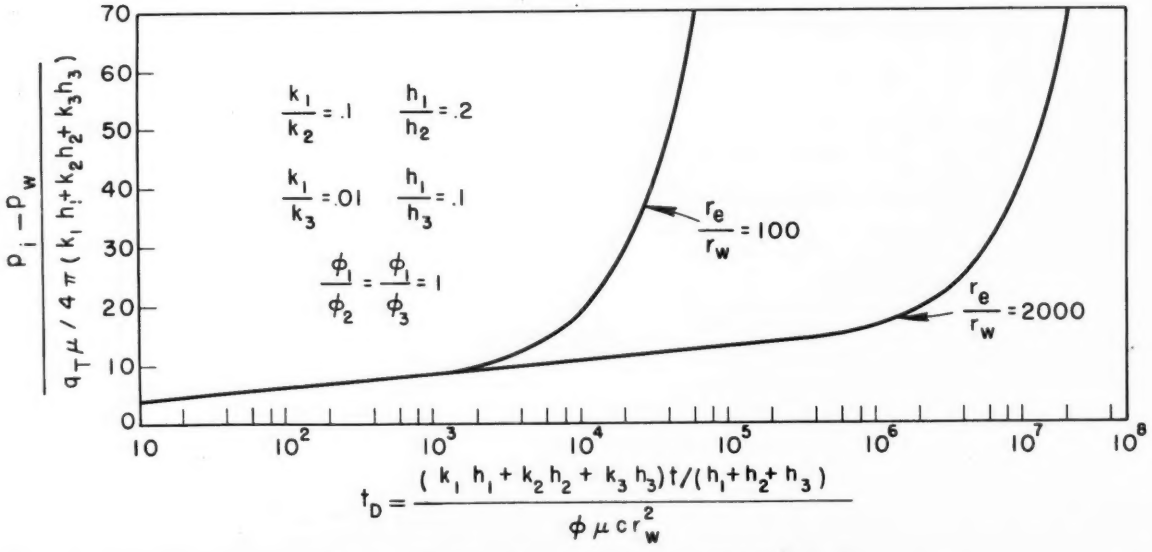

FIG. 15 – PRESSURE-DECLINE CURVES (3 LAYERS).

$$p_i - p_w(t) = \frac{q_T t}{A_1 + A_2} + \frac{q_T}{i_1 + i_2} + \frac{q_T (i_1 A_2 - i_2 A_1)^2}{i_1 i_2 (i_1 + i_2)(A_1 + A_2)^2} \times \left[1 - \exp\left(-\frac{i_1 i_2 (A_1 + A_2)}{(i_1 + i_2) A_1 A_2}\, t\right)\right] \quad \ldots\ldots\ldots\ldots\ldots\ldots\ldots (10)$$

$$p_i - \bar{p}_1(t) = \frac{q_T t}{A_1 + A_2} + \frac{q_T A_2 (A_2 i_1 - A_1 i_2)}{(A_1 + A_2)^2 i_1 i_2} \times \left[1 - \exp\left(-\frac{i_1 i_2 (A_1 + A_2)}{(i_1 + i_2) A_1 A_2}\, t\right)\right] \quad \ldots\ldots\ldots\ldots\ldots\ldots\ldots (11)$$

$$p_i - \bar{p}_2(t) = \frac{q_T t}{A_1 + A_2} - \frac{q_T A_1 (A_2 i_1 - A_1 i_2)}{(A_1 + A_2)^2 i_1 i_2} \times \left[1 - \exp\left(-\frac{i_1 i_2 (A_1 + A_2)}{(i_1 + i_2) A_1 A_2}\, t\right)\right] \quad \ldots\ldots\ldots\ldots\ldots\ldots\ldots (12)$$

Also,

$$Q_j(t) = A_j [p_i - p_j(t)]$$

$$q_1(t) = q_T \left[\frac{A_1}{A_1 + A_2} - \frac{A_2 i_1 - A_1 i_2}{A_1 (i_1 + i_2)} \exp\left(-\frac{i_1 i_2 (A_1 + A_2)}{(i_1 + i_2) A_1 A_2}\, t\right)\right] ; \ldots\ldots (13)$$

and $q_2(t)$ can be obtained from $q_2(t) = q_T - q_1(t)$. In these equations, A_j is the recovery per unit pressure drop of Layer j and i_j is the productivity index of Layer j, as defined by

$$A_j = c\phi_j \pi r_e^2 h_j \quad \ldots\ldots\ldots\ldots (14)$$

$$i_j = \frac{2\pi k_j h_j}{\mu\left(\ln \frac{r_e}{r_w} - \frac{3}{4}\right)} \quad \ldots\ldots\ldots\ldots (15)$$

APPLICATIONS

RELATIVE DEPLETION BETWEEN LAYERS

One application of the results of this study lies in the prediction of relative depletion between layers as a function of withdrawal rate.

If the rate of withdrawal q is not constant, the solutions for varying rate can be built up by appropriate superposition. The following example should make this clear.

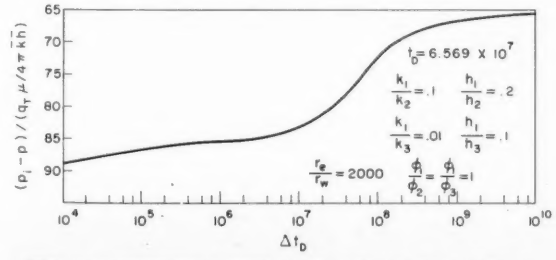

FIG. 16 – PRESSURE BUILD-UP CURVE (3 LAYERS).

Example

Let a well which penetrates two layers be produced at a rate of 100 B/D for 30 days, shut in one day, then produced at a rate of 50 B/D. Find the differential depletion between layers at the end of 60 days. The physical constants of the reservoir are as follow: $k_1 = 0.05$ darcy, $k_2 = 0.005$ darcy, $h_1 = 25$ ft, $h_2 = 75$ ft, $c = 10^{-5}$ psi^{-1}, $\mu = 0.5$ cp, $\phi = 0.2$, $r_e = 500$ ft and $r_w = 1/4$ ft; t' denotes production time in days.

Then

$$A_1 = \frac{c\phi\pi r_e^2 h_1}{5.615} = 6.99 \text{ bbl/psi},$$

$$A_2 = 20.97 \text{ bbl/psi},$$

$$i_1 = \frac{2\pi k_1 h_1}{\mu\left(\ln \frac{r_e}{r_w} - \frac{3}{4}\right)} \times \frac{1}{1.84} \times 30.48 \times \frac{1}{14.7} = 2.583 \text{ B/D} \times \text{psi},$$

$$i_2 = 0.775 \text{ B/D} \times \text{psi},$$

and

$$p_i - \bar{p}_1 = \frac{qt'}{27.96} + 0.652\, q(1 - e^{-0.1137 t'}).$$

For the production schedule outlined, we have at the end of 60 days,

$$p_i - \bar{p}_1 = \frac{100(60)}{27.96} + 0.652(100)\,[1 - e^{-0.1137(60)}] - \frac{100(60-30)}{27.96} - 0.652(100)[1 - e^{-0.1137(60-30)}] + \frac{50(60-31)}{27.96} + 0.652(50)[1 - e^{-0.1137(60-31)}] = 192 \text{ psi}.$$

$$p_i - \bar{p}_2 = \frac{100(30) + 50(29)}{20.97} - \frac{6.99}{20.97}(192) = 148 \text{ psi}.$$

$Q_1 = 6.99(192) = 1{,}342$ bbl or 53.6 bbl/ft sand,
$Q_2 = 20.97(148) = 3{,}103$ bbl or 41.4 bbl/ft sand.

For a rate of 300 B/D, the corresponding pressures at the same cumulative total production are

$$p_i - \bar{p}_1 = 319 \text{ psi},$$
$$p_i - \bar{p}_2 = 106 \text{ psi},$$

and the cumulative production per ft,

$$Q_1/h_1 = 89.1 \text{ bbl/ft sand},$$
$$Q_2/h_2 = 29.6 \text{ bbl/ft sand}.$$

The effect of rate on the differential depletion thus is emphasized. These equations can also be used to calculate how near the average pressures in each layer approach one another during shut-in. The effect of a skin in each layer is taken into account by changing r_w in each layer according to the manner of Eq. 8.

PRESSURE BUILD-UP FOR MULTILAYER CASES

As shown previously, the pressure build-up curves for multilayer cases have a "tail" which gives an essentially different shape to the build-up curve from that obtained for one-layer reservoirs. The method for obtaining the average pressure in

the drainage area of wells in such cases thus must be different from that for more homogeneous cases. The initial section of such a build-up curve is linear on a plot of pressure vs log $[\Delta t/(t + \Delta t)]$ as shown in Fig. 6 where Δt is the shut-in time. Next a slight flattening may occur, then a rise and, after a long time, a final flattening. In the initial straight-line portion, a value for $(k_1 b_1 + k_2 b_2)$ can be obtained from the slope by using

$$k_1 b_1 + k_2 b_2 = \frac{q_T' \mu / 4\pi}{\text{slope, psi}} \times (14.7)\,(2.303) \quad ,$$

where q_T is the total production rate measured at reservoir conditions at the time of shut-in.

The applicable equation for the section of the build-up curve subsequent to the straight-line section, provided the well has been producing long enough before shut-in, is

$$p_w(\Delta t, t) = \bar{p} - be^{C\Delta t} \quad , \quad \ldots\ldots\ldots \quad (16)$$

where b and C are constants. Thus, a plot of log $(\bar{p} - p)$ vs Δt should give a straight line. One method of determining $\bar{p}$ is to assume a value for $\bar{p}$, make this type of plot, and see whether or not a straight line is obtained. If not, a new value of p is assumed and the plotting is repeated. Fig. 17 shows a series of these plots for different assumed values of $\bar{p}$. The correct value is seen to be about 2,750 psi because the lines on either side curve away from each other.

It has been found that types of reservoirs other than multilayer reservoirs also show this same exponential behavior during build-up. Fig. 18 is a build-up curve from a fractured dolomite reservoir, the dotted line being the extrapolation to the average pressure determined by the plot in Fig. 19. In Fig. 20 a build-up curve from a hydrafracked reservoir is presented, the average pressure having been determined with the aid of Fig. 21. Fig. 22

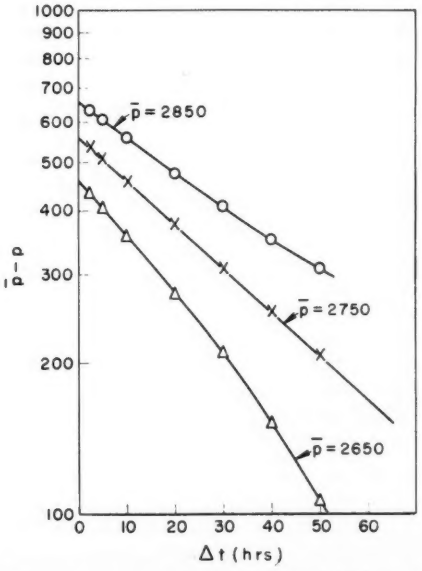

FIG. 17 – PLOT FOR DETERMINATION OF $\bar{p}$.

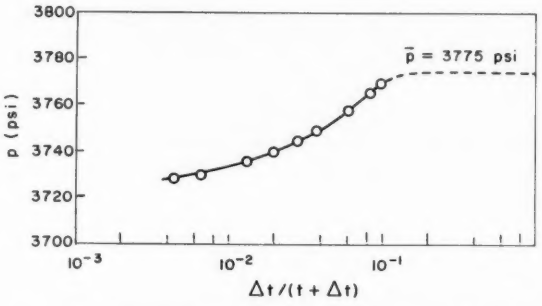

FIG. 18 – PRESSURE BUILD-UP CURVE, WILLISTON BASIN FIELD (FRACTURED DOLOMITE RESERVOIR) JUNE, 1953.

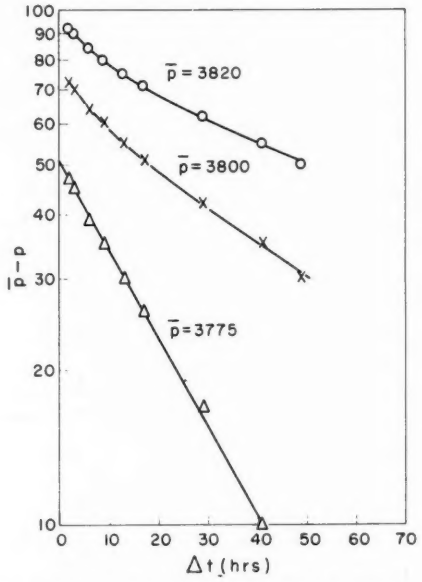

FIG. 19 – WILLISTON BASIN FIELD (FRACTURED DOLOMITE RESERVOIR) JUNE, 1953.

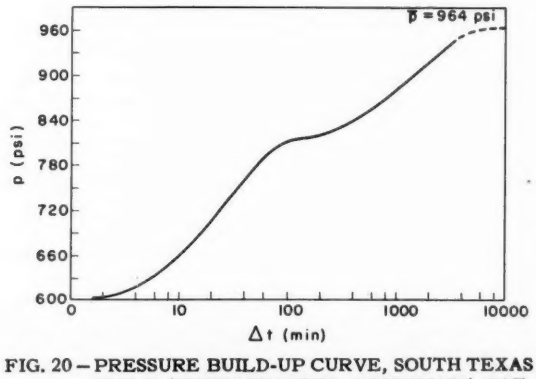

FIG. 20 – PRESSURE BUILD-UP CURVE, SOUTH TEXAS FIELD (HYDRAFRACKED RESERVOIR) OCT. 24 TO OCT. 27, 1952.

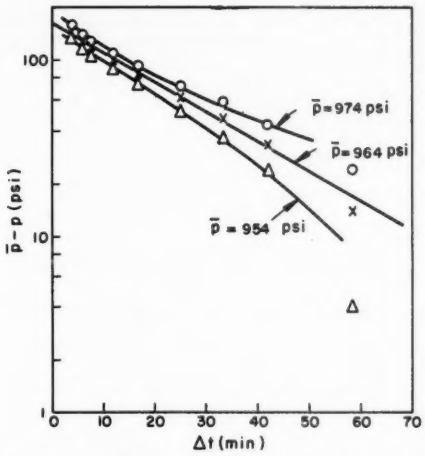

FIG. 21 – SOUTH TEXAS FIELD (HYDRA-FRACKED RESERVOIR) OCT. 24 TO OCT. 27, 1952.

is a build-up curve from a multilayer* reservoir in California. The exponential-rise type of build-up appears applicable to all three types of reservoirs.

CONCLUSIONS

The present investigation has shown that the simple formulas developed by Tempelaar-Lietz and generalized in this report can be used successfully for predicting differential depletion between layers of a multilayer reservoir except at very early times. The simpler formulas can also be used to predict pressure decline at the well. A method for determination of average pressures of these reservoirs is presented. This method can be applied to multilayer reservoirs and appears to be applicable to reservoirs of other types which have the same type of build-up behavior.

PART II — MATHEMATICAL DERIVATION

ASSUMPTIONS AND BASIC EQUATIONS

We assume that the reservoir to be studied is a bounded, horizontal cylindrical disk, with a completely penetrating well at its center, that its thickness is small enough that the forces of gravity can be neglected and that it is bounded above, below and on the outside by impermeable boundaries. The reservoir is divided horizontally into n parallel layers which are separated throughout the reservoir by impermeable boundaries through which no fluid can flow. The radius of the wellbore at the jth layer is denoted by $r_{w,j}$ and the exterior radius of the jth layer by $r_{e,j}$. Each layer is assumed to be homogeneous, isotropic, and filled with a fluid of small and constant compressibility c_j and constant viscosity μ_j ($j = 1, 2, \ldots, n$). For each

*For reservoirs composed of more than two layers, the applicable equation for build-up is of the type of Eq. 16, but it should contain $n - 1$ exponential terms if the reservoir contains n layers. Practically, however, it has been found that good results generally can be obtained by using only one exponential.

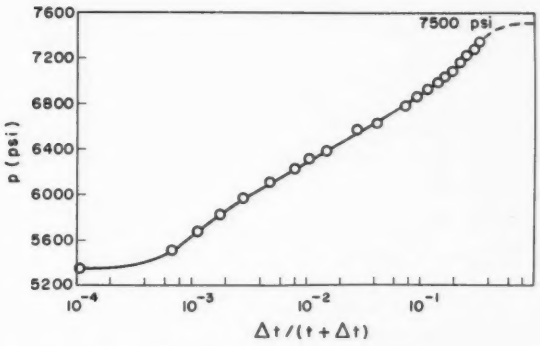

FIG. 22 – CALIFORNIA FIELD, PRESSURE BUILD-UP (MULTILAYER RESERVOIR) MAY, 1952.

layer, k_j denotes its permeability, ϕ_j its porosity and h_j its thickness. The reservoir is initially at a uniform pressure p_i; and, at all times $t > 0$, the fluid is withdrawn through the wellbore in such a manner that the total production rate q, measured at initial reservoir conditions, is held constant.

For simplicity of notation we let

$$\eta_j = \frac{k_j}{\phi_j \mu_j c_j}$$

$$a_j = \frac{r_{w,j}}{\sqrt{\eta_j}}$$

$$\beta_j = \frac{h_j k_j}{\mu_j}$$

$$\gamma_j = \frac{r_{e,j}}{\sqrt{\eta_j}}$$

$$j = 1, 2, \ldots, n$$

and define the pressure drops $P_j(r,t)$ by

$$P_j(r,t) = p_i - p_j(r,t) \qquad j = 1, 2, \ldots, n$$

where $p_j(r,t)$ denotes the pressure in the jth layer at a radial distance r and time t. Then, $P_j(r,t)$ must satisfy the equation

$$\frac{1}{r}\frac{\partial}{\partial r}\left(r\frac{\partial P_j}{\partial r}\right) = \frac{1}{\eta_j}\frac{\partial P_j}{\partial t} \qquad j = 1, 2, \ldots, n, \quad \ldots\ldots\ldots\ldots\ldots\ldots\ldots\ldots (1)$$

This system of equations must be solved subject to the following initial and boundary conditions.

1. At $t = 0$, the pressure drop in each layer is zero; i.e.,

$$P_j(r,0) = 0 \qquad j = 1, 2, \ldots, n. \quad \ldots (2)$$

2. There is no flow across the outer boundaries, so that

$$\frac{\partial P_j}{\partial r} = 0 \qquad \text{at } r = r_{e,j},\ j = 1, 2, \ldots, n. \quad \ldots (3)$$

3. The pressures in all layers at the well are equal and, hence, the pressure drops are also equal; i.e.,

$$P_j(r,t) = P_w(t) \text{ at } r = r_{w,j},\ j = 1, 2, \ldots, n. \quad (4)$$

the function $P_w(t)$ being independent of j.

4. The total production rate from all the layers

is constant and equal to q.

$$\sum_{i=1}^{n} q_j(t) = -2\pi \sum_{i=1}^{n} \beta_j \left(r \frac{\partial P_j}{\partial r} \right)_{r=r_{w,j}} = q \quad . \quad (5)$$

where $q_j(t)$ denotes the rate of flow from the jth layer into the well at time t.

THE TRANSFORMED EQUATIONS AND THEIR SOLUTION

Let $\bar{X}(z) = L[X(t)]$ denote the Laplace transform of $X(t)$ where z is the complex variable $x + iy$. Applying this transform to both sides of the Eqs. 1 and using Eq. 2, we obtain the system

$$\frac{1}{r} \frac{\partial}{\partial r} \left(r \frac{\partial \bar{P}_j}{\partial r} \right) - \frac{z}{n_j} \bar{P}_j = 0 \qquad j = 1, 2, \ldots, n$$

. . . . . (6)

which must be solved subject to the boundary conditions

$$\frac{\partial \bar{P}_j}{\partial r} = 0 \quad \text{at } r = r_{e,j}, \qquad j = 1, 2, \ldots, n$$

. . . . . (7)

$$\bar{P}_j(r,z) = \bar{P}_w(z), \text{ at } r = r_{w,j}, \; j = 1, 2, \ldots, n$$

. . . . . (8)

$$\sum_{i=1}^{n} \beta_j \left(r \frac{\partial \bar{P}_j}{\partial r} \right)_{r=r_{w,j}} = -\frac{q}{2\pi z} \quad . \quad . \quad . \quad (9)$$

Eq. 6 has general solutions of the form

$$\bar{P}_j(r,z) = A_j K_o \left(r\sqrt{\frac{z}{n_j}} \right) + B_j I_o \left(r\sqrt{\frac{z}{n_j}} \right)$$

and A_j and B_j are constants to be determined from Eqs. 7, 8 and 9. These conditions lead to the set of equations

$$\left.\begin{aligned} A_j K_1(\gamma_j\sqrt{z}) &= B_j I_1(\gamma_j\sqrt{z}) \\ A_j K_0(a_j\sqrt{z}) + B_j I_0(a_j\sqrt{z}) &= \bar{P}_w(z) \\ \Sigma\, \beta_j a_j [A_j K_1(a_j\sqrt{z}) - B_j I_1(a_j\sqrt{z})] &= \frac{q}{2\pi z^{3/2}} \end{aligned}\right\} \quad (10)$$

Letting

$$\psi_{0j}(z) = K_0(a_j\sqrt{z}) I_1(\gamma_j\sqrt{z}) + I_0(a_j\sqrt{z}) K_1(\gamma_j\sqrt{z}),$$

$$\psi_{1j}(z) = K_1(a_j\sqrt{z}) I_1(\gamma_j\sqrt{z}) - I_1(a_j\sqrt{z}) K_1(\gamma_j\sqrt{z}),$$

we obtain by simple manipulation

$$\bar{P}_w(z) = \frac{q}{2\pi z^{3/2}} \quad \frac{1}{\sum_{j=1}^{n} \beta_j a_j \dfrac{\psi_{1j}(z)}{\psi_{0j}(z)}} \quad , \quad . \quad . \quad . \quad (11)$$

and also

$$\bar{P}_j(r,z) = \frac{K_0\left(\dfrac{r}{r_{w,j}} a_j\sqrt{z}\right) I_1(\gamma_j\sqrt{z}) + I_0\left(\dfrac{r}{r_{w,j}} a_j\sqrt{z}\right) K_0(\gamma_j\sqrt{z})}{\psi_{0j}(z)} \bar{P}_w(z),$$

. . . . . (12)

$$\bar{q}_j(z) = 2\pi\beta_j a_j \sqrt{z} \frac{\psi_{1j}(z)}{\psi_{0j}(z)} \bar{P}_w(z) \quad . \quad . \quad . \quad . \quad . \quad (13)$$

INVERSION OF THE SOLUTIONS

In this section, we derive expressions for the inverses of the functions of Eqs. 11, 12 and 13 suitable for numerical calculations at large times.

Letting

$$F(z) = \sqrt{z} \sum_{j=1}^{n} \beta_j a_j \frac{\psi_{1j}(z)}{\psi_{0j}(z)} \; ,$$

so that

$$\bar{P}_w(z) = \frac{q}{2\pi z} \quad \frac{1}{F(z)} \quad ,$$

we first note that $\sqrt{z}\psi_{1j}(z)/\psi_{0j}(z)$ is a meromorphic function and that, therefore, the functions $\bar{P}_w(z)$, $\bar{P}_j(r,z)$ and $\bar{q}_j(z)$ are also meromorphic functions. From the stability of the physical system, it also can be deduced that these functions do not have poles with positive real part.

Expanding $1/F(z)$ about $z = 0$, we obtain

$$F(z) = \frac{2}{\sum_j \beta_j \gamma_j^2} \frac{1}{z} + \frac{\sum_j \beta_j \gamma_j^4 \left(\ln \dfrac{r_{ej}}{r_{wj}} - \dfrac{3}{4} \right)}{\left(\sum_j \beta_j \gamma_j^2 \right)^2} + 0(z),$$

so that

$$P_w(t) = \frac{q}{2\pi} \left[\frac{2t}{\sum_j \beta_j \gamma_j^2} + \frac{\sum_j \beta_j \gamma_j^4 \left(\ln \dfrac{r_{ej}}{r_{wj}} - \dfrac{3}{4} \right)}{\left(\sum_j \beta_j \gamma_j^2 \right)^2} \right] + Y(t) \quad , \quad . \quad . \quad . \quad . \quad . \quad . \quad . \quad (14)$$

where $Y(t)$ represents the contribution of the other poles of $\bar{P}_w(z)$. These poles are the non-vanishing roots of $F(z) = 0$. If we let $z = s^2$, this equation can be written

$$\sum_{j=1}^{n} \beta_j a_j \frac{K_1(a_j s) I_1(\gamma_j s) - I_1(a_j s) K_1(\gamma_j s)}{K_0(a_j s) I_1(\gamma_j s) + I_0(a_j s) K_1(\gamma_j s)} = 0. \quad (15)$$

It can be shown that the roots of this equation are conjugate complex and lie on the imaginary s axis.

Letting z_k, $k = 1, 2, \ldots$ denote the non-zero roots of $F(z) = 0$ and letting $\sqrt{z} = ix$, $z_k = -x_k^2$ so that the x_k are roots of

$G(x) =$

$$\sum_{j=1}^{n} \beta_j a_j \frac{Y_1(a_j x) J_1(\gamma_j x) - J_1(a_j x) Y_1(\gamma_j x)}{Y_0(a_j x) J_1(\gamma_j x) - J_0(a_j x) Y_1(\gamma_j x)} = 0, \quad (16)$$

we have

$$Y(t) = \frac{q}{\pi} \sum_{k=1}^{\infty} \frac{e^{-x_k^2 t}}{x_k^2 G'(x_k)} \quad . \quad . \quad . \quad . \quad . \quad . \quad . \quad . \quad (17)$$

Evaluating this expression with the aid of the eigenvalue Eq. 16, we obtain

$$Y(t) = -\frac{\pi q}{4} \sum_{k=1}^{\infty} \frac{e^{-x_k^2 t}}{\sum_{j=1}^{n} \beta_j \dfrac{1 - \dfrac{\pi^2}{4} a_j^2 x_k^2 \left(\phi_{0,jk}^2 + \phi_{1,jk}^2\right)}{\phi_{0,jk}^2}} \quad \ldots\ldots\ldots\ldots\ldots\ldots (18)$$

where

$$\phi_{0,jk} = Y_0(a_j x_k)\, J_1(\gamma_j x_k) - J_0(a_j x_k)\, Y_1(\gamma_j x_k)$$

$$\phi_{1,jk} = Y_1(a_j x_k) J_1(\gamma_j x_k) - J_1(a_j x_k)\, Y_1(\gamma_j x_k) .$$

This expression for $Y(t)$ is correct for all values of t. In the calculations performed, it was found that the times for which the solution was evaluated were large enough that only the smaller roots x_k were needed to evaluate $Y(t)$.

For such values of t, Eqs. 16 and 18 were simplified to

$$G(x) = \sum_{j=1}^{n} \frac{\beta_j J_1(\gamma_j x)}{\frac{2}{\pi} J_1(\gamma_j x) \ln \frac{\gamma}{2} a_j x - Y_1(\gamma_j x)} = 0 \quad (19)$$

and

$$Y(t) = -\frac{\pi q}{4} \sum_{k=1}^{\infty} \frac{e^{-x_k^2 t}}{\sum_j \beta_j \dfrac{1 - J_1^2(\gamma_j x_k)}{\left[\frac{2}{\pi} J_1(\gamma_j x_k) \ln \frac{\gamma}{2} a_j x_k - Y_1(\gamma_j x_k)\right]^2}} \quad \ldots\ldots\ldots\ldots\ldots\ldots (20)$$

respectively. The accuracy of the approximations checks in each case calculated.

If we assume that the first root of Eq. 19 is small, further approximations can be made for the calculation of this root. For the case of two layers, Eq. 19 then becomes

$$\sum_{j=1}^{2} \frac{1}{\beta_j} \left(\ln \frac{\gamma_j}{a_j} - \frac{\frac{1}{\gamma_j x} + \frac{1}{4} \gamma_j x}{\frac{1}{2} \gamma_j x - \frac{1}{16} \gamma_j^3 x^3} \right) = 0 .$$

From this, the smallest root x_1 can be approximated by

$$x_1^2 \simeq \frac{2\left(\gamma_1^2 \beta_1 + \gamma_2^2 \beta_2\right)}{\gamma_1^2 \gamma_2^2 \left[\beta_2 \left(\ln \frac{\gamma_1}{a_1} - \frac{3}{4}\right) + \beta_1 \left(\ln \frac{\gamma_2}{a_2} - \frac{3}{4}\right)\right]} . \quad \ldots\ldots\ldots\ldots\ldots\ldots (21)$$

It is interesting to note that this expression coincides with the exponent obtained in the simplified theory of Tempelaar-Lietz for two layers.

The transform of the production rate from the jth layer is given by

$$\bar{q}_j(z) = \frac{q}{z} \frac{\beta_j a_j \dfrac{\psi_{1j}(z)}{\psi_{0j}(z)}}{\sum_{j=1}^{n} \beta_j a_j \dfrac{\psi_{1j}(z)}{\psi_{0j}(z)}} .$$

By a procedure similar to the one used in obtaining $P_w(t)$, we obtain

$$\frac{q_j(t)}{q} = \frac{\beta_j \gamma_j^2}{\sum_j \beta_j \gamma_j^2} + Z_j(t) \quad \ldots\ldots\ldots\ldots (22)$$

where

$$Z_j(t) = -\frac{\pi^2}{2} \beta_j \sum_{k=1}^{\infty} \frac{a_j x_k \dfrac{\phi_{1,jk}}{\phi_{0,jk}} e^{-x_k^2 t}}{\sum_{j=1}^{n} \beta_j \dfrac{1 - \frac{\pi^2}{4} a_j^2 x_k^2 \left(\phi_{0,jk}^2 + \phi_{1,jk}^2\right)}{\phi_{0,jk}^2}} . \quad \ldots\ldots\ldots\ldots\ldots\ldots (23)$$

The x_k are the non-vanishing roots of Eq. 16.

Again for large values of t, a simplified expression for Eq. 23 can be constructed. This is

$$Z_j(t) = \pi \beta_j \sum_{k=1}^{\infty} \frac{\dfrac{J_1(\gamma_j x_k)}{\frac{2}{\pi} J_1(\gamma_j x_k) \ln \frac{\gamma}{2} a_j x_k - Y_1(\gamma_j x_k)} e^{-x_k^2 t}}{\sum_j \beta_j \dfrac{1 - J_1^2(\gamma_j x_k)}{\left(\frac{2}{\pi} J_1(\gamma_j x_k) \ln \frac{\gamma}{2} a_j x_k - Y_1(\gamma_j x_k)\right)^2}} \quad \ldots\ldots\ldots\ldots\ldots\ldots (24)$$

A similar treatment gives the solution $P_j(r,t)$.

THE PRESSURE AT SMALL TIMES

The use of the solutions derived in the preceding section is not convenient for small times, since too many terms in the expressions for $Y(t)$ and $Z_j(t)$ are required. However, since it is known that a bounded reservoir behaves as an infinite reservoir during its early life, the solutions corresponding to infinite and bounded reservoirs must coincide for all times smaller than the time at which the influence of the boundary is said to be felt upon the behavior of the reservoir.

The actual procedure used in the calculation of the results obtained in this paper was, first, to evaluate the solution corresponding to an infinite field, and, then, to evaluate the solution corresponding to the bounded reservoir, using enough terms in the series for the transient parts of the solutions to obtain a significant time range where the two solutions would overlap.

The solution to the problem of finding the well pressure in an infinite field composed of n horizontal layers has been solved by Horner.* The equations to be solved are the same as for the bounded reservoir, but the boundary equation in Eq. 3 must be replaced by the condition

$$P_j(r,t) \to 0 \quad \text{as } r \to \infty,\ t \geq 0,$$
$$j = 1, 2, \ldots, n. \quad \ldots\ldots\ldots (25)$$

The solution for $P_w(t)$ can be written

*The authors gratefully acknowledge this contribution which has only been published within the Shell companies.

$$P_w(t) = \frac{q}{4\pi \sum_{j=1}^{n} \beta_j} \left(\ln \gamma t - \frac{\sum_{j=1}^{n} \beta_j \ln \frac{\gamma^2 a_j^2}{4}}{\sum_{j=1}^{n} \beta_j} + J(t) \right), \quad \ldots\ldots\ldots\ldots\ldots\ldots\ldots\ldots (26)$$

where

$$J(t) = \int_0^\infty \frac{e^{-ut}}{u} \left\{ 1 - \frac{4 \sum_j \beta_j}{\pi^2} \right.$$

$$\left. \frac{\sum_{j=1}^{n} \frac{\beta_j}{J_{0j}^2 + Y_{0j}^2}}{u \left[\left(\sum_{j=1}^{n} a_j \beta_j \frac{J_{0j} J_{1j} + Y_{0j} Y_{1j}}{J_{0j}^2 + Y_{0j}^2} \right)^2 + \frac{4}{\pi^2 u} \left(\sum_{j=1}^{n} \frac{\beta_j}{J_{0j}^2 + Y_{0j}^2} \right)^2 \right]} \right\} du$$

$\ldots\ldots\ldots\ldots\ldots\ldots\ldots\ldots\ldots\ldots\ldots\ldots (27)$

The following abbreviations have been used.

$$J_{0j} = J_0(a_j \sqrt{u}),$$
$$J_{1j} = J_1(a_j \sqrt{u}),$$
$$Y_{0j} = Y_0(a_j \sqrt{u}),$$
$$Y_{1j} = Y_1(a_j \sqrt{u}).$$

The integral in the form given in Eq. 27 is quite intractable for numerical calculations. For the case of $n = 2$ (that is, when the reservoir is composed of only two layers), however, approximations can be obtained which make a numerical analysis possible.

Introducing approximations for the Bessel functions for small values of u, we can show that

$$-J(t) = \frac{\beta_1 \beta_2 \ln^2(a_1^2/a_2^2)}{(\beta_1 + \beta_2)^2} \int_0^\infty \frac{e^{-ut}\, du}{u[(\ln u - A)^2 + \pi^2]} \quad \ldots\ldots\ldots\ldots\ldots\ldots\ldots\ldots (28)$$

where

$$A = -\frac{\beta_1 \ln \frac{\gamma^2}{4} a_2^2 + \beta_2 \ln \frac{\gamma^2}{4} a_1^2}{\beta_1 + \beta_2}.$$

Now if we let $\tau = te^A$, the integral in Eq. 28 is transformed into the integral

$$\phi(\tau) = \int_0^\infty \frac{e^{-u\tau}\, du}{u(\ln^2 u + \pi^2)}.$$

This integral must be evaluated to calculate $J(t)$.

From the table of Laplace transforms of McLachlan, Humbert and Poli[5] it can be found that

$$\phi(\tau) = e^\tau - \int_0^\infty \frac{\tau^u du}{\Gamma(u+1)}.$$

This last integral can be further transformed as follows.

$$\int_0^\infty \frac{\tau^u\, du}{\Gamma(u+1)} = \sum_{n=0}^{\infty} \int_n^{n+1} \frac{\tau^u\, du}{\Gamma(u+1)} =$$

$$\sum_{n=0}^{\infty} \int_0^1 \frac{\tau^{u+n} du}{\Gamma(u+n+1)} = \int_0^1 F(\tau,u)\, du,$$

where

$$F(\tau,u) = \sum_{n=0}^{\infty} \frac{\tau^{n+u}}{\Gamma(u+n+1)}.$$

This function $F(\tau,u)$ satisfied the differential equation

$$\frac{dF}{d\tau} - F = \frac{\tau^{u-1}}{\Gamma(u)}$$

with the condition $F(0,u) = 0$. Solving this equation we find that

$$F(\tau,u) = \frac{e^\tau}{\Gamma(u)} \int_0^\tau e^{-v} v^{u-1}\, dv = e^\tau \left(1 - \frac{Q(u,\tau)}{\Gamma(u)}\right),$$

where

$$Q(u,\tau) = \int_\tau^\infty e^{-v} v^{u-1}\, dv$$

is an incomplete gamma function. Then, upon substitution of these results,

$$\phi(\tau) = e^\tau \int_0^1 \frac{Q(u,\tau)}{\Gamma(u)}\, du. \quad \ldots\ldots\ldots (29)$$

This expression is used to calculate $\phi(\tau)$ for values of $\tau \leq 10$. For values of $\tau > 10$, an asymptotic expression is used for $Q(u,\tau)$ which gives rise to the equation

$$\phi(\tau) \simeq \int_0^1 \frac{dv}{\tau^u \Gamma(1-v)} + \frac{1-\tau}{\tau^2} \int_0^1 \frac{v\, dv}{\tau^v \Gamma(1-v)} +$$

$$\frac{1}{\tau^2} \int_0^1 \frac{v^2\, dv}{\tau^v \Gamma(1-v)}. \quad (30)$$

It is found that the magnitude of the last two terms decreases rapidly with increasing values of τ.

An upper limit for $\phi(\tau)$ can be obtained in the following manner.

$$\phi(\tau) < \int_0^1 \frac{dv}{\tau^v} < \int_0^\infty \frac{dv}{\tau^v} = \frac{1}{\ln \tau}.$$

This upper limit gives a good approximation for $\phi(\tau)$ for large values of τ.

The values of $\phi(\tau)$ obtained are given in Table 1.

TABLE 1 – VALUES OF $\phi(\tau)$

τ	$\phi(\tau)$	τ	$\phi(\tau)$
1	0.452	1×10^4	0.1003
2	0.392	2×10^4	0.0939
3	0.359	4×10^4	0.0883
4	0.337	1×10^5	0.0818
6	0.308	2×10^5	0.0775
1×10	0.2765	4×10^5	0.0736
2×10	0.2398	1×10^6	0.0690
4×10	0.2100	2×10^6	0.0659
1×10^2	0.1792	4×10^6	0.0631
2×10^2	0.1608	1×10^7	0.0597
4×10^2	0.1456		
1×10^3	0.1291		
2×10^3	0.1189		
4×10^3	0.1101		

THE PRODUCTION RATE AT SMALL TIMES

The production rate at small times is obtained from the solution for an infinite reservoir evaluated in the case of two layers. The Laplace transform of the fraction production rate from the first layer is

$$\frac{\bar{q}_1(z)}{q} = \frac{1}{z} \frac{\beta_1 a_1 \dfrac{K_1(a_1\sqrt{z})}{K_0(a_1\sqrt{z})}}{\beta_1 a_1 \dfrac{K_1(a_1\sqrt{z})}{K_0(a_1\sqrt{z})} + \beta_2 a_2 \dfrac{K_1(a_2\sqrt{z})}{K_0(a_2\sqrt{z})}} \quad \ldots\ldots\ldots\ldots\ldots\ldots (31)$$

The corresponding solution is

$$\frac{q_1(t)}{q} = \frac{1}{2\pi i} \int_{\beta-i\infty}^{\beta+i\infty} \frac{\bar{q}_1(z)}{q} e^{zt}\, dz ,$$

the path of integration passing to the right of the origin. Replacing the Bessel functions by the approximations

$$K_0(a_j\sqrt{z}) \simeq -\ln\frac{\gamma}{2}\, a_j\sqrt{z} ,$$

$$K_1(a_j\sqrt{z}) \simeq \frac{1}{a_j\sqrt{z}} ,$$

and neglecting quantities of the order a_j^2, it can be shown that

$$\frac{q_1(t)}{q} = \frac{1}{2\pi i} \int_{\beta-i\infty}^{\beta+i\infty} \frac{\beta_1 \ln\frac{\gamma}{2} a_2\sqrt{z}}{\beta_1 \ln\frac{\gamma}{2} a_2\sqrt{z} + \beta_2 \ln\frac{\gamma}{2} a_1\sqrt{z}} \cdot \frac{e^{zt}}{z}\, dz ,$$

or

$$\frac{q_1(t)}{q} = \frac{1}{2\pi i} \int_{\beta-i\infty}^{\beta+i\infty} \left[\frac{\beta_1}{\beta_1+\beta_2} \frac{1}{z} + \frac{\beta_1\beta_2}{(\beta_1+\beta_2)^2} \ln\frac{a_2^2}{a_1^2} \frac{1}{z(\ln z - A)} \right] e^{zt}\, dz , \quad \ldots\ldots\ldots\ldots\ldots\ldots (32)$$

where A is defined as before. The first term in the integrand yields the constant $\beta_1/(\beta_1+\beta_2)$. The integral

$$\frac{1}{2\pi i} \int_{\beta-i\infty}^{\beta+i\infty} \frac{e^{zt}\, dz}{z(\ln z - A)} \quad \ldots\ldots\ldots (33)$$

is evaluated as follows. According to Doetsch,[6]

$$\frac{1}{z(\ln z - A)} \quad \ldots\ldots\ldots\ldots (34)$$

is the Laplace transform of

$$\int_0^\infty \frac{\tau^u}{\Gamma(u+1)}\, du \qquad (\tau = te^A) \quad \ldots\ldots (35)$$

The function Eq. 34 has a pole at $z = e^A$ which, however, does not contribute to the integral Eq. 33. This contribution, therefore, must be subtracted, yielding

$$\frac{1}{2\pi i} \int_{\beta-i\infty}^{\beta+i\infty} \frac{e^{zt}\, dz}{z(\ln z - A)} \int_0^\infty \frac{\tau^u\, du}{\Gamma(1+u)} - e^\tau = -\phi(\tau).$$

We can then write

$$\frac{q_1(t)}{q} = \frac{\beta_1}{\beta_1+\beta_2} - \frac{\beta_1\beta_2 \ln\dfrac{a_2^2}{a_1^2}}{(\beta_1+\beta_2)^2}\, \phi(\tau) \quad \ldots (36)$$

It can be noted that values of $\phi(\tau)$ have already been calculated for evaluation of the pressures.

The effects of the transient terms in the infinite solutions are both proportional to $\phi(\tau)$; but, whereas this effect is negligible in the pressure equation for all but very small times, the effect of this term on the rate solution is in general of considerable magnitude.

INCLUSION OF THE SKIN EFFECT

The skin factor S_j of the jth layer is defined by the equation*

$$S_j = \frac{P_w - P_{fj}}{q_f(t)\,\mu_j/2\pi k_j b_j} \quad \ldots\ldots\ldots (37)$$

The equations to be solved are the same in the presence of a skin as without one, except that the boundary condition (that the pressures at the well are the same in all layers) must be restated to say that the pressures inside the wellbore are the same in all layers. This can be stated as

$$\frac{S_j q_j(t)\mu_j}{2\pi k_j b_j} + P_{fj}(t) = P_w(t) \qquad j = 1, 2, \ldots, n \quad \ldots\ldots\ldots\ldots\ldots\ldots (38)$$

where $P_w(t)$ is independent of j.

The method of analysis used to solve this problem is identical to the method outlined for solving the equations without the skin; the equations are similar, and only some extra terms containing S_j are present.

The transform of $P_w(t)$ can be obtained as

$$\bar{P}_w(z) = \frac{q}{2\pi z} \frac{1}{\sqrt{z}\sum_j \beta_j a_j \dfrac{\psi_{1j}(z)}{\psi_j(z)}} , \quad \ldots (39)$$

where

$$\psi_j(z) = a_j S_j \sqrt{z}\, \psi_{1j}(z) + \psi_{0j}(z) ,$$

and $\psi_{0j}(z)$ and $\psi_{1j}(z)$ have the same meaning as as before. Similarly

$$\bar{q}_j(z) = 2\pi\beta_j a_j \sqrt{z} \frac{\psi_{1j}(z)}{\psi_j(z)} \bar{P}_w(z) \quad \ldots\ldots (40)$$

The functions $\bar{P}_w(z)$ and $\bar{q}_j(z)$ are again meromorphic functions of z, and the inversion proceeds in the same manner as before. Then,

*Where P_{fj} denotes the pressure drop at the well in the formation in Layer j.

$$P_w(t) = \frac{q}{2\pi}\left[\frac{2t}{\sum_{j=1}^{n}\beta_j\gamma_j^2} + \frac{\sum_{j=1}^{n}\beta_j\gamma_j^4\left(\ln\frac{\beta_j}{\alpha_j} - \frac{3}{4} + S_j\right)}{\left(\sum_{j=1}^{n}\gamma_j\beta_j^2\right)^2}\right] + Y_s(t) \quad (41)$$

where $Y_s(t)$ represents the transient solution.

With the same approximations as before and in the time range of validity of these approximations, the skin factors S_j always appear in such a fashion that they can be completely absorbed by replacing α_j by α_j^*, which is defined by

$$\alpha_j^* = \alpha_j e^{-S_j} \quad (42)$$

The solution for the infinite reservoir with skins was found by a method similar to the one used by Horner; it was concluded that again, in the time range of validity of the approximations taken when no skin was present, the presence of the skin factors in the equations could be absorbed into the quantities α_j in the manner of Eq. 42.

Hence, it can be concluded that, for times of practical importance, the effect of a skin with skin factor S_j in each one of the layers can be described completely by assigning a fictitious well radius $r_{w,j}^*$ to each layer, the relation between the true well radius $r_{w,j}$ and $r_{w,j}^*$ being given by

$$r_{w,j}^* = r_{w,j}e^{-S_j} \quad (43)$$

NOMENCLATURE

A_j = recovery/unit pressure drop of Layer j (Eq. 14)

b_j = thickness of jth layer, cm

$\bar{b}$ = $b_1 + b_2$, total thickness, cm

i_j = productivity index of Layer j (Eq. 15)

k_j = permeability of jth layer, darcy

$\bar{k}$ = $(k_1b_1 + k_2b_2)/(b_1 + b_2)$, weighted mean of permeabilities, darcy

$p_j(r,t)$ = pressure in the jth layer at position r and time t, atm

$p_w(t)$ = pressure at the well at time t, atm

$\bar{p}_j(t)$ = average pressure in the jth layer at time t

p^* = pressure obtained by straight-line extrapolation of first linear portion of p_w vs $\ln[\Delta t/(t + \Delta t)]$

p_{fj} = pressure in the formation of Layer j at the well

$P_j(r,t)$ = pressure drop in the jth layer at position r and time t

$P_w(t)$ = pressure drop function at the well

q_T = total production rate from multilayer reservoir in cc/sec, measured at initial reservoir conditions

q_T' = total production rate in cc/sec measured at average reservoir conditions

$q_j(t)$ = production rate from jth layer at time t, in cc/sec, measured at initial reservoir conditions

$q_j(\Delta t,t)$ = flow rate out of jth layer at shut-in time Δt for a well closed in at production time t

$q_c(\Delta t)$ = production rate during after-production at dimensionless shut-in time Δt

$Q_j(t)$ = cumulative production from Layer j at time t, in cc, measured at initial reservoir conditions

r_w^* = fictitious well radius to represent skin effect, cm

S_j = skin factor of jth layer, dimensionless

t' = production time, days

t_r = time at which the pressure disturbance reaches the point r, sec

$Y(t)$ = transient solution in well-pressure equation

$Z_j(t)$ = transient solution in rate equation for jth layer

α = loading constant (dimensionless) with respect to T

$\Delta D(t)$ = differential depletion per unit thickness at time t between the layers of a two-layer reservoir

Δt = shut-in time, sec

Δt_D = dimensionless shut-in time = $\bar{k}\Delta t/\bar{\phi}\mu c r_w^2$

ϕ_j = oil-filled porosity of the jth layer, dimensionless

$\bar{\phi}$ = $(\phi_1b_1 + \phi_2b_2)/(b_1 + b_2)$ weighted mean of porosities

γ = Euler's constant, $\ln\gamma = 0.5772$

REFERENCES

1. Horner, D. R.: "Pressure Behavior in a Well Producing from a Number of Different Horizons", Shell Oil Co. Report.
2. Tempelaar-Lietz, W.: "The Effect of the Rate of Oil Production upon the Performance of Wells Producing from More than One Horizon", *Soc. Pet. Eng. Jour.* (March, 1961) 26.
3. Matthews, C. S., Brons, F. and Hazebrook, P.: "A Method for Determination of Average Pressure in a Bounded Reservoir", *Trans.*, AIME (1954) Vol. 201, 182.
4. van Everdingen, A. F.: "The Skin Effect and Its Influence on the Productive Capacity of a Well", *Trans.*, AIME (1953) Vol. 198, 171.
5. McLachlan, N. W., Humbert, P. and Poli, L.: "Supplement au Formulaire pour le Calcul Symbolique", *Memorial pour les Sciences Mathématiques* (1950) CXIII.
6. Doetsch, G.: *Tabellen zur Laplace — Transformation und Anleitung zum Gebrauch*, Springer-Verlag (1947) Berlin und Göttingen.

***

. . . . . About The Authors

WILLIAM E. BRIGHAM is a senior research engineer in the recovery processes section of Continental Oil Co.'s Production Research Div. at Ponca City, Okla. First joining Continental as a research engineer in 1958, he received his MS degree in chemical engineering from the U. of Oklahoma in 1956 and spent the next two years as a chemical engineering instructor.

PHILIP W. REED (left) is a research engineer in the Production Research Div. of Continental Oil Co., Ponca City, Okla. He joined Continental in 1955 following receipt of an MS degree in petroleum and natural gas engineering from Pennsylvania State U. JOHN N. DEW (right), also with Continental at Ponca City, is supervisor of the company's recovery processes section, Production Research Div. Formerly associated with the Research and Development Div. of the New Mexico School of Mines, he holds a BS degree from the U. of Oklahoma and MSE and PhD degrees in chemical engineering from the U. of Michigan.

W. TEMPELAARLIETZ, a native of The Netherlands, heads Shell Oil Co.'s West Coast Area laboratory in Los Angeles. A graduate of Delft Technical U., The Netherlands, he came to the United States in 1938 and joined Shell two years later. In his present position, he is concerned with research covering exploration, production, drilling and mechanical engineering problems.

S. A. HOVANESSIAN (left) is a research engineer in the reservoir analysis and applied math section of the California Research Corp., La Habra, Calif. He obtained BS, MS and PhD degrees in engineering from the U. of California at Los Angeles and served on the Engineering Dept. faculty of the School before joining Cal Research in 1958. F. J. FAYERS (right) until recently a group supervisor with Cal Research at La Habra, is now with the English Electric Co., Atomic Power Div., Leicester, England. Born in Italy of British parents, he obtained his education in England, receiving a PhD degree in physics from the U. of Reading in 1955. He joined Cal Research in 1956.

R. L. PERRINE is an associate professor in the Dept. of Engineering at the U. of Southern California, Los Angeles. A native Californian, he is a graduate of San Jose State College and Stanford U. and holds BS, MS and PhD degrees in physical chemistry. He joined California Research Corp. at La Habra, Calif. in 1953.

D. KUNII (left), assistant professor of chemical engineering at the U. of Tokyo, was a visiting professor at Northwestern U. from 1958 through 1960. His chief interests have been in the field of heat transfer, and he has published many articles and books on this subject both in the United States and in Japan. J. M. SMITH is Walter P. Murphy Distinguished Professor of chemical engineering at Northwestern U. His research activities in recent years have been in the areas of heat and mass transfer.

H. C. LEFKOVITS (left) works in the operations analysis group of Shell Development Co.'s Exploration and Production Research Div., Houston. He holds BA and MA degrees from The U. of Texas and a PhD degree in math from Rice U. He joined Shell Development's reservoir mechanics section in 1951 and later transferred to his present position. P. HAZEBROEK (right), also with Shell Development in Houston, is a native of The Netherlands. He received undergraduate and ScD degree in math and physics from the U. of Leyden, The Netherlands. From 1938 until 1954, he was employed by the N. V. de Bataafsche Petroleum Maatschappij at The Hague, moving to his present position in 1955.

E. ELIZABETH ALLEN (left) heads the computer project in the Basic Research Div. of Shell Development Co., Houston. She has been with the company since 1946, when she graduated from Rice U. with a BS degree in physics. C. S. MATTHEWS (right), formerly chief reservoir engineer for Shell Oil Co.'s Technical Services Div., is now senior reservoir engineer with Shell Development in Houston. He joined Shell Oil as a chemical engineer immediately following his graduation from Rice U. with a PhD degree in chemistry.

Order Now While All Volumes Available

Complete Your Library of Permanent Literature With Petroleum Transactions Covering Years 1925 through 1960

CONTENT OF VOLUMES

Reprinting of AIME Petroleum Transactions has been accomplished by combining two of the original volumes into one book for Volumes G-25 through 179. Material on production statistics and certain chapters of non-technical material were omitted in the reprinting. The books in this series, containing two of the original volumes, are six by nine inches in size.

Volumes 186 through 198 were reprinted in their original form, with one book of 8½ by 10¾ inches in size containing a single volume.

BINDING, PACKAGING, PRICES

Books are bound in standard AIME red cloth binding, and individually packaged in cardboard cartons for delivery. Prices are listed on the order form at right for cash purchase of individual books, with a discount of 30 per cent to AIME members as shown. No provision is made for credit or installment purchases, or for discount on purchase of complete set of books. Delivery will be postpaid.

BONUS BOOKS

One copy of Index to Petroleum Publications, AIME (1921-1952) and Index (1953-1959) will be given as a bonus with a purchase of any eight of the reprinted books listed at the right. The hard-back Index published in 1953 by the Society of Petroleum Engineers covers all petroleum publications of the Institute through 1952. Prices are $5.00 to Non-Members and $3.50 to Members. The paper-bound Index covering years 1953-1959 is available at $1.00 per copy. These are valuable additions to a set of Transactions.

ORDER FORM

INDICATE NUMBER OF BOOKS DESIRED IN COLUMN SHOWN

Years Covered	*Original Volume Numbers*	*PRICES To Non-AIME Members* Price Per Book	*PRICES To Non-AIME Members* Number Copies Desired	*PRICES To AIME Members* Price Per Book	*PRICES To AIME Members* Number Copies Desired	*Add Amounts in This Column*
1925-1926	G-25—G-26 Small Book	$9.00		$6.30		
1927-28-29	77- 82 "	$9.00		$6.30		
1930-31	86- 92 "	$9.00		$6.30		
1932-33	98-103 "	$9.00		$6.30		
1934-35	107-114 "	$9.00		$6.30		
1936-37	118-123 "	$9.00		$6.30		
1938-39	127-132 "	$9.00		$6.30		
1940-41	136-142 "	$9.00		$6.30		
1942-43	146-151 "	$9.00		$6.30		
1944-45	155-160 "	$9.00		$6.30		
1946-47	165-170 "	$9.00		$6.30		
1948-49	174-179 "	$9.00		$6.30		
1949	186 Large Book	$7.00		$4.90		
1950	189 " "	$7.00		$4.90		
1951	192 " "	$7.00		$4.90		
1952	195 " "	$7.00		$4.90		
1953	198 " "	$7.00		$4.90		
1954	201 " "	$7.00		$4.90		
1955	204 " "	$7.00		$4.90		
1956	207 " "	$7.00		$4.90		
1957	210 " "	$7.00		$4.90		
1958	213 " "	$7.00		$4.90		
1959	216 " "	$7.00		$4.90		
1960	219 " "	$7.00		$4.90		
Index	(1921-1953)	$5.00		$3.50		
Index	(1953-1959)	$1.00		$1.00		
					TOTAL AMOUNT ENCLOSED	

Please Send Remittance With Order Form to:

SOCIETY OF PETROLEUM ENGINEERS
OF AIME
6300 NORTH CENTRAL EXPRESSWAY
DALLAS 6, TEXAS

Your Name_____
(Please Print)

Mailing Address_____

_____

City_____ State_____

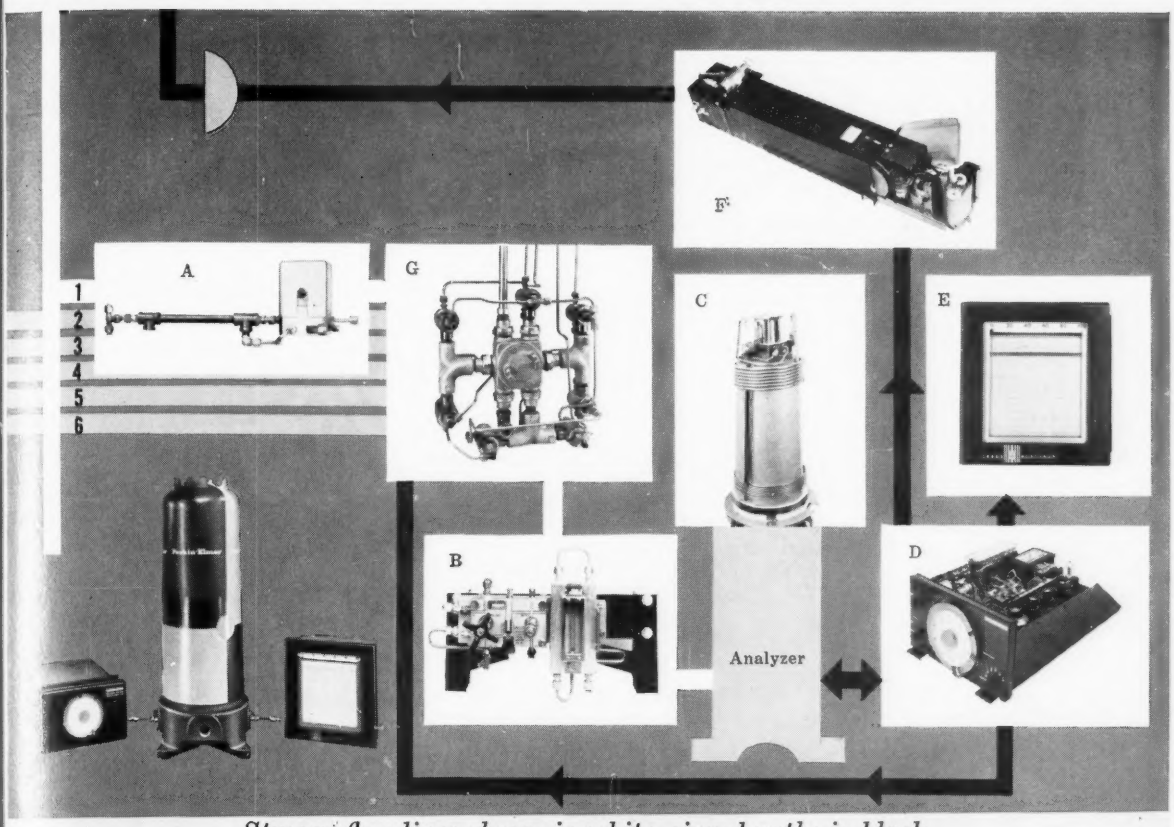

Stream flow lines shown in white, signal paths in black

This block diagram shows how six process streams can be selectively analyzed by the P-E Model 184-B. For brevity, Stream #1 only will be followed through the system.

Stream #1 is tapped, and the sample vaporized in the Liquid Sample Vaporizer (A). Sample #1 then flows (with the other five vaporized samples) into the enclosed, heated Multi-Stream Solenoid Switching Manifold (G). The solenoids are electrically directed by the Programmer (D). As it is selected, Sample #1 is valved into the Final Sampling Assembly (B), where it is filtered and metered into the Analyzer. The Analyzer quantitatively and qualitatively separates the sample's components by gas chromatography, produces signals which appear as a bar graph on Recorder (E).

The signal can also be fed into a Pneumatic Control Accessory (F) which produces a 15 psi signal for automatic control of one variable component of the stream.

The Analyzer with Reverse Flow Valve (C) allows for the analysis of light components individually plus a "total heavies" measurement; it back-flushes and analyzes heavy ends as a single peak, shortening analysis time in the process. The Programmer (D) is available in a variety of modes for multi-component and multi-stream analysis. It controls the Switching Manifold (G) and the Analyzer, and the read-out of the Recorder (E).

All flow lines and sampling building blocks are kept above the dew point, where necessary, by steam tracing.

UNTIL NOW—PROCESS CONTROL INSTRUMENTATION LIKE THIS HAD TO BE CUSTOM-BUILT

Standard building blocks give the new P-E Model 184-B Process Vapor Fractometer the flexibility of the most advanced special engineering developments in process gas chromatography.

A new, highly versatile instrument, the Model 184-B brings automatic process control by gas chromatography within the reach of virtually any petroleum or chemical processing plant.

The Model 184-B uses *building block* sampling and sensing units in various combinations to produce process analytical systems which mean continuing extra dividends through reduced maintenance, low-cost training and highest reliability.

These standard building blocks include multi-port sampling valves for backflushing and analyzing heavy ends . . . versatile multi-column systems . . . multi-stream programmer kits . . . pneumatic units for automatic control . . . and a wide variety of sampling devices.

Perkin-Elmer, the world's largest manufacturer of gas chromatographic instruments, will help you in your process instrumentation requirements. For more information, write for a new descriptive booklet.

All building blocks in any P-E system conform to standard refinery and chemical plant safety practices.

INSTRUMENT DIVISION

Perkin-Elmer *Corporation*

NORWALK, CONNECTICUT

BENDIX
G-20 COMPUTER
'SPACE'
PROGRAMMING

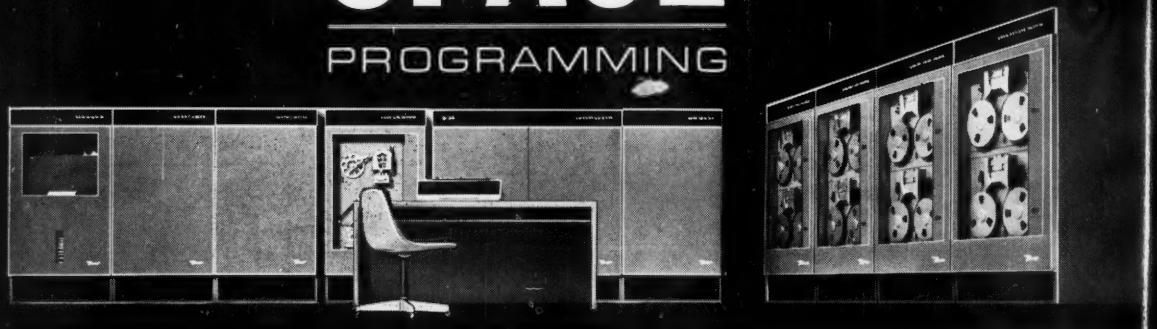

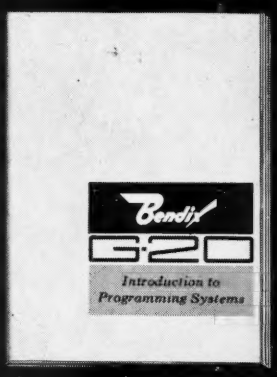

GIVES YOU DOWN-TO-EARTH RESULTS

SPACE—the Bendix G-20 Automatic Programming "package"—sets new standards for ease of use, power and efficiency. Designed in concert with the G-20 computer system, SPACE is complemented by numerous advanced equipment features. Here are the automatic programming methods which form an integral part of SPACE . . . and Bendix G-20 systems, large or small:

SPAR—Symbolic Assembly Programming. Allows the programmer to maintain direct control over all G-20 operations. Provides the efficiency of machine language programming without the complexities.

ALCOM—an Algebraic Compiler based on the international notation of ALGOL. Easy-to-use ALCOM permits the statement of scientific problems in natural mathematical language . . . simplifies and speeds problem solving.

COBOL—Common Business Oriented Language permits statement of data processing problems in natural business language for high-speed computer solution . . . makes flexible use of alphabetic, decimal, and special characters.

EXECUTIVE—provides automatic program scheduling and component assignment . . . permits maximum-efficiency in parallel processing and utilization of components.

See for yourself how SPACE . . . combined with outstanding equipment capabilities . . . has put the G-20 in a class by itself. Investigate today. For your copy of "Introduction to G-20 Programming Systems," write, wire or call:

THE Bendix CORPORATION

Bendix Computer Division

Dept. AQ-30, Los Angeles 45, California